

CZECH TECHNICAL UNIVERSITY IN PRAGUE



MASTER'S THESIS

**Development and Prototypical Implementation of a Universal
Concept for a Trailer Rear View Camera**

Sören Böttger

Supervisor: **Ing. Tomáš Pajdla, Ph.D.**

A thesis submitted in fulfilment of the requirements for the Degree in
Master of Science in Space Science and Technology

August 2016

Host University



In Collaboration with



Co-funded by the
Erasmus+ Programme
of the European Union

DIPLOMA THESIS ASSIGNMENT

Student: **Sören Böttger**

Study programme: Cybernetics and Robotics
Specialisation: Systems and Control

Title of Diploma Thesis: **Development and Prototypical Implementation of a Universal Concept for a Trailer Rear View Camera**

Guidelines:

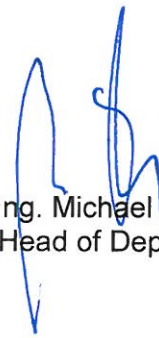
1. Review the literature about the dynamics of a vehicle including a trailer for a parking situation. Furthermore, the basic principles of camera projections shall be studied.
2. Based on the steering and car-trailer angle, which are detected by sensors and existing algorithms, the trajectory of the system shall be predicted and later mapped to the camera image. Furthermore, camera calibration and drawbar recognition have to be implemented on top of existing algorithms in C++ and OpenCV.
3. The concept should be simulated and tested on a test vehicle under real conditions. An analysis of the test results should discuss reliability and feasible improvements.

Bibliography/Sources:

- [1] Multiple View Geometry in Computer Vision - Hartley, Zisserman
- [2] Eliminating Blind Spots for Assisted Driving - Ehlgen, Pajdla, Ammon
- [3] Dynamical Analysis of Vehicle Systems - Schiehlen

Diploma Thesis Supervisor: Ing. Tomáš Pajdla, Ph.D.

Valid until the summer semester 2016/2017


prof. Ing. Michael Šebek, DrSc.
Head of Department




prof. Ing. Pavel Ripka, CSc.
Dean

Prague, February 24, 2016

Disclaimer

This project has been funded with support from the European Commission. This publication [communication] reflects the views only of the author, and the Commission cannot be held responsible for any use which may be made of the information contained therein.

Declaration of Originality and Compliance of Academic Ethics

I herewith declare that this thesis contains literature survey and original research work by the undersigned candidate, as part of his studies.

All information in this document has been obtained and presented in accordance with academic rules and ethical conduct.

I also declare that, as required by these rules and conduct, I have fully cited and referenced all material and results that are not original to this work.

Prague,

.....

Abstract

Manoeuvring a vehicle with additionally attached trailers is a tedious task. Albeit driver assistance systems support the driver in nearly any situation in these days, tools facilitating the manoeuvring process of extended vehicles can only rarely be found in research and especially in the market. This thesis deals with the prototypical implementation of a rear view camera parking assistance system. In particular, the visualisation of the predicted driving path of the tractor-trailer combination in the camera image is emphasised, following the representation of existing parking assistance systems for individual vehicles. A general approach is aiming at the portability of the system to nearly any kind of trailer.

The superimposed guidelines are based on a state space model, which is derived on top of assumptions agreeing with results found in the literature. Due to the strong assumptions and simplifications, the model is tested in three different ways and moreover for different types of trailers. All underlying methods are described in detail and furthermore tested in several scenarios, if necessary. Special importance is attached to the comparison of the actual driven paths with their previous predictions, for which a new method has been derived, implemented and tested successfully.

Beside the implementation of the guideline projection to the camera's image, the human-machine interface is augmented by a Bird's Eye view animation, too. A final test of the integrated system for different types of trailers shows the proper operation of the overall system during parking situations.

Acknowledgement

Without the help of many different people, the work of this thesis would not have been accomplished in the same manner. Obviously, it is not possible to mention every individual person, but I try to express my thanks at least to the most important ones. In case I forgot anybody, I would like to apologise to them.

First of all, I would like to thank my person in charge at *IAV*, Christoph Hein, who always gave me advice driving the outcome of this work in the resulting direction. Moreover I would like to thank you for the annotations to the written report. Without the help of my supervisor especially in his field of research, Tomáš Pajdla, the investigations of the validity of the derived model would not have been possible. I would like to thank you further for the lucrative skype meetings and for the admission of the thesis, despite organisational hurdles. I would like to thank the whole team of *VI-D53* at *IAV* in Chemnitz, for the helping discussions during meetings, supporting the experiments but especially for the joy and fun we had during the breaks. Thanks go especially to Maria Kremsreiter, Ludwig Winkler, Diana Schif, Christoph Hartwig, Nils Werner, Pia Wald, Tim Schrader, Maryam Sadat Boka, Aditiya Kamath and especially the leader of our team Matthias Sachse.

I would like to thank Jörg Bauer, the head of the department of *VI-D5* of *IAV*, letting me working quite independently despite the troubles with the arrangement of confidentiality. I appreciate your engagement in the final correcting phase as well.

The work of Thomas Ullmann and Peter Burkhardt should not be forgotten, too. Without their cooperation regarding the design and manufacturing of the camera mounting, the system would not have achieved its final functionality.

During the whole period of my studies, I met many new people, whom I want to thank for their collaboration in tough study periods but especially for the joy they gave me beside the work. It is hard to mention only a few, but omitting the following would be a shame: Jendrik Jördening, Franz Weigel, Thomas Rapp, Roger Gutierrez Ramon and Christian Grosse. Further thanks go to the whole SpaceMaster team of round 10.

I would like to thank my family especially, which supported me during my long way of education and all coming along decisions. Thank you for your love, joy and sympathy.

Last but not least I would like to thank Anne Huster for the effort of checking the work for language mistakes. Thank you further for encouraging me in tough periods and giving me joy and love beside the studies.

Finally, I would like to thank the Education, Audiovisual and Culture Executive Agency of the Commission of the European Communities for the support within the Erasmus Mundus Framework.

Contents

List of Figures	i
List of Tables	iii
Nomenclature	v
1 Introduction	1
1.1 State-of-the-Art	1
1.1.1 Model of Tractor-Trailer Systems	1
1.1.2 Off-the-Shelf Parking Assistance Systems	2
1.1.3 Path Planning	3
1.1.4 Manoeuvring Assistance Systems in Research and in the Market	3
1.2 Problem Formulation	4
2 Theoretical Background	5
2.1 Vehicle Dynamics	5
2.1.1 Classification	5
2.1.2 Lateral Dynamics	5
2.1.3 Bicycle Model	6
2.2 Computer Vision	7
2.2.1 Projective Camera Model	7
2.2.2 Lens Distortion	8
2.2.3 Camera Calibration	9
2.3 Driver Assistance Systems	9
2.3.1 Classification of Driver Assistance Systems	9
2.3.2 Classification of Parking Assistance Systems	10
3 System Identification	11
3.1 Types of Trailers	11
3.2 Simplification of Trailer Models	12
3.3 Virtual Trailer Properties	14
3.4 From Real Trailers to a Chain of Virtual Trailers	15
4 System Analysis and Modelling	17
4.1 Derivation of Kinematics Equations	17
4.1.1 Description of the System	17
4.1.2 State Vector of the System	19
4.1.3 Tractor Vehicle Kinematics	20
4.1.4 Kink Angle Kinematics	21
4.1.5 Entire State Space Model	24
4.1.6 Comparison with Existing Models in the Literature	25

4.2	Steering Model	27
5	Calculation of Guidelines	29
5.1	Integration of the State Space Model	29
5.2	Point Transformation and Guideline Calculation	31
5.3	Guideline Projection	33
5.4	Accuracy of Guideline Projection	35
6	Analysis of the Model	37
6.1	Kink Angle Progress for Different Steering Angles	37
6.2	Kink Angle Progress for Different Initial Conditions	38
6.3	Threshold Kink Angle	38
6.4	Static Turn Steering Angle	39
6.5	Critical Kink Angles	40
6.6	Error Behaviour and Stability Analysis	40
7	Validation of the Model	43
7.1	Constraints Stating the Reliability of the Model	43
7.2	Lateral Slip Analysis	44
7.2.1	Results	44
7.3	Kink Angle Behaviour	45
7.3.1	Results: Single-Axle Trailer	45
7.3.2	Results: Two-Axle Trailer	47
7.4	Absolute measurement	50
7.4.1	Camera Calibration	50
7.4.2	Image-to-World Projection	54
7.4.3	Accuracy of Target Determination	55
7.4.4	Trajectory Comparison	58
7.4.5	Results: Single-Axle Trailer	60
7.4.6	Results: Two-Axle Trailer	62
7.5	Conclusion	63
8	The Overall System	65
8.1	Integration	65
8.2	Performance	67
8.2.1	Single-Axle Trailer	67
8.2.2	Two-Axle Trailer	68
8.3	Conclusion	69
9	Conclusion and Outlook	71
9.1	Outlook	72
10	Appendix	73
10.1	Analysis of the Single-Axle Trailer	74
10.1.1	Scenario: $\varepsilon \approx 0^\circ$	74
10.1.2	Scenario: $\varepsilon \approx +90^\circ$	75
10.1.3	Scenario: $\varepsilon \approx -90^\circ$	76
10.1.4	Scenario: $\varepsilon \approx +180^\circ$	77
10.1.5	Scenario: $\varepsilon \approx +490^\circ$	78
10.1.6	Scenario: $\varepsilon \approx -490^\circ$	79

10.2 Analysis of the Two-Axle Trailer	80
10.2.1 Scenario: $\varepsilon \approx +90^\circ$	80
10.2.2 Scenario: $\varepsilon \approx -90^\circ$	81
10.2.3 Scenario: $\varepsilon \approx +180^\circ$	82
10.2.4 Scenario: $\varepsilon \approx -180^\circ$	83
10.2.5 Scenario: $\varepsilon \approx +490^\circ$	84
10.2.6 Scenario: $\varepsilon \approx -490^\circ$	85
CD Content	91

List of Figures

1.1	Rear view camera images with displayed auxiliary lines	2
2.1	Forces, moments and coordinate frames of a vehicle (from Reif [Rei14])	6
2.2	Ackermann turning geometry (from Rajamani [Raj11])	6
2.3	Single-track (bicycle) model of a vehicle (after Rajamani [Raj11])	6
2.4	Projection of world point to an image plane behind a fisheye lens	9
3.1	Example of a general trailer	12
3.2	Simplified model of a complex trailer: two trailer segments with only one (gen- eralised) axle	13
3.3	Properties of a virtual trailer	14
4.1	Definition of the properties of the tractor-trailer system model	18
4.2	System of tractor and trailer (from [Ada14])	25
4.3	Cubic fit - steering model	28
5.1	Initial pose of the tractor-trailer system	31
5.2	Virtual pose after a passed distance s (dashed), compared to the initial pose (solid)	32
5.3	Transformation of a point from frame i to its previous neighbour.	32
5.4	Transformation of a point of the guideline to the camera's frame	34
5.5	Chessboard pattern for the evaluation of the accuracy of the projection algo- rithm	35
5.6	Projection of known coordinates (red) to the camera image (top: raw image, bottom: undistorted image)	35
6.1	Responses of the model to different steering angles	38
6.2	Responses of the model to different initial kink angles	39
6.3	Maximum driven path s_{final} for various steering and initial kink angles	41
7.1	Kink angle development along driven distance for a single-axle trailer	45
7.2	Kink angle deviation along driven distance for a single-axle trailer	46
7.3	Kink angle development along driven distance for a two-axle trailer with used model (3.3)	48
7.4	Kink angle deviation along driven distance for a two-axle trailer with used model (3.3)	48
7.5	Kink angle development along driven distance for a two-axle trailer with used model (3.2)	49
7.6	Kink angle deviation along driven distance for a two-axle trailer with used model (3.2)	49
7.7	Calibration chessboard pattern at different views with detected inner corners	51

7.8	Used target structure for the extrinsic camera calibration	52
7.9	Recorded frame before (left) and after (right) undistortion	53
7.10	Calculation of world coordinates from absolute distances	53
7.11	Detected points of accuracy measurement	56
7.12	Mean error histogramm of the point in the centre	57
7.13	Mean error histogramm of the right-most point	57
7.14	Mean error histogramm of the right-most point at a height of 0.53 m	57
7.15	Method of trajectory comparison	59
8.1	Mounting system of the rear view camera	66
8.2	Wiring of the rear view camera	66
8.3	HMI - enabled Bird's Eye view and undistorted camera image	66
8.4	HMI - disabled Bird's Eye view with raw camera image only	66
8.5	Used method of performance test for the single-axle trailer	68
8.6	Comparison of the driving path for two different steering angles for a single-axle trailer	68
8.7	Rear view scenes during the targeting test: the trailer is approaching the target (top to bottom)	69
8.8	Initial position, prediction and final position of the system during the parking test	69
8.9	Final position of the tractor-trailer system after the targeting test	70
10.1	Analysis of single-axle trailer for 0° steering angle	74
10.2	Analysis of single-axle trailer for $+90^\circ$ steering angle	75
10.3	Analysis of single-axle trailer for -90° steering angle	76
10.4	Analysis of single-axle trailer for $+180^\circ$ steering angle	77
10.5	Analysis of single-axle trailer for maximum steering angle	78
10.6	Analysis of single-axle trailer for minimum steering angle	79
10.7	Analysis of two-axle trailer for $+90^\circ$ steering angle	80
10.8	Analysis of two-axle trailer for -90° steering angle	81
10.9	Analysis of two-axle trailer for $+180^\circ$ steering angle	82
10.10	Analysis of two-axle trailer for -180° steering angle	83
10.11	Analysis of two-axle trailer for maximum steering angle	84
10.12	Analysis of two-axle trailer for minimum steering angle	85

List of Tables

3.1	Properties of a virtual trailer	14
4.1	Properties of the tractor-trailer system	19
4.2	Comparison of properties between both models - first model from [Ada14] . .	25
7.1	Accuracy results of both points on the floor and the right-most point at a height of 0.53 m	58
7.2	Results of the absolute deviation for a single-axle trailer	62
7.3	Results of the absolute deviation for a two-axle trailer	63
10.1	CD Content	91

Nomenclature

Abbreviations

ADAS	Advanced Driver Assistance Systems
CAN	Controller Area Network
CV	Computer Vision
DAS	Driver Assistance Systems
DLS	Direct Least-Squares - a method of optimisation
FOV	Field of View
HMI	Human-Machine Interface
OpenCV	Open Source Computer Vision - the OpenCV library
PnP	Perspective-n-Point - extrinsic calibration problem
RADAR	Radio Detection and Ranging

Conventions

Coordinate Frame	The terms coordinate frame and coordinate system are used equivalently
Driving Corridor	See Guideline, used equivalently
Driving Path	See Guideline, used equivalently
Guideline	Predicted path of the system, formed by its outer contour (possibly determined by a sub-vehicle only)
Initial Condition	Initial conditions are specified with a lower note, separated by a comma
Segment	See Trailer Segment, used equivalently
Steering Angle	If the context is clear, steering angle is used instead of axle angle

Sub-Vehicle	A member of the Tractor-Trailer system, either the towing vehicle or an attached (virtual) trailer
System	See Tractor-Trailer System, used equivalently
Tractor-Trailer System	The combination, consisting of a towing vehicle and an arbitrary number of attached trailers
Trailer Segment	A part of a trailer, which is steerable with respect to other parts. It can contain an arbitrary number of axles.
Trigonometric Functions	Sine and Cosine are sometimes abbreviated with their first letter in equations
Undistortion	The process of removing the fisheye-effect of images

1 Introduction

Rear view parking assistance systems for combinations of towing vehicles and additional attached trailers appear only rarely in the market. A development of a rear-view parking assistance system, with the aim, to make it ready for series production can be an interesting task, if only the versatile use of trailers is considered. Still, the manoeuvring procedure of a tractor-trailer system is a tough task. This thesis is aiming at a prototypical implementation of a rear view parking assistance system, emphasising additional hints to the driver beside the mere camera image.

Therefore, the thesis is organised as follows: The current chapter gives an overview of the state-of-the-art technology related to the topic. In the end, the specific problem is formulated. For the sake of providing the minimum amount of basics, in order to understand the following content of this thesis, chapter 2 provides the necessary theoretical background. Followed by an identification of the system in chapter 3, a model is derived based on existing approaches in the literature in chapter 4. During chapter 5 the calculation of the driving path from the system's state is presented as well as the way of its projection to the camera's image. An investigation of the derived model's behaviour in chapter 6, gives rise to the actual validation of the model in chapter 7. Beside the analysis of the model's assumptions, the estimated driving corridors are proven. Only in chapter 8 the integration of the camera system to the trailer as well as several parking test situations are described. The conclusion in chapter 9 summarizes the most important results of this thesis and suggests further reasonable investigations, in order to bring the system in a ready for the market state.

1.1 State-of-the-Art

The technology related to driver assistance systems undergoes a huge growth. At the same time, assistance systems for tractor-trailer combinations, do not seem attractive, at least, if one refers to the available technologies. And yet the manoeuvring of a tractor-trailer system is often a tedious task [WHW⁺11], [WHLS15], so that assistance systems could facilitate the driving situation enormously. However, some approaches have been done so far. The step towards a functional system involves several fields of research. That is why the state-of-the-art description is split, respectively.

1.1.1 Model of Tractor-Trailer Systems

Systems consisting of a towing tractor vehicle and attached trailer(s) are widely discussed in the literature, especially in the field of robotic motion, e.g. in [TMS93], [TSBS95], [BTS95], [Alt00]. Based on the non-holonomic roll-constraint, neglecting lateral slip and the bicycle

approach, pure kinematic models are derived and the behaviour of the whole system in terms of control applications is discussed. Most of the papers refer to a chain, consisting of a tractor and n trailers. Although, the application of these models seems escapist in the first regard, the opinion changes by thinking of luggage trains, which are used in airports [TMS93]. However, the application of these models refers mostly to simulations (e.g. [ZPW00]) or models of tractor-trailer systems (e.g. [MK15]). Only in [EPA08] and [Sch06], a real application has been found.

1.1.2 Off-the-Shelf Parking Assistance Systems

The camera image of nowadays rear view parking assistance systems are normally superposed by auxiliary lines, in order to provide additional information to the driver of the current situation. Static distance markers as well as dynamic guidelines, which describe the predicted path of the vehicle for static steering wheel angles, are usually displayed. The survey of Stratmann [Jen15] was used for a comparison of available parking assistance systems. Four examples are shown in Figure 1.1. All examples display the mentioned static distances, as well as the driving path, albeit their representation is different. Usually, rear cameras are characterized by a large field of view, in order to survey a wide region behind the vehicle. Distortion effects arise due to the structure of the lenses, which can, upon a certain level, be eliminated with software operations. Clearly, some manufactures like *Volkswagen* and *Audi* have decided to present an undistorted image (Figure 1.1a and 1.1c), whereas other manufacturers like *Mercedes* and *Nissan* display the raw image (Figure 1.1b and 1.1d) or with small undistortion operations only.



(a) Volkswagen (from [WHW⁺11])



(b) Mercedes (from [Jen15])



(c) Audi (from [Jen15])



(d) Nissan (from [Jen15])

Figure 1.1: Rear view camera images with displayed auxiliary lines

The static markers represent distances of the rear bumper of the vehicle perpendicular to its

surface. *Volkswagen* usually shows three static markers at different distances. The colour is identifying if the distance is critical or not (red: closest distance, green: furthest distances). *Audi* and *Mercedes* depict one static marker, only. Similar to *Volkswagen*, the distances are shown in vehicles from *Nissan*.

The predicted driving path is usually displayed in a yellowish colour. A nice hint to the driver is given by *Volkswagen*, but especially by *Mercedes*: Along the predicted driving path, distance markers are shown. In the latter case, finer distances are displayed, resulting in a carpet-like representation. Beside the actual rear view, *Volkswagen* and *Audi* show a Bird's eye view of the vehicle, providing a better understanding of the current situation.

Albeit the mode of operation of the parking assistance system of all manufacturers are nearly the same, differences arise in the human-machine interface (HMI).

1.1.3 Path Planning

One of the most interesting topics, in which the models, discussed in section 1.1.1, are used, is the path or motion planning problem. The main objective is to find a path, which brings the tractor-trailer system from one state to another [SV95]. A realistic application could be the steering of the system into a pre-detected parking spot. Related problems are discussed in [SV95], [ZPW00] and [MK15], to mention only a few. The authors of these papers propose a passive control system, advising the human operator of the vehicle [MK15]. Such a system could be considered in the implementation on top of the driving path projection, since it requires no additional hardware and is moreover simple to implement.

1.1.4 Manoeuvring Assistance Systems in Research and in the Market

Parking is a part of the umbrella term of manoeuvring. A system, assisting the driver of a truck-trailer combination has been proposed, implemented and tested by Ehlgen et al. [EPA08]. Via four cameras, a Bird's eye view is constructed, eliminating blind spots for all situations. On top of that, the predicted driving path, based on models described in section 1.1.1, is superposed to the constructed image, in order to support the driver. A similar approach could have been considered in the present thesis, too.

Still, after a very time-consuming research on the internet, only a single work has been found, where the predicted driving path is projected into a camera image, obtained by a camera, mounted at the rear side of a trailer. A survey with many test persons showed, that a rear view parking assistance system could lead to a great facilitation of the manoeuvring process [Sch06]. Nevertheless, there are many realisations, which have been concerned in a different way. Although the authors of [MK15] have mounted a camera at the rear side of the last trailer of their model, the image was only used for the detection of the final position of the system. This result gave a further impulse, to implement the system with a rear view camera. Nevertheless, there exist trailer assistance systems as commercial off-the-shelf products already. The *Trailer Assist*, introduced by *Volkswagen*, enjoyed a good reputation during the last years. The driver can pretend the kink angle between the tractor and the trailer, which the system automatically regulates during the reversing [Vol14]. Hence, constant circles can be driven, having such a system included. Beside the publicity, there are still some disadvantages of the system. At first, the huge blind spot regions behind the trailer are still not accessible to the driver. Moreover, it seems quite a challenging task to guess the write radius of the wanted path, according to which the kink angle has to be set. For both issues, the

Bird's eye system proposed in [EPA08] seems more suitable. On top of that, the *Trailer Assist* is an expensive add-on.

1.2 Problem Formulation

After an extensive research about existing methods and technologies, the problem statement of this thesis has to be defined. According to the title, a rear view system shall be implemented. Nevertheless, the research of Ehlgen [EPA08] gave rise to reconsider the camera concept, although the rear view system should be aimed at. In all cases, the image should be presented to the operator in a proper fashion, that makes a pre-processing of the raw image indispensable. In the case of the rear view system, this would mean, that the image has to be undistorted, according to its lens distortion coefficients. The driver should be able to assess distances in the camera image respectively. For a better evaluation, static distance markers as discussed in section 1.1.2 shall be overlaid to the pre-processed image.

Clearly, the dynamic guidelines can be a very helpful assistant to the operator. Based on existing models in the literature, the path of the system shall be predicted and the resulting boundary lines displayed in the image. Although the models, presented in e.g. [TMS93], [TSBS95], [BTS95], [Alt00] are widely accepted in robotic applications and has further been tested in the Bird's eye view system of Ehlgen [EPA08], the model shall be validated for the case of a real passenger car-trailer combination.

In all aspects, the system should be kept as general as possible, so that it can easily be attached to any tractor-trailer combination. Moreover, the system should be easy to use and close to the series maturity phase in the end.

2 Theoretical Background

The thesis combines basically two large fields of study, namely *Vehicle Dynamics* as well as *Computer Vision and Projective Geometry*. Although the two fields have nothing in common, they are required to fulfil the given task. Moreover the strict separation allows an approach, which firstly deals with the accomplishment of both components independently. Only in the end, the results can be combined in order to deliver the conceptual solution.

This section refreshes the basic principles of *Vehicle Dynamics* as well as *Computer Vision and Projective Geometry*. At the same time, the most significant information for the research in this thesis is emphasised.

2.1 Vehicle Dynamics

The dynamics of vehicles are highly complex mathematical problems. According to [MW14], a vehicle, consisting of four wheels and its main body, can be described as a system of 5 objects, connected through springs, dampers and other mechanical constructions. A free body in 3D space has 6 degrees of freedom, namely three translational as well as three rotational. In total, this would lead to 30 degrees of freedom for an individual car, neglecting further movable parts and moreover not to mention attached trailers, which engage the essential part in this thesis. Although the movements of the parts are coupled, individual problems can be regarded separately keeping the deviations of the real system acceptable small. It is not necessary to mention that the problem of vehicle dynamics is therefore divided in multiple separate problems, which give beside the understanding of the specific behaviour a general overview of the characteristics of the vehicle in total.

2.1.1 Classification

A vehicle moving on a surface is exposed to external forces and torques, which are responsible for the reaction of the system. Certainly, these forces and moments can be described in various coordinate frames as depicted in Figure 2.1 [Rei14]. The influences of these forces mainly lead to the different fields of vehicle dynamics.

2.1.2 Lateral Dynamics

The area of vehicle dynamics describing trajectory calculation is mainly found in lateral dynamics. As a fact of separation of vehicle dynamics in sub-areas, some assumptions have to be made, with the aim of decoupling the dynamics from other effects. For lateral dynamics,

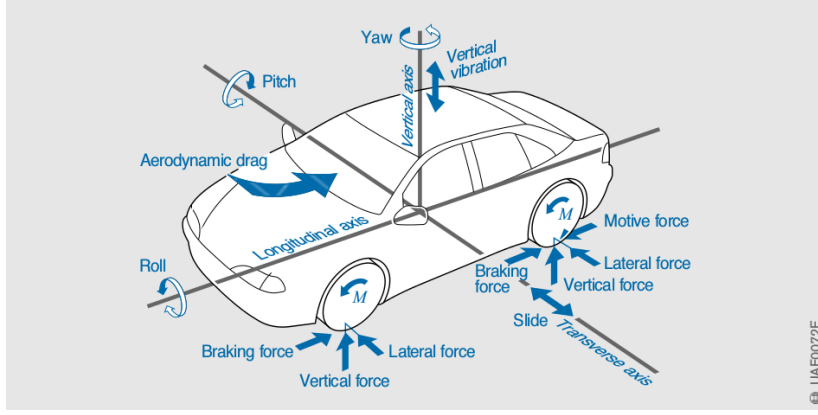


Figure 2.1: Forces, moments and coordinate frames of a vehicle (from Reif [Rei14])

the centre of mass is shifted to the ground, stating the negligence of rolling and pitching of the vehicle [MW14]. Furthermore, the different stress, encountered by the inner and outer tires are assumed to be equivalent. The dynamics can be described as a pure 2D model. However, a parking situation is characterized by low speeds, so that lateral forces may be neglected further[Raj11]. In mathematical equations, this issue can be described by

$$(\mathbf{e}_y^I)^T \cdot \mathbf{v}^I = 0, \quad (2.1)$$

meaning that the lateral velocity at all axes is vanishing. The trajectory prediction then simplifies to a pure kinematic problem, described by geometric relations. An example of vehicle kinematics is the trajectory of a four-wheeled vehicle, influenced only by its steering angle. The resulting trajectory is a circle, described by Ackermann geometry [Raj11], illustrated in Figure 2.2.

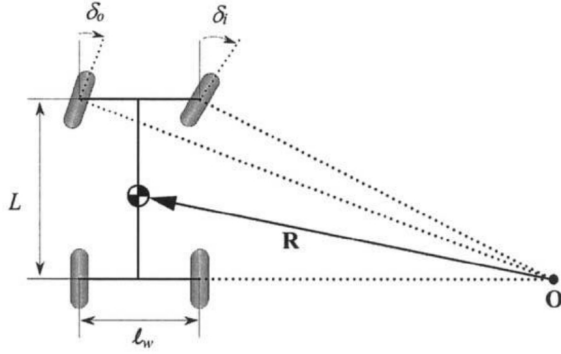


Figure 2.2: Ackermann turning geometry (from Rajamani [Raj11])

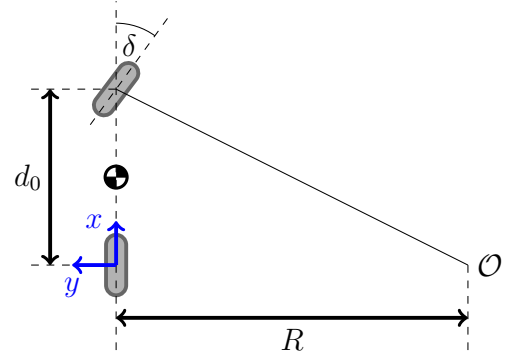


Figure 2.3: Single-track (bicycle) model of a vehicle (after Rajamani [Raj11])

2.1.3 Bicycle Model

Although the inner δ_i and outer δ_o steering angles are not necessarily equivalent, the reduction to a single-track model, called the *Bicycle Model*, may be valid for special cases, e.g. very low speed conditions, as demonstrated in many references (e.g. [Raj11], [MW14]). Especially in parking situations, speeds are limited, so that the mentioned model may deliver fairly

well results [WHW⁺11]. The model approximates outer and inner steering angles by one generalized (front) steering angle δ . Moreover the vehicle is described by a one-dimensional axis through the centre of mass of the system. Figure 2.3 justifies the name of the model by its analogy to a real bicycle. According to the geometry, the radius of the turning circle can be computed with the mean steering angle δ :

$$R = \frac{d_0}{\tan \delta}, \quad (2.2)$$

where d_0 denotes the wheelbase of the vehicle. The turning radius is related to the y -axis of the vehicle's coordinate system, which is placed at the rear axle (Figure 2.3).

2.2 Computer Vision

2.2.1 Projective Camera Model

Camera models describe the way, 3D world points are mapped to the image plane. Hence, a camera model is a mathematical function, taking the coordinates of points in 3D space as input and delivering image coordinates as an output. However, camera models do not belong to the group of classical transformations. The reason for that is the reduction of dimensions: while a classical transformation maps vectors to the same set, a camera model transforms points from three to two coordinates. Moreover, the phenomenon called projection arises in this process, the reason why a camera model contains always a projective transformation. A projective transformation requires a new type of vectors, since the classical tuples fail in the projective approach. That is why homogeneous coordinates are introduced, which add basically one dimension to the classical vectors. A projection from the 3D world to the 2D image is described by a mapping from a 4-tuple to a 3-tuple. Classical coordinates can then be extracted from the homogeneous coordinates [HZ04].

Camera models contain several parts, each describing a different phenomenon. A classical coordinate transformation, containing rotation and translation, is always a part of the camera model. In general, the world coordinate frame and camera coordinate frame are not matching, that is why a coordinate transformation is indispensable. The representation of a world point, expressed in homogeneous coordinates $\mathbf{X}^{\text{World}}$, can be transformed to the camera frame according to [HZ04]

$$\mathbf{X}^{\text{Cam}} = \begin{bmatrix} \mathbf{R} & \mathbf{t} \\ 0 & 1 \end{bmatrix} \mathbf{X}^{\text{World}}, \quad (2.3)$$

with the classical rotation matrix \mathbf{R} and a translation vector $\mathbf{t} = -\mathbf{R}\tilde{\mathbf{C}}$, where $\tilde{\mathbf{C}}$ is the camera origin expressed in the world coordinate frame [HZ04]. The dimension of the matrix in equation (2.3) is 4x4, since it maps homogeneous 4-vectors to homogeneous 4-vectors.

After the coordinate transformation, the actual camera model comes into play. The simplest model, namely the pinhole camera model, directly projects the transformed coordinate to the image plane with a simple projective transformation, as it can be found even in the standard literature of computer vision (e.g. [HZ04]). More complicated approaches take lens distortion into account as well (e.g. [KB06]). However, the lens effects have to be described, before the projection, because the rays are influenced by the optical system. The projection itself is

described by a 3x3 matrix. The matrix looks as follows [HZ04]

$$\mathbf{K} = \begin{bmatrix} \alpha_x & s & c_x \\ 0 & \alpha_y & c_y \\ 0 & 0 & 1 \end{bmatrix}. \quad (2.4)$$

Whereas the rotation and translation are known as the extrinsic camera parameters, all components of the matrix (2.4) are called the intrinsic parameters of the camera. α_x and α_y are the focal length referred to pixel dimensions in the given direction, c_x and c_y the offset of the crossing of the optical axis with respect to the image plane to the centre of the image and s the skew factor, which can be neglected for most real cameras [HZ04]. Denoting homogeneous 3-vectors with small letters and homogeneous 4-vectors with capital letters, the whole projection from a world point, to an image point becomes

$$\mathbf{x}^{\text{Cam}} = \mathbf{K}[\mathbf{R}|\mathbf{t}]\mathbf{X}^{\text{World}} \quad (2.5)$$

2.2.2 Lens Distortion

The classical projective pinhole model is a strong idealization of the reality and would lead to prohibitive errors. However, with modelling of lens distortion effects, the error can be suppressed until a certain limit. During all performed experiments, only cameras with fisheye effects are used. That is why the model, describing this type of camera, shall be emphasized here. The distortion effect arises between the coordinate transformation mapping and the projective mapping in equation (2.5), since the lenses influence the incoming rays. In [KB06], a precise model of a fisheye camera is described. Compared to the pinhole model, the relationship between the angle of the incoming ray θ and the resulting distance of the intersection of the ray with the image plane to the optical axis r is modelled differently:

$$r = f \tan \theta \quad \Rightarrow \quad r = f\theta \quad (2.6)$$

However, it is mentioned in [KB06], that this model will not be enough for many real lenses. That is why a polynomial approach should be suitable for more cases:

$$r(\theta) = k_1\theta + k_2\theta^3 + k_3\theta^5 + k_4\theta^7 + k_5\theta^9 + \dots \quad (2.7)$$

Sometimes, the relation (2.7) is expressed for a change in the angle [Bra00]

$$\theta_d = \tilde{k}_1\theta + \tilde{k}_2\theta^3 + \tilde{k}_3\theta^5 + \tilde{k}_4\theta^7 + \tilde{k}_5\theta^9, \quad (2.8)$$

where θ_d denotes the distorted angle resulted from the fisheye lens. The problem is illustrated in Figure 2.4. A world point with the coordinates (X, Y, Z) (violet, position vector in blue) is projected to the image plane, with the resulting coordinates (u, v) . With respect to the optical axis, the point appears at an angle of θ_d . However, if the camera would be a pinhole camera, the same point would appear at the point denoted with $(u, v)_{\text{undist}}$. Equation (2.8) relates exactly these two angles. The distorted ray (dashed line, marked in red) represents the projection of the point to the image plane, with the camera matrix (2.4). The individual projection parameters would lead to an appearance of the original point at (X', Y', Z) .

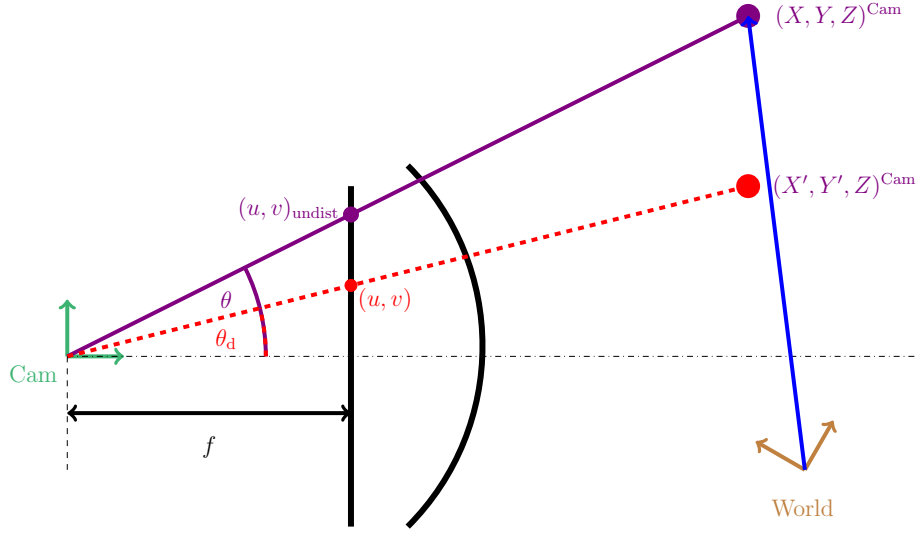


Figure 2.4: Projection of world point to an image plane behind a fisheye lens

2.2.3 Camera Calibration

Camera calibration is required, if metric information of the content of an image shall be determined [Zha00], or if world points shall be projected into an image. During the calibration procedure, all degrees of freedom of the mapping are determined, in order to be able to apply the projection to every world point. Especially the intrinsic parameters as well as the distortion coefficients k_i (equation (2.7)) are of interest. Moreover, the extrinsic parameters, containing rotational and translational information are determined, albeit these are only valid, if the camera has a fixed pose with respect to the world frame. As soon as the camera pose is changing, an extrinsic calibration, determining the extrinsic parameters only, has to be performed again.

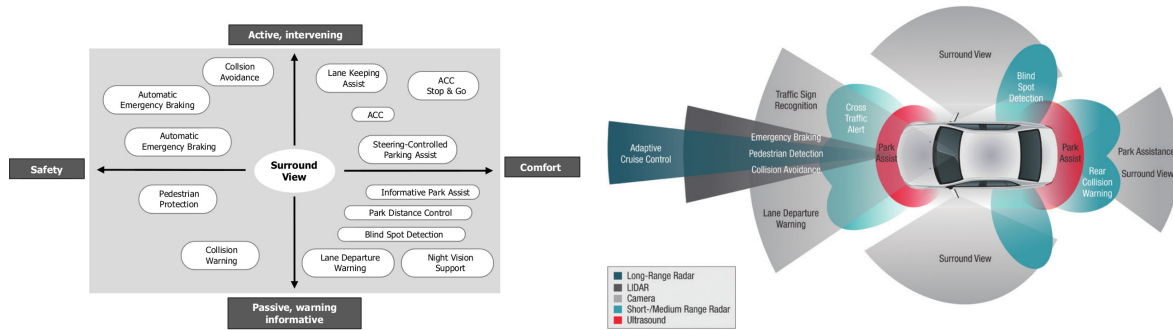
2.3 Driver Assistance Systems

Today, nearly any vehicle system provides support to the driver using electronic devices, called driver assistance systems (in brief: DAS). Different types of sensors observe the environment, surrounding the vehicle (Figure 2.5b) [Tex15]. The data provided by the sensors can be processed and used to increase the driver's safety and convenience. A rear view camera parking assistance system for a tractor-trailer combination is clearly an instance of DAS. An overview of DAS should clarify, in which section the system can be classified.

2.3.1 Classification of Driver Assistance Systems

Nowadays DAS spread in many directions. According to [Hue14] and [RDG10], there exist two main criteria for the classification of DAS. First of all, DAS are distinguished according to its purpose: While many DAS try to increase the safety on the road, there exist systems for reasons of comfort only, which facilitate drivers processes, but do not have any safety reasons. The second criteria describes, how the processed data is used for the support of the driver.

On the one hand, data can be used to trigger the actuators of the system, so that an active reaction is caused by the DAS. On the other hand, data can be used to inform the driver about the current situation of the environment, only. Instances of the latter case are called passive systems. However, a strict separation of the discussed criteria is not possible. Rather a scale, which evaluates the systems according to their classification is used. Figure 2.5a gives a proper overview about the classification of DAS [Hue14]. Clearly, parking assistance systems are classified to the comfort side of the chart. Still, active and passive systems are possible. On top of the classification of DAS, Figure 2.5b gives an overview about the used sensors



(a) Classification of Driver Assistance Systems (taken from [Hue14], original image from [RDG10]) (b) Sensors for Driver Assistance Systems [Tex15]

used in DAS [Tex15]. The focused rear camera for trailers extends available park assistance rear view systems.

2.3.2 Classification of Parking Assistance Systems

In the wide field of DAS, parking assistance systems form a group, which can be further split according to their functions and performances. The handbook of driver assistance systems [WHW⁺11] and [WHL15] classify the systems according to 4 categories, related to their complexity and increasing autonomy. Informing parking systems are quite standard nowadays. Based on ultrasonic or RADAR measurements, the driver is informed by the system about the distance of the vehicle to the closest obstacle, basically in the longitudinal direction. Although there exist many different ways of presenting the distance, acoustical signals supported by a display surround view of the car are most popular [WHW⁺11]. Existing systems, which provide the size of parking slots, belong to informing systems as well. Guided parking systems embody the next step towards autonomous parking. Additional to pure information about distances, the system evaluates the data resulting in instructions to the driver. These could either be steering instructions, in order to reach a certain parking spot or the display of the driving path, according to the current steering angle. Based on the latter statement, the trailer rear view camera parking assistance system is classified to guided parking systems. The so far discussed parking assistance systems are passive. Clearly, autonomous parking requires an active control of the actuator of the vehicular system. Semiautomatic parking systems do the transverse control arm automatically by influencing the steering angle. Nevertheless, the driver can influence the speed of the system by controlling the throttle pedal. Although complete automated parking systems were tested successfully in the past, they are still not available in the market. Reasons of safety might be the most decisive barriers [WHW⁺11].

3 System Identification

Before a model of the system can be derived, an analysis of the system is inevitable. The word *system* refers here to the towing vehicle, called the *tractor*, including all attached *trailers*. *Tractor-trailer system* shall be used equivalently.

Since parking assistant systems based on cameras for tractor-only systems already exist, the discussion shall be reduced to the influence of the attached trailers to the system.

3.1 Types of Trailers

Especially the properties of the attached trailers influence the kinematics and dynamics of the tractor-trailer system. Therefore, existing types of trailers have to be investigated. According to the vehicle standard paper [Bul99] and the everyday experience, the following types of trailers exist:

- Caravans
- Box Trailers
- Tray Bodies
- Vehicle Transport Trailers
- Animal Transport Trailers
- Plant Transport Trailers
- Dog Trailers

Despite the plenty of different types of trailers, only the influencing characteristics of the kinematics are of interest, which reduce to the following properties (neglecting trailer dynamics, which depends furthermore on the mass load):

1. Movable parts
2. Number of axles

Movable parts of a trailer refer to sections, which are steerable with respect to others. In the following, those parts shall be denoted as *trailer segments* (or *segments* in short). Clearly, each segment has its own kinematics and/or dynamics, which brings more complexity to the system. The number of axles is related to their attached section of the trailer. Moreover, the axles are assumed to be fixed with respect to each other. Only segments can rotate against

one another, due to their interconnection through hitches.

According to the mentioned properties and the found examples in the literature [Bul99], a general trailer may look like shown in Figure 3.1.

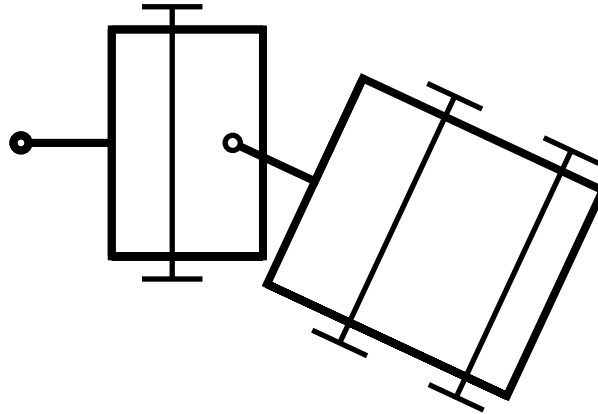


Figure 3.1: Example of a general trailer

The depicted trailer has two movable segments. The first is containing one axle only whereas the second is equipped with a pair of axles. A trailer can therefore have multiple movable parts, each with an arbitrary number of axles.

3.2 Simplification of Trailer Models

Aiming at the simplicity of the model, the derivation should be restricted to kinematics only. Dynamic models require too many parameters, which can not be determined in every situation. As an example, the model should be independent on the mass by reason of possibly changing loads of the same attached trailer. Such a dependency is undesirable, if the system is aimed to be placed in the market. Obviously, some simplifications have to be made, in order to achieve the model based on kinematics only. Still, acceptable deviations have to be met.

Corresponding to the most important properties specifying the kinematics, mentioned in the previous section, the most basic existing trailer one can think of is containing only one axle, which is furthermore not movable. Single-axle trailers can be described with kinematics only, if a certain deviation is tolerated. Theoretically, this axle can turn in place around its centre, without any slip. Lateral slip of the tires is a dynamic effect and should be therefore avoided in the model. Movable parts do not change the situation dramatically. Albeit every movable part brings an additional degree of freedom and therefore more complexity into play, the treatment of each individual part remains the same. That is why movable parts may be treated as a chain of individual trailers. However, with an increasing number of fixed axles the occurrence of lateral slip is unavoidable, since the turning point of the trailer can not be placed coinciding with all axles. A possible way out could be the introduction of a *generalised axle*. This idea has been discussed in the literature already (e.g. in [FW07]), albeit for a truck only. For this scenario, the model showed very good results. If it is assumed, that the distance of the axle of the sub-vehicles with respect to their junctions, which would connect a further trailer is small, the model may be used for trailers, too. With the use of the notation of this

thesis, the stated equation, describing the distance of the joint to the axle is

$$d_{i,\text{eq}} = d_{i,\text{gc}} + \frac{\sum_{k=1}^N (d_{i,\text{gc}} - d_{i,k})^2}{d_{i,\text{gc}}} \cdot \left(1 + \frac{C_{\text{ar}}}{C_{\text{af}}}\right), \quad (3.1)$$

where $d_{i,k}$ denotes the distance of the k -th axle of the i -th trailer segment with respect to the junction between the i -1-st and i -th trailer segment. $d_{i,\text{gc}}$ describes the geometrical mean of the distances

$$d_{i,\text{gc}} = \frac{1}{N} \sum_{k=1}^N d_{i,k}. \quad (3.2)$$

Maybe, even this equation is sufficient for a description of the generalised axle of a trailer segment. Equation (3.1) is still containing dynamic properties, namely the sums of the cornering stiffness C_{ar} and C_{af} of all rear and front tires, respectively. The formula refers to a work by Winkler [WA98], based on the assumption of lateral force balance during a turning manoeuvre of a truck. A presented calculation example assumes the equality of the participating cornering stiffness of all tires, so that the ratio $\frac{C_{\text{ar}}}{C_{\text{af}}}$ reduces to the ratio of the number of rear and front tires $\frac{\#_{\text{rw}}}{\#_{\text{fw}}}$, avoiding the use of dynamic properties at all. Obviously, equation (3.1) simplifies to

$$d_{i,\text{eq}} = d_{i,\text{gc}} + \frac{\sum_{k=1}^N (d_{i,\text{gc}} - d_{i,k})^2}{d_{i,\text{gc}}} \cdot \left(1 + \frac{\#_{\text{rw}}}{\#_{\text{fw}}}\right). \quad (3.3)$$

Depending on the distance of the axles, the forces differ at every axle, resulting in even different polarity. That is why the general axis is rather off the geometric centre (3.3). In any case, the validity of equation (3.3) has to be tested, since the derivation was originally done for a truck, where the steering axis intersects the body axis. This is clearly not the case for trailers.

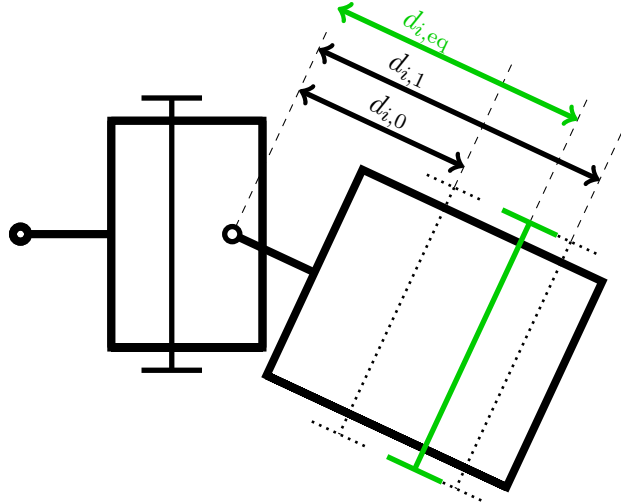


Figure 3.2: Simplified model of a complex trailer: two trailer segments with only one (generalised) axle

A segment whose generalised axle is computed shall be denoted with *virtual trailer*, due to its correspondence with the most basic trailer, containing a single axle only.

With the proposed adaptations, the example of the trailer introduced in Figure 3.1 would change to a chain of two single-axle virtual trailers, depicted in Figure 3.2. Clearly, the original

complex trailer has been reduced to a chain of two segments. For the second segment, a generalised axle had to be introduced (marked in green).

3.3 Virtual Trailer Properties

The previous section introduced the idea of virtual trailers. The identification of the properties, which influence the kinematics of the whole system, is necessary for the derivation of a model. A virtual trailer together with its denoted characteristic dimensions is shown in Figure 3.3. Table 3.1 explains the visualised quantities.

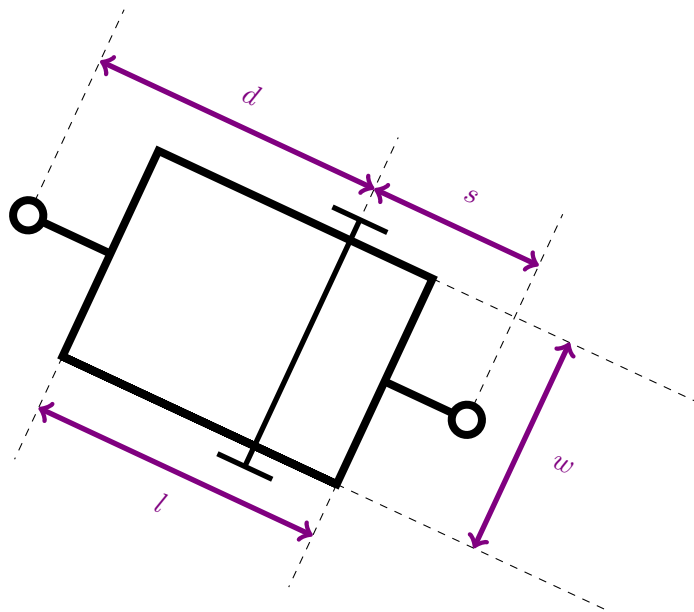


Figure 3.3: Properties of a virtual trailer

Table 3.1: Properties of a virtual trailer

Property	Explanation
l	Length of the trailer, without the front (and, if existing, rear) hitch
w	Width of the trailer
d	Distance from the front junction to the (generalised) axle of the trailer segment
s	Distance to the next junction, measured from the (generalised) axle

The width and the length of the virtual trailer do not influence the kinematics. However, they are necessary for the representation in the customer display. Furthermore, the width is the crucial property, specifying the guidelines of the trailer.

Only the distances of the (generalised) axle to the front and rear junction remain as influencing parameters for the kinematics of the system. This becomes clear, if one has a closer look into the problem: the virtual trailer with only one axle can be interpreted as a lever, with

a movable pivot in the tangential direction of the trailer's wheels. If the front junction is pushed or pulled in one direction, the rear end of the trailer will show a contrary movement, but rotated around the point of turning, located at the intersection with the axle. Also, the front end can be influenced from impacts on the rear side. The kinematics of the simplified lever together with the width of the trailer define the guidelines completely. Contrary to the distances of the axle, width and length of the virtual trailer are directly inherited from the dimensions of the corresponding trailer segment.

Although the imagination of a real lever leads to two arms, one in each direction of the pivot, the rear junction could be situated directly at the pivot (this is the case in quite many real situations, if only one axle is movable) or even in front of it. In these situations, the distance to the next junction is zero or even negative. Still, the kinematic equations would be equivalent.

3.4 From Real Trailers to a Chain of Virtual Trailers

With the introduction of virtual trailers, the system has been encapsulated and simplified. Since the demand of this work is to keep the problem as general as possible, an assumption about the number of attached trailers would counteract the stated goal. All resulting virtual trailers, obtained from their real trailer segment correspondences are then assumed to form a chain of trailers. The kinematics of the total system can then be described with a drawing vehicle with a chain of attached virtual trailers. Beside the trailer's segments, the train of virtual trailers can be extended by any number of actual existing trailers.

4 System Analysis and Modelling

4.1 Derivation of Kinematics Equations

The derivation of the kinematics equations are done in the same fashion as proposed by Rill [Geo11], but extended for multiple attached trailers. In all cases, the bicycle approach was used (section 2.1.3) together with the negligence of lateral slip. Resulting in a state space model, the derivation delivers a good preparation for the following task, namely the construction of the guidelines.

4.1.1 Description of the System

The starting point of the derivation is the result of section 3: a chain of virtual trailers. In addition to the already identified kinematic properties of the trailers, the position of at least one sub-vehicle to an inertial reference frame, as well as the orientation of all sub-vehicles have to be known, in order to be able to predict the guidelines of any sub-vehicle completely. All sub-vehicles, namely the tractor and all virtual trailers in the chain get their own fixed coordinate frame. It is centred in the middle of the axle (rear axle in case of the towing vehicle) of the corresponding sub-vehicle. The x-axis is aligned with the sub-vehicle's roll-axis, whereas the z-axis is coinciding with the inertial z-axis. Finally, the y-axis completes a right-handed system. Within the sub-vehicle frame, its kinematic properties, namely the distances from the axle to the joints, are fixed, even if external rotations occur.

As the absolute position of the total system with respect to the inertial frame, the origin of the tractor was chosen. In contrary to the front axle it has the advantage, that the orientation remains fixed, relative to the roll-axis of the tractor, no matter which steering angle is applied. Instead of the yaw angle with respect to the inertial frame, it was decided to describe the sub-vehicle's orientation with respect to the *previous* frame. *Previous* means, that all sub-vehicles are numbered, starting with 0 at the tractor and increasing along the chain of virtual trailers. Clearly, the orientation angle of the tractor is equal to its yaw angle, since the *previous* frame of the tractor is the inertial frame. With this approach of relative orientation angles, two birds are killed with one stone: The relative angles are equivalent to the kink angles between sub-vehicles, which are easier to identify, compared to the absolute angles. Furthermore, the absolute orientation of a sub-vehicle with respect to the inertial frame can still be calculated, with the help of the sum of all relative angles along the chain of virtual trailers. Figure 4.1 shows a sketch of a system containing two trailers. All kinematic properties as well as the kink angles κ_i are shown. The relative frames of the sub-vehicles are coloured in magenta. Moreover, the position vector of all sub-vehicles are added and marked in blue, albeit the position vector of the tractor is used in the system's state only. All shown properties are

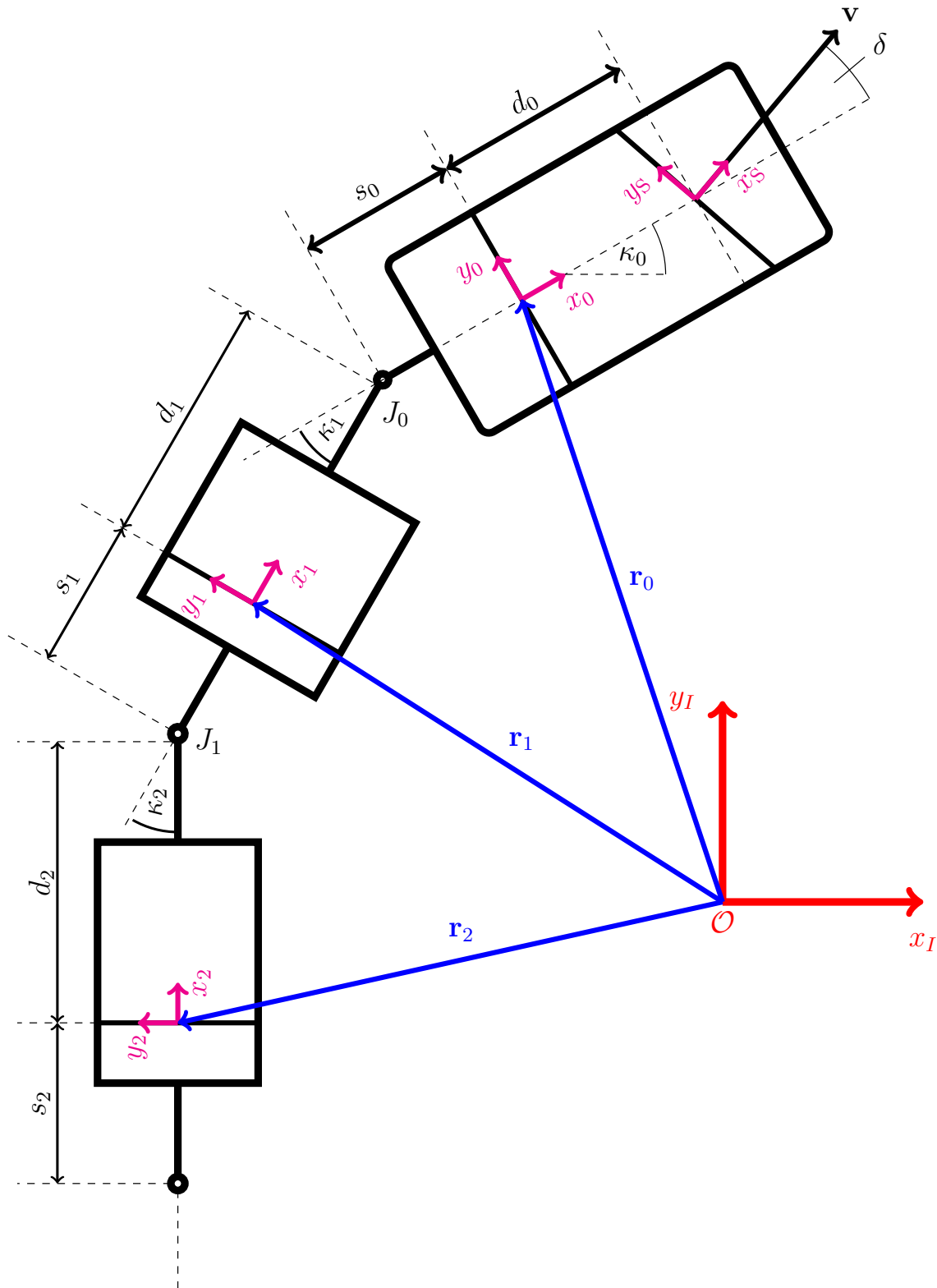


Figure 4.1: Definition of the properties of the tractor-trailer system model

described in Table 4.1. Before the derivation can be done, some notes have to be made. During the derivation, vectors have to be expressed in different coordinate frames. Therefore,

Table 4.1: Properties of the tractor-trailer system

Property	Description
\mathbf{r}_i	Position vector of the i-th sub-vehicle with respect to the inertial frame
(x_I, y_I)	Inertial frame
\mathcal{O}	Origin of the inertial frame
(x_i, y_i)	Relative frame of i-th sub-vehicle
d_i	distance joint to axle (or wheelbase in the case of the tractor)
s_i	distance axle next joint
κ_i	relative angle towards the previous frame (kink angle)
δ	Steering Angle
J_i	Joint between (i-1)-st and i-th sub-vehicle

a strict labelling has to be met. In principal, the number of the coordinate frame, in which the vector is expressed, is shown as an upper note. The lower notes have two components, separated by a hyphen. In the case of a position vector (\mathbf{r}), the first part is the origin of the position vector, whereas the second part denotes the end point. If such a point is just labelled as a letter (e.g. i), then the origin of the i th frame is meant. If the lower notes describe a velocity vector (\mathbf{v}) or an angular velocity vector ($\boldsymbol{\omega}$), then the first part symbolises the origin of the coordinate frame, the velocity vector refers to. On the other hand, the second part denotes the point in space, whose velocity is of interest. Again, a single identifier would refer to an origin of the corresponding reference frame, with respect to the inertial frame.

In order to avoid confusion, some examples shall be given:

1. $\mathbf{r}_{J_1-2}^2$
2. $\mathbf{v}_{\mathcal{O}-1}^1 = \mathbf{v}_1^1$
3. $\boldsymbol{\omega}_{1-2}^2$

The position vector (1.) is presented with respect to the second frame. In detail, it describes the vector from the point J_1 in space to the origin of the second frame. Furthermore, the velocity vector (2.) is represented in the first frame and describes the velocity of the origin of the first coordinate frame towards the origin of the inertial frame. Finally, the angular velocity vector (3.) denotes the angular speed between the first and the second frame, represented in the second frame.

If the purpose of vectors is clear (e.g. unit vectors $\mathbf{e}_x, \mathbf{e}_y, \mathbf{e}_z$ of the corresponding frame), then only the representing frame is given as a note. An appropriate labelling of rotation matrices is remaining. Here, the lower note represents the number of the source frame, whereas the upper note denotes the destination frame. As an example,

$$\mathbf{R}_1^2$$

transforms the representation of a vector from the first to the second frame.

4.1.2 State Vector of the System

The individual tractor normally has 6 degrees of freedom, namely three in translation as well as three in rotation. Since the system is restricted to the x-y-plane (theoretically, any other

plane could have been chosen, but the x-y-plane reaches most simplicity), three degrees of freedom vanish: the tractor can not move in the z-direction and moreover not turn around roll- and pitch-axes. The remaining three quantities can describe the tractor completely. The position vector \mathbf{r}_0 with the components x_0 and y_0 and the yaw angle κ_0 fulfil this demand. Clearly, another option could have been chosen.

Every attached trailer adds only one degree of freedom to the system. As well as the tractor, the trailer can not roll, pitch and move along the z-axis. Moreover, x_i and y_i position are restricted, because the hitch is directly connected to the previous sub-vehicle (holonomic constraint). That is why x_i and y_i are fully defined by an orientation angle of the trailer, what can be the kink angle, for example.

Cutting the story short, the state vector, which shall describe the tractor-trailer system, consisting of a tractor and n trailers, was chosen to be

$$\begin{pmatrix} x_0 \\ y_0 \\ \kappa_0 \\ \kappa_1 \\ \vdots \\ \kappa_n \end{pmatrix} \quad (4.1)$$

The goal of the development of a system model is to find a state space description, which delivers a system of first order differential equations:

$$\dot{\mathbf{x}} = \mathbf{f}(\mathbf{x}, \mathbf{u}), \quad (4.2)$$

where \mathbf{x} denotes the state of the system and \mathbf{u} the input vector to the system. After an integration, the state is known for several points in time. The extraction of the guidelines is then a pure geometric task.

4.1.3 Tractor Vehicle Kinematics

The kinematics of the tractor vehicle deals with the development of the sub state

$$\begin{pmatrix} x_0 \\ y_0 \\ \kappa_0 \end{pmatrix} \quad (4.3)$$

Clearly, the input vector \mathbf{u} of the system consists of a speed v and the steering angle δ . It was decided to use the tangential speed component at the rear axle of the tractor, consistent with the placement of the tractor vehicle frame. Instead of v , the speed shall be denoted with v_R , to emphasize the speed of the rear axle. Hence the input vector to the system is

$$\mathbf{u} = \begin{pmatrix} v_R \\ \delta \end{pmatrix} \quad (4.4)$$

However, the components of the position of the tractor are not directly dependent on the steering angle. If the rear speed is known, the time increment is found quite easy [Geo11]:

$$\begin{aligned} \dot{x}_0 &= v_R \cdot \cos \kappa_0 \\ \dot{y}_0 &= v_R \cdot \sin \kappa_0 \end{aligned}$$

Certainly, the components are indirectly dependent on the steering angle, if the front axle is driving the system. Then, the rear speed is influenced by the yaw rate, which itself is dependent on the steering angle. The reason for this coupling is the rule for the transformation of velocities between relatively rotating frames. A closer look into the transformation between speed at front and rear axle helps to understand the problem.

Contrary to the previous statement, the derivation starts with the rear speed v_R of the tractor, instead of using the speed of the front axle. The goal is to find the velocity at the front axle. Therefore, a coordinate frame in the centre of the front axle, rotated by the steering angle with respect to the tractor axis, is introduced (see Figure 4.1 - frame with label S). According to the velocity transformation rule, the front axle velocity in the steered frame is

$$\begin{aligned}
 \mathbf{v}_{O-S}^S &= \mathbf{R}_0^S \cdot \mathbf{v}_{O-0}^0 + \boldsymbol{\omega}_{O-S}^S \times \mathbf{R}_0^S \cdot \mathbf{r}_{0-S}^0 \\
 &= \mathbf{R}_0^S \cdot \begin{pmatrix} v_R \\ 0 \\ 0 \end{pmatrix} + \begin{pmatrix} 0 \\ 0 \\ \dot{\kappa}_0 \end{pmatrix} \times \mathbf{R}_0^S \cdot \begin{pmatrix} d_0 \\ 0 \\ 0 \end{pmatrix} \\
 &= \begin{pmatrix} v_R \cdot \cos(\delta) \\ -v_R \cdot \sin(\delta) \\ 0 \end{pmatrix} + \begin{pmatrix} 0 \\ 0 \\ \dot{\kappa}_0 \end{pmatrix} \times \begin{pmatrix} d_0 \cdot \cos(\delta) \\ -d_0 \cdot \sin(\delta) \\ 0 \end{pmatrix} \\
 &= \begin{pmatrix} v_R \cdot \cos(\delta) \\ -v_R \cdot \sin(\delta) \\ 0 \end{pmatrix} + \begin{pmatrix} \dot{\kappa}_0 \cdot d_0 \cdot \sin(\delta) \\ \dot{\kappa}_0 \cdot d_0 \cdot \cos(\delta) \\ 0 \end{pmatrix}
 \end{aligned}$$

Keeping in mind, that the goal was to find the yaw rate of the tractor vehicle, the y-component of above's equation in addition to the no-lateral-slip assumption can be used, to calculate the angular speed [Geo11]:

$$\begin{aligned}
 \mathbf{v}_{O-S,y}^S &\stackrel{!}{=} 0 = -v_R \cdot \sin(\delta) + \dot{\kappa}_0 \cdot d_0 \cos(\delta) \\
 \dot{\kappa}_0 &= \frac{v_R}{d_0} \tan(\delta)
 \end{aligned}$$

The equation for $\dot{\kappa}_0$ completes the state equations for the sub-state:

$$\begin{pmatrix} \dot{x}_0 \\ \dot{y}_0 \\ \dot{\kappa}_0 \end{pmatrix} = \begin{pmatrix} v_R \cdot \cos \kappa_0 \\ v_R \cdot \sin \kappa_0 \\ \frac{v_R}{d_0} \tan(\delta) \end{pmatrix} \quad (4.5)$$

4.1.4 Kink Angle Kinematics

The purpose of labelling the orientation angles in the given order instead of introducing new variable names for e.g. yaw angle of the tractor and kink angle of the trailers is to achieve a generalized formula for any number of trailers in the system. Especially the dynamics of the system is of interest: Out of the system parameters, the kink angle rate has to be found. Together with the system properties, the path of the tractor-trailer system can be reconstructed from the kink angles as functions of time. The following derivation shows step-by-step, how the formula of the kink angle rate can be found in a system of any number of trailers.

Equivalent to the derivation of the tractor's equations, the key approach is based on the assumption of no lateral slip at every axle [Geo11]. In equations, the assumption can be expressed with

$$(\mathbf{e}_y^T)^i \cdot \mathbf{v}_{\mathcal{O}-i}^i = 0$$

Care has to be taken, with the transformation of velocities between different frames. A general well-known formula is

$$\mathbf{v}_{\mathcal{O}-P}^i = \mathbf{v}_{\mathcal{O}-i}^i + \boldsymbol{\omega}_{\mathcal{O}-i}^i \times \mathbf{r}_{i-P}^i,$$

which can compute the absolute velocity of the point P with respect to the inertial frame, but expressed in the i-th frame. \mathbf{r}_{i-P}^i has to be fixed with respect to the origin of the i-th coordinate frame. The general formula can be applied to the (n-1)-st junction, represented in the frame of the n-th trailer.

$$\mathbf{v}_{\mathcal{O}-n}^n = \mathbf{v}_{\mathcal{O}-J_{n-1}}^n + \boldsymbol{\omega}_{\mathcal{O}-n}^n \times \mathbf{r}_{J_{n-1}-n}^n$$

However, the goal should be to get the velocity at the n-th trailer from the velocity of the (n-1)-st trailer. Luckily, the distance of the junction J_{n-1} is fixed with respect to the origins both frames, so that

$$\mathbf{v}_{\mathcal{O}-J_{n-1}}^n = \mathbf{v}_{\mathcal{O}-(n-1)}^n + \boldsymbol{\omega}_{\mathcal{O}-(n-1)}^n \times \mathbf{r}_{(n-1)-J_{n-1}}^n$$

is valid, too. Putting both results together, the n-th velocity can be calculated from the (n-1)-st velocity with the helping hand of the system parameters:

$$\mathbf{v}_{\mathcal{O}-n}^n = \mathbf{v}_{\mathcal{O}-(n-1)}^n + \boldsymbol{\omega}_{\mathcal{O}-(n-1)}^n \times \mathbf{r}_{(n-1)-J_{n-1}}^n + \boldsymbol{\omega}_{\mathcal{O}-n}^n \times \mathbf{r}_{J_{n-1}-n}^n$$

The tractor-trailer system is moving in the 2D x-y-plane. Hence, the angular rates only have a z-component. Moreover they are equivalent in every frame, therefore

$$= \mathbf{v}_{\mathcal{O}-(n-1)}^n + \begin{pmatrix} 0 \\ 0 \\ \dot{\kappa}_{\mathcal{O}-(n-1)} \end{pmatrix} \times \mathbf{r}_{(n-1)-J_{n-1}}^n + \begin{pmatrix} 0 \\ 0 \\ \dot{\kappa}_{\mathcal{O}-n} \end{pmatrix} \times \mathbf{r}_{J_{n-1}-n}^n$$

$\mathbf{r}_{J_{n-1}-n}^n$ is fix in the n-th frame and should be therefore described with respect to \mathcal{O}_n . The opposite holds for $\mathbf{r}_{(n-1)-J_{n-1}}^n$. This distance vector should be represented with respect to \mathcal{O}_{n-1} . Thus, this vector has to be transformed with the according rotation matrix.

$$= \mathbf{v}_{\mathcal{O}-(n-1)}^n + \begin{pmatrix} 0 \\ 0 \\ \dot{\kappa}_{\mathcal{O}-(n-1)} \end{pmatrix} \times \mathbf{R}_{n-1}^n \mathbf{r}_{(n-1)-J_{n-1}}^{n-1} + \begin{pmatrix} 0 \\ 0 \\ \dot{\kappa}_{\mathcal{O}-n} \end{pmatrix} \times \mathbf{r}_{J_{n-1}-n}^n$$

In the appropriate coordinate frame, the distance vectors have simple representations, according to Figure 4.1

$$= \mathbf{v}_{\mathcal{O}-(n-1)}^n + \begin{pmatrix} 0 \\ 0 \\ \dot{\kappa}_{\mathcal{O}-(n-1)} \end{pmatrix} \times \mathbf{R}_{n-1}^n \begin{pmatrix} -s_{n-1} \\ 0 \\ 0 \end{pmatrix} + \begin{pmatrix} 0 \\ 0 \\ \dot{\kappa}_{\mathcal{O}-n} \end{pmatrix} \times \begin{pmatrix} -d_n \\ 0 \\ 0 \end{pmatrix}$$

Since the angular rates only have z-components and furthermore have the same representation in each frame, they can be simply added. According to the definition of the kink angles, the following is true:

$$= \mathbf{v}_{\mathcal{O}-(n-1)}^n + \begin{pmatrix} 0 \\ 0 \\ \sum_{i=0}^{n-1} \dot{\kappa}_i \end{pmatrix} \times \mathbf{R}_{n-1}^n \begin{pmatrix} -s_{n-1} \\ 0 \\ 0 \end{pmatrix} + \\ + \begin{pmatrix} 0 \\ 0 \\ \sum_{i=0}^n \dot{\kappa}_i \end{pmatrix} \times \begin{pmatrix} -d_n \\ 0 \\ 0 \end{pmatrix}$$

Moreover, the velocity of the (n-1)-st origin is known already, but in the (n-1)-st frame. That is why a transformation becomes necessary as well.

$$= \mathbf{R}_{n-1}^n \mathbf{v}_{\mathcal{O}-(n-1)}^{n-1} + \begin{pmatrix} 0 \\ 0 \\ \sum_{i=0}^{n-1} \dot{\kappa}_i \end{pmatrix} \times \mathbf{R}_{n-1}^n \begin{pmatrix} -s_{n-1} \\ 0 \\ 0 \end{pmatrix} + \\ + \begin{pmatrix} 0 \\ 0 \\ \sum_{i=0}^n \dot{\kappa}_i \end{pmatrix} \times \begin{pmatrix} -d_n \\ 0 \\ 0 \end{pmatrix}$$

Performing the transformations and the cross products and assuming, that $\mathbf{v}_{\mathcal{O}-n-1}^{n-1}$ has an x-component only (no lateral slip), the result becomes

$$= \begin{pmatrix} v_{\mathcal{O}-(n-1)} \cos \kappa_n \\ -v_{\mathcal{O}-(n-1)} \sin \kappa_n \\ 0 \end{pmatrix} + \begin{pmatrix} -\sum_{i=0}^{n-1} \dot{\kappa}_i s_{n-1} \sin \kappa_n \\ -\sum_{i=0}^{n-1} \dot{\kappa}_i s_{n-1} \cos \kappa_n \\ 0 \end{pmatrix} + \begin{pmatrix} 0 \\ -\sum_{i=0}^n \dot{\kappa}_i d_n \\ 0 \end{pmatrix}.$$

According to the no-lateral-slip assumption, the velocity of the n-th origin should only have an x-component, too, labelled as the n-th speed.

$$\stackrel{!}{=} \begin{pmatrix} v_{\mathcal{O}-n} \\ 0 \\ 0 \end{pmatrix}$$

The above derivation yields two equations. While the x-component gives the formula for the n-th speed out of the (n-1)-st speed

$$\boxed{v_{\mathcal{O}-n} = v_{\mathcal{O}-(n-1)} \cos \kappa_n - \sum_{i=0}^{n-1} \dot{\kappa}_i s_{n-1} \sin \kappa_n,} \quad (4.6)$$

the y-component can be used for the calculation of the desired rate of change of the n-th kink angle:

$$v_{\mathcal{O}-(n-1)} \sin \kappa_n = - \sum_{i=0}^{n-1} \dot{\kappa}_i s_{n-1} \cos \kappa_n - \sum_{i=0}^n \dot{\kappa}_i d_n \\ = - \sum_{i=0}^{n-1} \dot{\kappa}_i (s_{n-1} \cos \kappa_n + d_n) - \dot{\kappa}_n d_n$$

$$\dot{\kappa}_n = -\frac{1}{d_n} \left\{ v_{\mathcal{O}-(n-1)} \sin \kappa_n + \sum_{i=0}^{n-1} \dot{\kappa}_i (s_{n-1} \cos \kappa_n + d_n) \right\} \quad (4.7)$$

Equations (4.6) and (4.7) are easy to implement in an iterative way.

4.1.5 Entire State Space Model

Finally the system can be described with the following state space model:

$$\begin{pmatrix} \dot{x}_0 \\ \dot{y}_0 \\ \dot{\kappa}_0 \\ \dot{\kappa}_1 \\ \vdots \\ \dot{\kappa}_n \end{pmatrix} = \begin{pmatrix} v_R \cdot \cos \kappa_0 \\ v_R \cdot \sin \kappa_0 \\ \frac{v_R}{d_0} \cdot \tan \delta \\ -\frac{v_R}{d_0} \left\{ \left(\frac{s_0}{d_1} \cos \kappa_1 + 1 \right) \tan \delta + \frac{d_0}{d_1} \sin \kappa_1 \right\} \\ \vdots \\ -\frac{1}{d_n} \left\{ v_{\mathcal{O}-(n-1)} \sin \kappa_n + \sum_{i=0}^{n-1} \dot{\kappa}_i (s_{n-1} \cos \kappa_n + d_n) \right\} \end{pmatrix} \quad (4.8)$$

The fourth equation of the model is equivalent to the result in [Geo11]. For the representation of the trajectory, the time information is not necessarily required. Thus, the integration of the system should be stopped after a given distance, rather than after a given time. Moreover, the trajectory should be displayed, even if the vehicle system is not moving. A virtual speed has to be assumed in this case. The question arises, whether the integration of the system can be done over the driven distance, instead of time.

The incremental position changes can be expressed (with the use of (4.8)) as follows

$$\begin{aligned} dx_0 &= v_R \cdot \cos \kappa_0 \, dt \\ dy_0 &= v_R \cdot \sin \kappa_0 \, dt, \end{aligned}$$

resulting in the infinitesimal travelled distance of the tractor vehicle's rear axle:

$$ds = \sqrt{(dx_0)^2 + (dy_0)^2} = \sqrt{(v_R \cdot \cos \kappa_0 \, dt)^2 + (v_R \cdot \sin \kappa_0 \, dt)^2} = \sqrt{v_R^2 \, dt^2} = \text{sign}(v_R) \cdot v_R \, dt$$

Using this outcome, dt in the system equation (4.8) can be replaced by ds :

$$\frac{d}{ds} \begin{pmatrix} x_0 \\ y_0 \\ \kappa_0 \\ \kappa_1 \\ \vdots \\ \kappa_n \end{pmatrix} = \begin{pmatrix} \text{sign}(v_R) \cdot \cos \kappa_0 \\ \text{sign}(v_R) \cdot \sin \kappa_0 \\ \text{sign}(v_R) \cdot \frac{1}{d_0} \cdot \tan \delta \\ -\frac{\text{sign}(v_R)}{d_0} \left\{ \left(\frac{s_0}{d_1} \cos \kappa_1 + 1 \right) \tan \delta + \frac{d_0}{d_1} \sin \kappa_1 \right\} \\ \vdots \\ -\frac{1}{d_n} \left\{ \tilde{v}_{\mathcal{O}-(n-1)} \sin \kappa_n + \sum_{i=0}^{n-1} \dot{\kappa}_i (s_{n-1} \cos \kappa_n + d_n) \right\} \end{pmatrix} \quad (4.9)$$

Here, $\tilde{v}_{\mathcal{O}-(n-1)}$ is not a speed any more. Moreover, it is obtained by equation (4.6), but with $v_{\mathcal{O}-0} = \text{sign}(v_R)$ as initial condition. The system equation is now independent on the speed. This gives rise to the idea, that the speed does not have to be read from the CAN bus, so that the input vector \mathbf{u} to the system becomes

$$\mathbf{u} = (\delta), \quad (4.10)$$

consisting of the steering angle only.

4.1.6 Comparison with Existing Models in the Literature

A model describing a tractor vehicle with a single attached single-axle trailer was found in [Ada14]. Moreover, the author used the bicycle approach as well. A sketch of the system can be seen in Figure 4.2. All denoted properties are explained in Table 4.2. Furthermore, the equivalent properties of the new model are emphasized. A first analysis of the system in

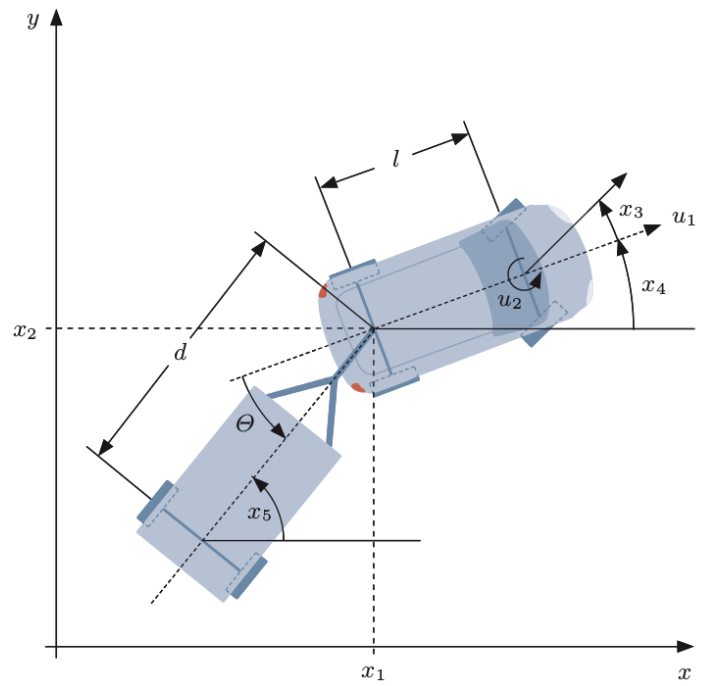


Figure 4.2: System of tractor and trailer (from [Ada14])

Table 4.2: Comparison of properties between both models - first model from [Ada14]

Property	Description	Equivalent property
x_1	x-position of the tractor	x_0
x_2	y-position of the tractor	y_0
x_3	steering angle of the tractor	-
x_4	yaw angle of the tractor	κ_0
x_5	yaw angle of the trailer	-
u_1	speed of the tractor	-
u_2	steering rate	-
l	wheelbase	d_0
d	distance joint to axle of trailer	d_1
θ	kink angle	κ_1

Figure 4.2 leads to the conclusion, that the junction between tractor and trailer coincides with the origin of the tractor frame. This is a pure simplification, taken by the author. Still, the system consists of only two sub-vehicles. In comparison to the model, presented in [Ada14],

the new model seems more general. That is why a reduction of the new model is the first step to be able to compare the systems:

$$\begin{pmatrix} \dot{x}_0 \\ \dot{y}_0 \\ \dot{\kappa}_0 \\ \dot{\kappa}_1 \end{pmatrix} = \begin{pmatrix} v_R \cdot \cos \kappa_0 \\ v_R \cdot \sin \kappa_0 \\ \frac{v_R}{d_0} \cdot \tan \delta \\ -\frac{v_R}{d_0} \left\{ \left(\frac{s_0}{d_1} \cos \kappa_1 + 1 \right) \tan \delta + \frac{d_0}{d_1} \sin \kappa_1 \right\} \end{pmatrix}$$

If the system properties from Table 4.2 are inserted in above's sub-model, the new model is adapted to

$$\begin{pmatrix} \dot{x}_1 \\ \dot{x}_2 \\ \dot{x}_4 \\ \dot{\theta} \end{pmatrix} = \begin{pmatrix} v_R \cdot \cos x_4 \\ v_R \cdot \sin x_4 \\ \frac{v_R}{l} \cdot \tan x_3 \\ -\frac{v_R}{l} \cdot \tan x_3 - \frac{v_R}{d} \sin \theta \end{pmatrix} \quad (4.11)$$

The system, described in [Ada14], has the following representation:

$$\begin{pmatrix} \dot{x}_1 \\ \dot{x}_2 \\ \dot{x}_3 \\ \dot{x}_4 \\ \dot{x}_5 \end{pmatrix} = \begin{pmatrix} u_1 \cdot \cos(x_3) \cos(x_4) \\ u_1 \cdot \cos(x_3) \sin(x_4) \\ 0 \\ u_1 \cdot \frac{1}{l} \sin(x_3) \\ u_1 \cdot \frac{1}{d} \cos(x_3) \sin(x_4 - x_5) \end{pmatrix} + \begin{pmatrix} 0 \\ 0 \\ u_2 \\ 0 \\ 0 \end{pmatrix} \quad (4.12)$$

Clearly, the third component describes the steering angle progress, which is not modelled by the new system. For the parking assistance system, which should be developed, it is, however, not necessary. That is why the third component of (4.12) is neglected from now on. As a conclusion, both models now have four dimensions. However, the most tricky remaining problem is, that the model from [Ada14] uses the speed at the front axle in the direction of steering whereas the new model uses the tangential speed at the rear axle. Hence, a transformation has to be done. In section 4.1.3, this transformation was derived already, where the x-component of the final equation is the required transformation of the speeds:

$$v_S = v_R \cdot \cos(\delta) + \dot{\kappa}_0 \cdot d_0 \sin(\delta)$$

v_S denotes the same speed as u_1 in the model of [Ada14]. If $\dot{\kappa}_0$ is replaced by its expression in the new model (4.8), the above equation transforms to

$$v_S = v_R \cdot \cos(\delta) + \frac{v_R}{d_0} \cdot \tan(\delta) \cdot d_0 \sin(\delta) = \frac{v_R}{\cos(\delta)},$$

what is a simple transformation formula between both speeds (note: the formula is only valid, if the no-lateral-slip assumption is valid). Now, the result can be inserted into the adapted model (4.11).

$$\begin{pmatrix} \dot{x}_1 \\ \dot{x}_2 \\ \dot{x}_4 \\ \dot{\theta} \end{pmatrix} = \begin{pmatrix} u_1 \cdot \cos x_3 \cdot \cos x_4 \\ u_1 \cdot \cos x_3 \cdot \sin x_4 \\ \frac{u_1 \cdot \cos x_3}{l} \cdot \tan x_3 \\ -\frac{u_1 \cdot \cos x_3}{l} \cdot \tan x_3 - \frac{u_1 \cdot \cos x_3}{d} \sin \theta \end{pmatrix} = \begin{pmatrix} u_1 \cdot \cos x_3 \cdot \cos x_4 \\ u_1 \cdot \cos x_3 \cdot \sin x_4 \\ \frac{u_1}{l} \cdot \sin x_3 \\ -\frac{u_1 \cdot \sin x_3}{l} - \frac{u_1 \cdot \cos x_3}{d} \sin \theta \end{pmatrix} \quad (4.13)$$

Clearly, the first three rows are now equivalent. Only the kinematics of the trailer remains. Figure 4.2 gives rise to the fact, that the kink angle can be expressed as the difference of yaw

angles of trailer and tractor:

$$\theta = x_5 - x_4$$

If this is inserted in (4.13), the last row changes to

$$\dot{x}_5 - \dot{x}_4 = -\frac{u_1 \cdot \sin x_3}{l} - \frac{u_1 \cdot \cos x_3}{d} \sin(x_5 - x_4).$$

The state space equation for x_5 becomes

$$\dot{x}_5 = -\frac{u_1 \cdot \sin x_3}{l} - \frac{u_1 \cdot \cos x_3}{d} \sin(x_5 - x_4) + \underbrace{\dot{x}_4}_{=\frac{u_1}{l} \sin x_3} = \frac{u_1 \cdot \cos x_3}{d} \sin(x_4 - x_5)$$

Clearly, the model of [Ada14] is embedded in the new model, which shall emphasize the correctness of the derivation of the state space equations (4.8).

4.2 Steering Model

The only input to the derived model (4.9) of the previous section is the steering angle of the tractor, which describes the angle between the tires of the tractor with respect to the body axis. However, the steering angle can not be measured directly and is therefore not available on the CAN bus. Rather than the steering angle, the angle of the steering wheel is available. The goal is to find a relation between the steering wheel angle and the steering angle, in order to get the input to the system correctly.

Nowadays steering systems are characterized by their high complexity. Especially the comparison to a bicycle reveals the problem: the steering angle of the tires is not the same as the steering wheel rotation angle, but are rather related by a function involving system and environmental properties. Although the relation of steering wheel angle to steering angle of the steering system can be known in theory, the workload of a precise model is too high for the development of a rear view parking assistance system. Moreover, the function is dependent on the road properties, which can further vary by reason of weather conditions, to mention only one. Those properties can not and are not wanted to be considered in the desired system. That is why a function with fit-parameters should do the job. For the test vehicle, a series of measurements was performed, delivering several steering wheel to axle angle correspondences. The axle angles have been estimated from the radius of the driven circle, according to equation (2.2)., The results are shown in Figure 4.3. Compared to [Gil92], where a steering ratio between both angles was introduced, it was decided to use a cubic function, in order to achieve a precise relation even at high steering wheel angles. This phenomena is coinciding with the described decrease of the steering ratio with increasing steering wheel angles for servo steering systems in [MW14].

The result of the fit parameters of the function

$$\delta = k_0 \varepsilon^3 + k_1 \varepsilon^2 + k_2 \varepsilon + k_3 \quad (4.14)$$

are

$$\begin{aligned} k_0 &= 9.18e-09 (\text{°})^{-2} \\ k_1 &= 1.43e-06 (\text{°})^{-1} \\ k_2 &= 6.66368277e-02 \end{aligned}$$

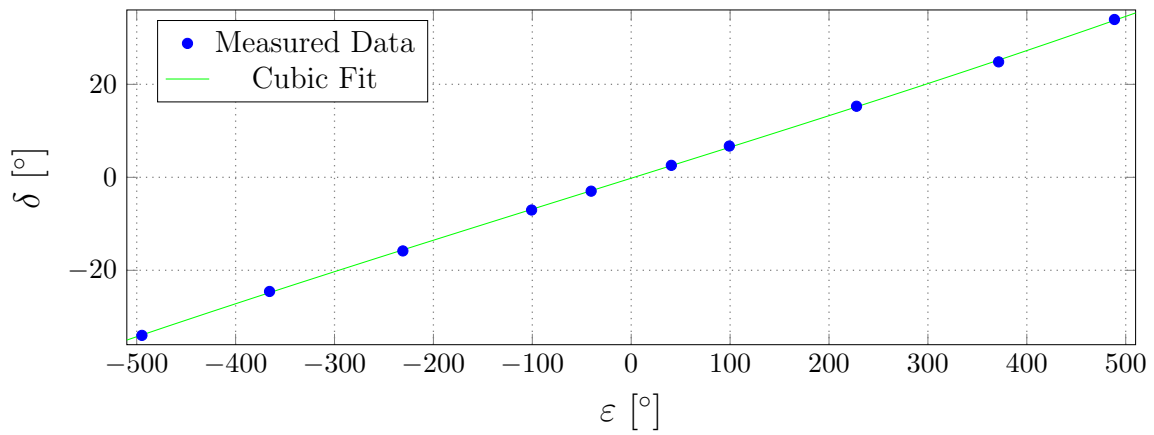


Figure 4.3: Cubic fit - steering model

$$k_3 = -1.94262055e - 01^\circ.$$

Clearly, the linear term dominates, as proposed in [Gil92], albeit the cubic term has the second most influence.

5 Calculation of Guidelines

Although the state space model (4.9) of the tractor-trailer system is fully derived, it has to be clarified, how the guidelines can be extracted from a state (4.1). Clearly, an integration of the model is required, in order to obtain a state trajectory, representing the progress of the state (4.1) along the driven path s . The result is

$$\begin{pmatrix} x_0 \\ y_0 \\ \kappa_0 \\ \kappa_1 \\ \vdots \\ \kappa_n \end{pmatrix} (s) \quad (5.1)$$

in a continuous case or

$$\begin{pmatrix} x_0 \\ y_0 \\ \kappa_0 \\ \kappa_1 \\ \vdots \\ \kappa_n \end{pmatrix}_k \quad (5.2)$$

in the discrete case. Each state in the trajectory (5.1) or (5.2) corresponds to a pair of points in the guideline, so that for the whole guideline, the total predicted trajectory (5.1) or (5.2) is required.

This section deals firstly with the integration of the model (4.9), the subsequent extraction and finally with the projection of the guidelines into the camera image.

5.1 Integration of the State Space Model

An integration of a state space model can be done either in an analytical or a numerical way. As long as the equations are friendly, an analytical integration should be preferred by virtue of two reasons: beside the fact, that integration errors can be avoided, the result is moreover a continuous function, which can be evaluated for every value the independent parameter (the integration variable) can take. Problems for the model (4.9) arise due to the structure of the equations for the kink angles. The equation for the first kink angle rate depends on trigonometric functions of itself already. In general, the differential equation has the form

$$\dot{x} = c_0 + c_1 \cdot \sin(x) + c_2 \cdot \cos(x).$$

Although an integration for this type of differential equation can be found, it's structure is quite unhandy. Moreover, the complexity of the kink-angle-equations for a train of trailers increases with the number of attached trailers. Equation (4.7) gave rise for the use of a numerical solver already, due to it's convenience of implementation, by reason of it's implicit form. Although the first three components of the state (position and orientation of the towing vehicle) can be solved with an analytical function, the kink angle equation claims therefore for a numerical handling. For the sake of equal treatment of all differential equations, it was decided to integrate every state equation in a numerical way.

Dedicated numerical solvers are the *Runge-Kutta-Methods*. They exist in different orders. It was decided to use a *Runge-Kutta solver* of order four with a constant step size by virtue of two reasons:

1. One of the most popular numerical solvers is the Runge-Kutta-Fehlberg method (RKF45) [Sta11], with automatic step size control. Its schemes are of order four and five, so that the step size can be adapted according to the difference of their estimations. [Sta11]. Before 1970, the classical Runge-Kutta method of order four was the most popular one [Sta11], what further emphasized the choice of the mentioned solver.
2. Step size control has its origin in improving the efficiency of computing. However, the differential equations of the model (4.9) are not too complex. Moreover, the integration range is quite short compared to other physical problems. That is why efficiency and computing time are not crucial. Furthermore, adaptive step size would cause a problem in the calculation of the guidelines. While in most physical problems, the final state is of interest, the trajectory of the model has to be calculated in this task. Between every state in the trajectory, the model can only be interpolated. An adaptive step-size would result in different distance along the state trajectory and hence in the guidelines. That is clearly not wanted in the representation.

For the sake of solving a system of differential equations, some known conditions are required. Usually, the initial conditions are used to remove the integration constants. For the state space model (4.9), the following initial state seems to be a good choice:

$$\mathbf{x}_0 = \begin{pmatrix} 0 \\ 0 \\ 0 \\ \kappa_{1,0} \\ \vdots \\ \kappa_{n,0} \end{pmatrix}, \quad (5.3)$$

where $\kappa_{i,0}$ represent the initial kink angles. All parameters of the tractor vehicle are set to zero in the initial state. The reason is, that the guidelines are of interest with respect to the current pose of the car. Moreover, the origin of the inertial frame is more or less arbitrary. In the interest of simplification, the tractor reference frame can be assumed to coincide with the inertial frame at the initial condition. Nevertheless, the initial kink angles are required. There are different technologies available in order to determine the current kink angle. The kink angle sensor used in Ehlgen's project [EPA08] is based on the anisotropic magneto-resistive effect. Another possibility would be a system, involving a camera and clever algorithms. Beside the detection of the drawbar, the current kink angle may be computed from the camera's image only. A proposal can be found in [CSMH13], where the authors estimate the kink angle from single video frames. In order to increase the reliability, training algorithms were used. However, in this thesis, the kink angles are assumed to be available, no matter

through which types of sensors and underlying algorithms, the data is obtained.

5.2 Point Transformation and Guideline Calculation

After the integration of the state equations, it is necessary to clarify, how the guidelines can be extracted from a trajectory of states of the type (5.1) and (5.2). Usually, the guidelines are formed by the outer contours of the sub-vehicle of interest. In detail, the maximum width, shifted to the rear side of the corresponding sub-vehicle should be used. However, in order to describe the guidelines with respect to the tractor vehicle at rest, the transformation of a fixed point in the reference frame of the sub-vehicle, whose guidelines shall be calculated, to the tractor vehicle rest frame has to be performed.

Therefore, the following derivation shows, how any fixed point $\mathbf{r}_{\text{fix}}^i$, represented in the i -th sub-vehicle frame can be transformed to the tractor system at rest.

For every position of the tractor-trailer system, the guidelines are calculated. At the same time, the position and orientation of the tractor-trailer system is assumed to be zero. Figure 5.1 shows the assumed pose of the tractor-trailer system. Clearly, the position as well as the orientation is zero with respect to the inertial frame, marked in red. For the current steering angle δ , the guidelines (marked in orange at the rear end of the trailer) shall be predicted. The integration gives a trajectory of states, dependent on the virtually driven distance s . Virtual means, that the integrator calculates, what would happen, if the system is moving backwards with the current steering angle. Figure 5.2 shows, how an arbitrary

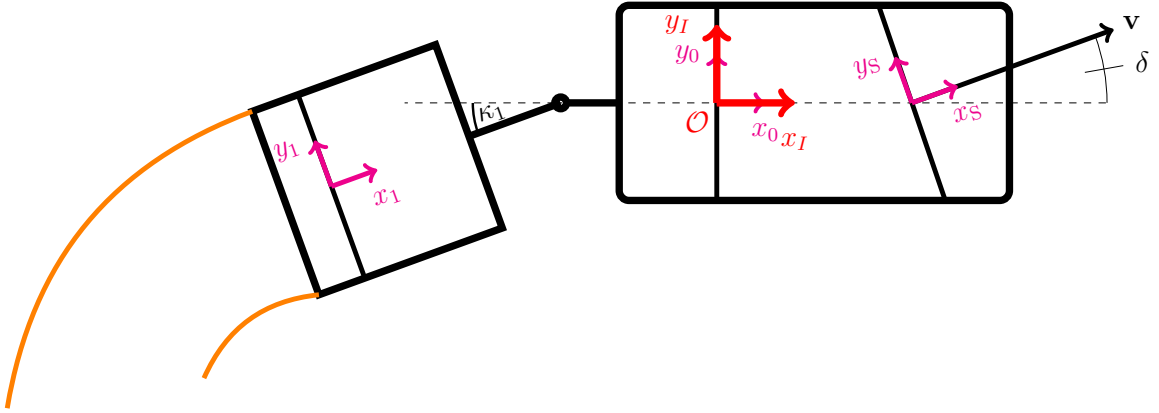


Figure 5.1: Initial pose of the tractor-trailer system

pose within the predicted trajectory could look like. For a better comparison, the original position is drawn with continuous lines, whereas the new pose is illustrated with the help of dashed lines. Clearly, the rear-most points of the virtual pose of the trailer intersect with the previous drawn guidelines. However, the process of the calculation is executed in the opposite way: Out of the state vector at a driven distance s , the guidelines are calculated.

The starting point are the coordinates of a fixed point in the frame of the n -th trailer $(x_{\text{fix}}, y_{\text{fix}})^n$. This vector has to be transformed along the chain of trailers until the inertial frame (what is the rest frame of the tractor) is reached. The underlying fundamental transformation is the change of the representation of a vector from a frame i to its previous neighbour $i - 1$. However, for reasons of simplicity, two intermediate frames at the junction between both trailers (or trailer and tractor) are introduced with the label J_{i-1} and J'_{i-1} (see Figure 5.3). The vector $\mathbf{r}_{\text{fix}}^i$, represented in the i -th frame can be transformed by a pure

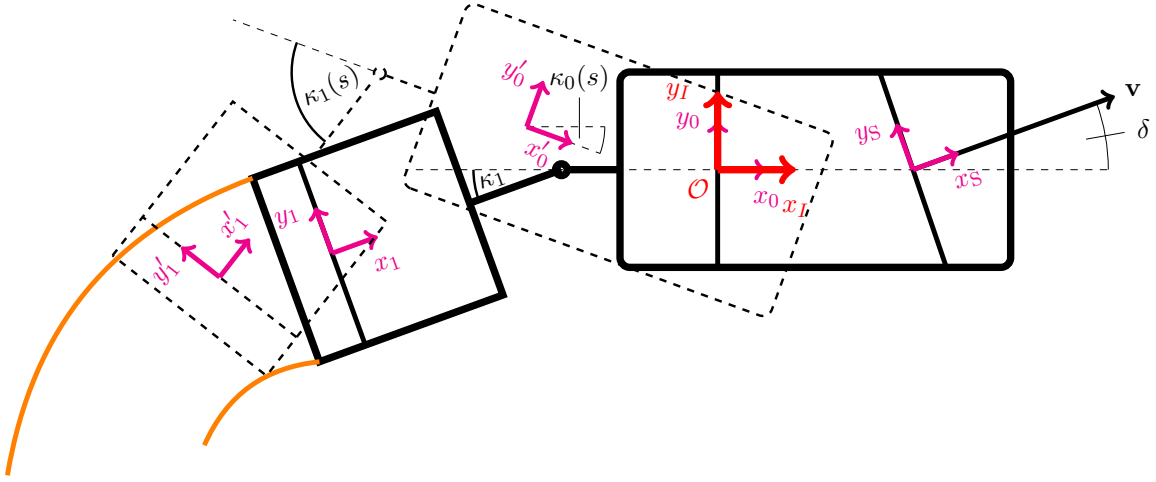


Figure 5.2: Virtual pose after a passed distance s (dashed), compared to the initial pose (solid)

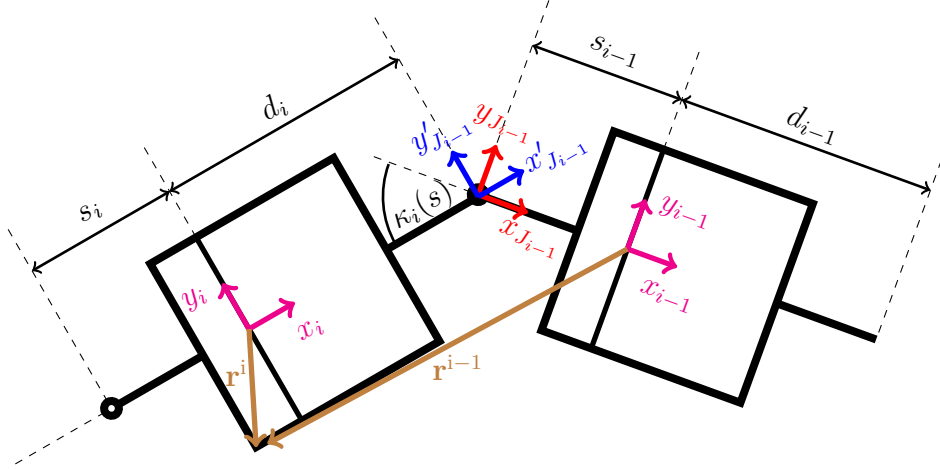


Figure 5.3: Transformation of a point from frame i to its previous neighbour.

translation to the system at J'_{i-1} (blue frame in Figure 5.3), since the frames have the same orientation, but are shifted by a distance of d_i with respect to each other (5.4). In order to obtain the vector in a frame with the same orientation as frame $i-1$, the transformed vector is rotated about the kink angle $\kappa_i(s)$ (5.5). From J_{i-1} (red frame in Figure 5.3) to $i-1$, the transformation is again a pure translation along the x-axis with the distance s_{i-1} (5.6). The total transformation, containing the explained intermediate steps of any point \mathbf{r} , represented in the frame i , to the previous frame $i-1$ is illustrated in Figure 5.3. In mathematical terms, the transformation can be expressed as follows:

$$\mathbf{r}_{\text{fix}}^{J'_{i-1}} = \mathbf{r}_{\text{fix}}^i + \begin{pmatrix} -d_i \\ 0 \\ 0 \end{pmatrix} \quad (5.4)$$

$$\mathbf{r}_{\text{fix}}^{J_{i-1}} = \mathbf{R}_i^{i-1} \mathbf{r}_{\text{fix}}^{J'_{i-1}} \quad (5.5)$$

$$\mathbf{r}_{\text{fix}}^{i-1} = \mathbf{r}_{\text{fix}}^{J_{i-1}} + \begin{pmatrix} -s_{i-1} \\ 0 \\ 0 \end{pmatrix} \quad (5.6)$$

or in one term

$$\mathbf{r}_{\text{fix}}^{i-1} = \mathbf{R}_i^{i-1} \left[\mathbf{r}_{\text{fix}}^i + \begin{pmatrix} -d_i \\ 0 \\ 0 \end{pmatrix} \right] + \begin{pmatrix} -s_{i-1} \\ 0 \\ 0 \end{pmatrix} \quad (5.7)$$

The rotation matrix \mathbf{R}_i^{i-1} refers to the predicted kink angle $\kappa_i(s)$ along the path:

$$\mathbf{R}_i^{i-1} = \begin{pmatrix} c\kappa_i(s) & -s\kappa_i(s) & 0 \\ s\kappa_i(s) & c\kappa_i(s) & 0 \\ 0 & 0 & 1 \end{pmatrix}$$

The explained transformation has to be repeated, until the representation of the original point is obtained in the frame of the virtual tractor vehicle. The last step is to transform the representation to the inertial frame. In comparison to the previous steps, an intermediate frame is not required. Rather a transformation with the translation $(x_0(s), y_0(s))$ and a rotation $\kappa_0(s)$ is performed.

If all these steps are repeated for every state vector along the path, a vector of guideline points in the frame of the tractor at rest is obtained.

5.3 Guideline Projection

The result of the previous section was a set of guideline points, formed by the endmost attached trailer in the frame of the resting tractor vehicle. For a Bird's eye view system, this result would be enough, since the virtual camera is situated above the towing vehicle normally. However, the goal of this thesis is to project the estimated driving path into the camera's image, placed at the rear side of the endmost trailer (see Figure 5.4). Beside the plenty of introduced coordinate frames for the trailers, the camera requires an additional coordinate system. Theoretically, a projection of a world point to the camera image can only be performed correctly, if its coordinates are represented with respect to the camera's frame. Knowing the camera's pose, namely its position and orientation, the transformation between the inertial frame (which is the towing vehicle's frame at rest) and the camera frame can be performed. The camera's pose however, is obtained by an extrinsic calibration of the camera. The actual projection, namely the transformation from world points to its representations in the camera's image, is only dependent on the intrinsic parameters, including the distortion coefficients. A lot of research has been done in this topic, making the projection of world coordinates to their corresponding representation in the camera's image to a standard task. *OpenCV* provides several routines for different intrinsic camera models, which project the world points to the image plane. That is why the pure projection of world points is not discussed in this section, but rather the calculation of the camera's pose, which is a required parameter to the existing routines [Bra00].

Figure 5.4 illustrates the problem: any vector \mathbf{r}^0 , represented in the vehicle's frame at rest therefore has to be transformed to the camera's frame \mathbf{r}^{Cam} (see brownish arrows in Figure 5.4). This can be done using the *OpenCV* routine, if the camera's pose is known, with respect to the vehicle's frame at rest. The extrinsic calibration is, however, slightly more complicated, compared to the calibration of a rear camera, mounted at the rear side of the towing vehicle. Whereas the camera's pose in a classical parking assistance system is fixed with respect to the vehicle's frame, the camera, mounted at the endmost trailer changes its pose with respect to the tractor's frame, as the intermediate kink angles change (see Figure 5.4). Nevertheless, the rear view camera is fixed with respect to the endmost trailer. The

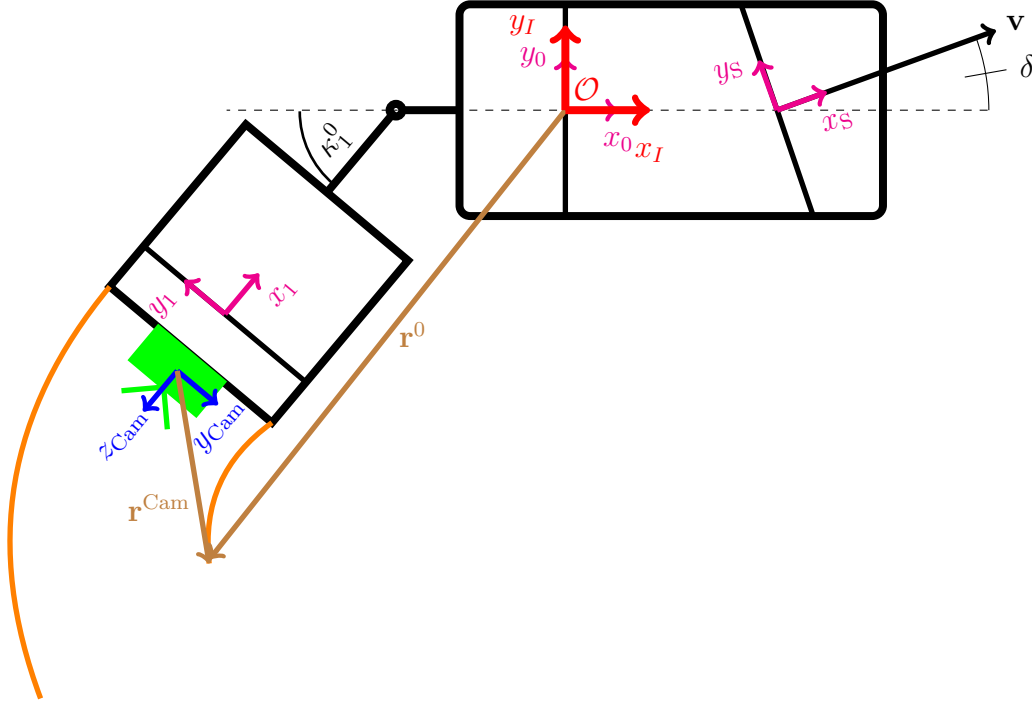


Figure 5.4: Transformation of a point of the guideline to the camera's frame

idea for the correct extrinsic calibration of the camera is, to calibrate the camera first with respect to the frame of the endmost trailer. According to the actual state of the system, the current position and orientation of the endmost trailer can be calculated. Therefore, equation (5.7) can be used, but with $\mathbf{r}_{\text{fix}}^n = 0$, since the origin of the endmost trailer (n -th trailer) is regarded. Together with the camera's pose with respect to the trailer, the whole calibration can be calculated, with respect to the vehicle's frame at rest. The complete translation vector of the camera can therefore be expressed with

$$\mathbf{r}_{0-\text{Cam}}^0 = \mathbf{r}_n^0 + \mathbf{R}_n^0 \mathbf{r}_{n-\text{Cam}}^n, \quad (5.8)$$

where $\mathbf{r}_{n-\text{Cam}}^n$ is the position vector of the camera, in the endmost trailers frame, obtained by the extrinsic calibration with respect to its axle. \mathbf{r}_n^0 is the position of the endmost trailer, represented in the towing vehicle's frame. Together with the current orientation matrix \mathbf{R}_n^0 , which is obtained by the kink angles:

$$\mathbf{R}_n^0 = \mathbf{R}_z\left(\sum_{i=1}^n \kappa_i^0\right), \quad (5.9)$$

these quantities have to be updated for every new state of the system. A similar approach was done in [EPA08]. This makes the extrinsic calibration more complicated and error sensitive compared to the case, where the camera is mounted on a fixed platform. The orientation of the camera has to be adapted according the kink angles as well

$$\mathbf{R}_0^{\text{Cam}} = \mathbf{R}_n^{\text{Cam}} \mathbf{R}_0^0, \quad (5.10)$$

where the rotation matrix $\mathbf{R}_n^{\text{Cam}}$ represents the extrinsic calibration parameters with respect to the endmost trailer's frame.

5.4 Accuracy of Guideline Projection

The projection of world points to the camera's image may suffer from different effects. First of all, the camera model may be inaccurate, so that a displacement appears in the projection algorithm of world points to their image correspondences. Moreover, the undistortion of the raw image takes some assumptions, which may not hold in reality. On top of that, the extrinsic calibration with respect to the trailer is dependent on the kink angle measurement, whose accuracy is limited by a certain value. In order to investigate the accuracy of the projection, a chessboard was used, whose pattern size was known (see Figure 5.5).

Placing the longer side of the pattern 5.5 coinciding with the rear end of the trailer and moreover centred exactly, the coordinates of the corners of the chessboard can be calculated with respect to the frame of the towing vehicle, together with the knowledge of the system's current configuration. Additional lines were added to the chessboard (Figure 5.5) with a distance of 1.9 cm. With the help of these lines, the projection accuracy could be evaluated quantitatively. The result can be seen in Figure 5.6. Neither in the projection to the raw image nor to the undistorted image, any point is exceeding the distance to the next line, which are described above. That leads to the conclusion, that the deviation of the projected points is below 1.9 cm, which is negligibly small compared to the thickness, a projected guideline takes.

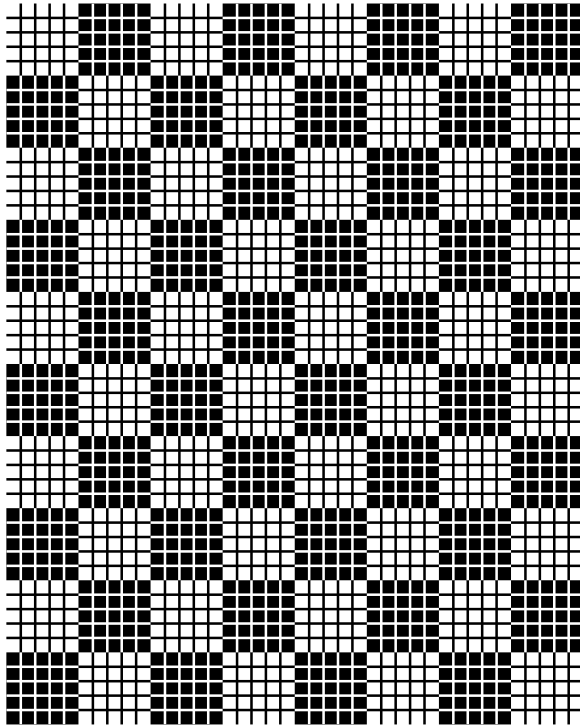


Figure 5.5: Chessboard pattern for the evaluation of the accuracy of the projection algorithm

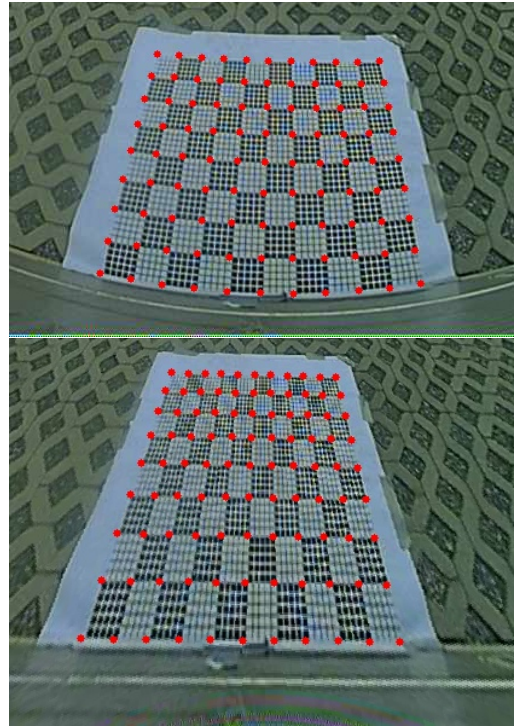


Figure 5.6: Projection of known coordinates (red) to the camera image (top: raw image, bottom: undistorted image)

6 Analysis of the Model

The input parameters of the model (4.9) are limited to the steering angle δ . Together with the initial condition of the state, the reaction of the system can be influenced by these quantities only. Section 5 showed, that the position of the tractor as well as the yaw angle are assumed to be zero, at least in the initial state. Hence, only the initial conditions of the kink angles may influence the system's reaction.

For a combination consisting of a tractor and a single trailer, the behaviour of the state vector along the driven path is of interest, in order to obtain a feeling of the system's behaviour. The above-mentioned assumptions reduce the degrees of freedom of the model enormously. Therefore, the progress should be studied for different steering angles as well as for variable initial conditions of the kink angle. Since the state of the regarded system has four components only, namely

$$\mathbf{x} = \begin{pmatrix} x_0 \\ y_0 \\ \kappa_0 \\ \kappa_1 \end{pmatrix},$$

of which the first three describe the kinematics of the individual tractor, it is sufficient to analyse the kink angle progress along the driven path. The kinematics of the tractor is assumed to be valid. The overall discussions are made for a tractor-trailer system with the following properties:

$$d_0 = 2.5 \text{ m} \quad s_0 = 1.0 \text{ m} \quad d_1 = 2.5 \text{ m}$$

6.1 Kink Angle Progress for Different Steering Angles

Especially the study of the model's response to different steering angles should be emphasised, because the steering angle is the only opportunity the driver can influence the system. A standard passenger car has a limited range of possible steering angles, usually inside $\delta \in [-40^\circ, 40^\circ]$. Coinciding with the system boundaries, the system's responses to several steering angles is analysed and presented in Figure 6.1.

Clearly, the system shows a symmetrical behaviour to the steering angle of 0° , as long as the initial kink angle is zero. It turns out, that the kink angle remains in its initial condition for a steering angle of zero degrees, resulting in the symmetry of the system's kink angle progress for positive and negative steering angles. As one might expect, the greater the (absolute value of) steering angle, the faster (fast in the sense of driven distance) the trailer is bent. Against the expectation in advance, the kink angle progress has the greatest rate of change between its minimum and maximum for all steering angles. An explanation is the dependency of the kink angle rate on trigonometric functions of the kink angle itself.

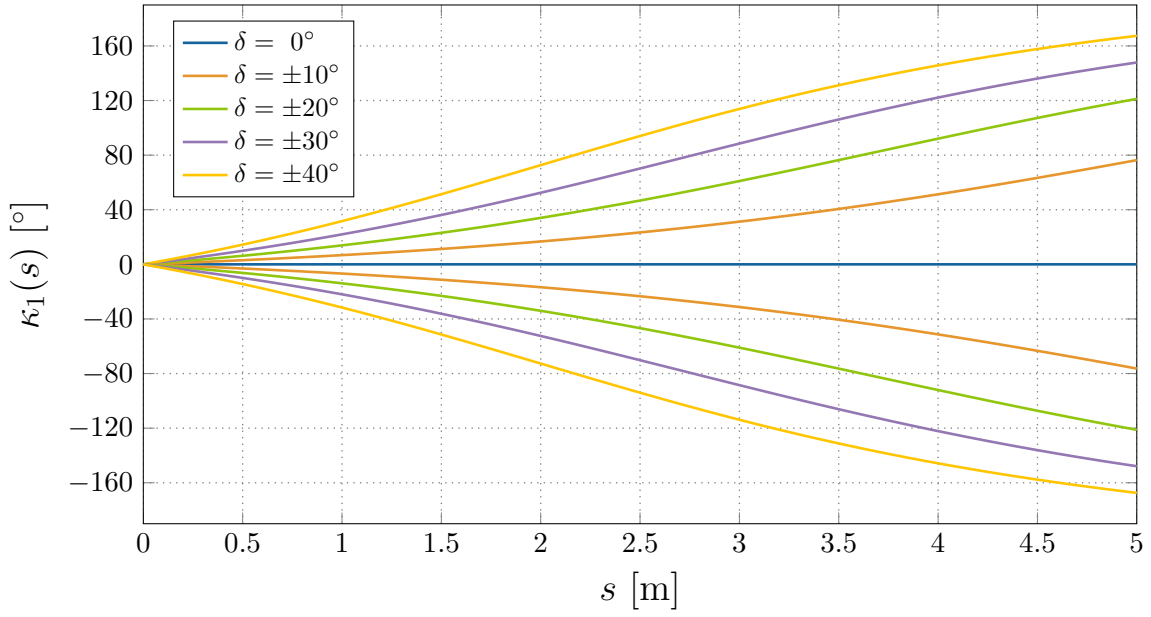


Figure 6.1: Responses of the model to different steering angles

6.2 Kink Angle Progress for Different Initial Conditions

For the investigation of the system's responses to different initial kink angles, a fixed steering angle has to be assumed, which was chosen to be $\delta = -7^\circ$. The analysed range of initial kink angles was $\kappa_{1,0} \in [-30^\circ, 30^\circ]$, with the system's response shown in Figure 6.2.

Compared to the investigation of different steering angles at a fixed initial condition for the kink angle, the system seems not to be symmetric any more, at least not to an initial kink angle of zero degrees. Clearly, the symmetry line is rather shifted to the initial kink angle, which is leading the system to remain in its configuration. It turns out, that there exists a value for the initial kink angle, which will not be changed, when the steering angle is kept. Clearly, this threshold in the given example is around 10° (reddish line in Figure 6.2). Exactly this phenomenon is causing the shift of the symmetry line, compared to the Figure 6.1 in the previous section.

Still, there is another outcome, which has to be regarded in more detail. If one has a closer look at Figure 6.2 again, the maximum kink angle rate for all curves seems to be equivalent. This gives rise to the fact, that for a fixed steering angle, there exists only one curve of the kink angle development along the driven path. According to the initial condition, this curve is just shifted along the x-axis, until the actual initial kink angle is obtained. In other words, this would mean, that the behaviour of the system with an initial kink angle of 0° would show the same behaviour from the point in space, when it reaches a kink angle of 5° , as if it would have had an initial kink angle of 5° .

6.3 Threshold Kink Angle

Figure 6.2 showed, that there exists a kink angle for a given steering angle, for which the kink angle rate almost disappears. An analysis of the mathematical model gives information about the angle, which should be called *threshold kink angle* with the symbol $\kappa_{1,\text{thresh}}$ from

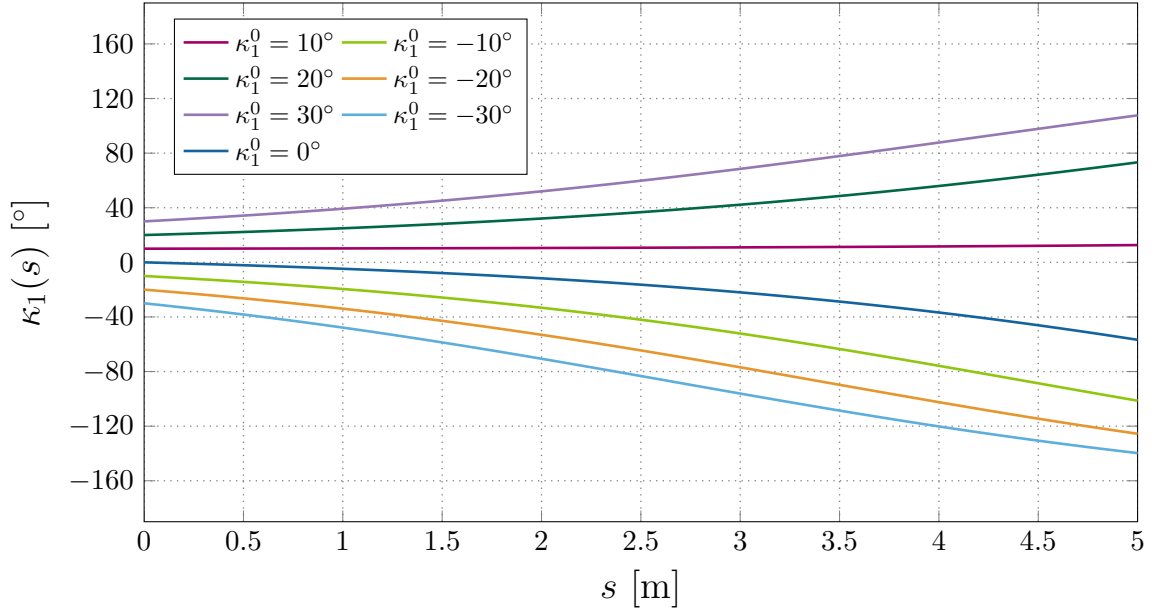


Figure 6.2: Responses of the model to different initial kink angles

now on. If the rate of the kink angle has to disappear, the parameters, which influence the rate have to be analysed. Recalling the equation again

$$\kappa_1' = \frac{1}{d_0} \left\{ \left(\frac{s_0}{d_1} \cos \kappa_1 + 1 \right) \tan \delta + \frac{d_0}{d_1} \sin \kappa_1 \right\},$$

it becomes obvious, that the steering angle δ and the current kink angle κ_1 are the only influencing properties, as a part of the system's state.

The threshold kink angle shall describe the situation, when the kink angle rate disappears, hence

$$0 \stackrel{!}{=} \left(\frac{s_0}{d_1} \cdot \cos \kappa_1 + 1 \right) \tan \delta + \frac{d_0}{d_1} \sin \kappa_1. \quad (6.1)$$

is the condition for the threshold kink angle. The equation above can not be rearranged for the kink angle analytically, so that the threshold kink angle has to be found with numerical algorithms. A good choice can be Newton's method. The solution shall be denoted with

$$\kappa_{1,\text{thresh}}(\delta), \quad (6.2)$$

expressing its dependency on the current steering angle.

6.4 Static Turn Steering Angle

The so far discussion just aimed at the kink angle. However, the tables can be turned, considering the steering angle instead. The question arises, which steering angle the operator has to choose, so that the system in the given configuration has a vanishing kink angle rate. In comparison to the determination of the threshold kink angle, the static steering angle can be

calculated analytically, namely by rearranging equation (6.1) for the steering angle:

$$\delta_{\text{static}} = \arctan \left(-\frac{\frac{d_0}{d_1} \cdot \sin \kappa_{1,0}}{\frac{s_0}{d_1} \cdot \cos \kappa_{1,0} + 1} \right). \quad (6.3)$$

Applying the static turn steering angle δ_{static} , the system will remain in its configuration.

6.5 Critical Kink Angles

Theoretically, the kink angle rate can have both signs. The question which should be outlined in this section is, if the system can escape its configuration by the restriction of driving backward only. Escaping means, that positive kink angles can be decreased and negative kink angles increased. Recalling the limits of the steering system, labelled with δ_{\min} and δ_{\max} respectively, a critical kink angle in both directions is expected, for which the system can not escape the related configuration any more. The critical kink angles shall be denoted with $\kappa_{1,\text{crit},\min}$ and $\kappa_{1,\text{crit},\max}$. In mathematical terms, the question can then be formulated as follows

$$? \exists \delta \in [\delta_{\min}, \delta_{\max}] : \kappa_1^0 = \kappa_{\text{crit},\min} \Rightarrow \frac{d\kappa_1^0}{ds} > 0 \quad \wedge \quad \kappa_1^0 = \kappa_{\text{crit},\max} \Rightarrow \frac{d\kappa_1^0}{ds} < 0.$$

If the above condition is wrong, then the critical kink angle is exceeded. It turns out, that equation (6.2), evaluated for δ_{\min} and δ_{\max} delivers the limit, at which the mathematical statement is just true:

$$\kappa_{1,\text{crit},\min} = \kappa_{1,\text{thresh}}(\delta_{\max}) \quad (6.4)$$

$$\kappa_{1,\text{crit},\max} = \kappa_{1,\text{thresh}}(\delta_{\min}) \quad (6.5)$$

6.6 Error Behaviour and Stability Analysis

Figure 6.1 and 6.2 have shown the reaction of a system for various steering angles and initial kink angles, respectively. The initial kink angle and the steering angle are obtained by sensor measurements, which may suffer from inaccuracies and errors. Therefore, it is crucial to know the quality of the prediction, even if the steering angle and the initial kink angle are not known precisely. Problematic is the choice of the measure, which describes the quality of the prediction. Clearly, a difference of the resulting trajectories should be considered. However, the difference of trajectories is a tough task, as it is discussed in section 7.4.4 and in [RMJ07]. Nevertheless, the kink angle will reach a maximum value after a certain travelled distance, except the specific case of zero kink angle rate. The idea is to use the difference of the total travelled distance, until the maximum kink angle is reached. For this purpose, the total distance s_{final} is visualized based on the colorbar on the right for various steering angles and initial kink angles (Figure 6.3). A maximum kink angle of 90° was assumed. Moreover, the total travelled distance was limited to 10 m. Theoretically, an infinite travelled distance is possible for some configurations, where the kink angle rate disappears. Still, the integration has to be stopped at a certain distance. 10 m was chosen, since it has a good relationship to the average travelled distances, but still being the largest possible. A good way to evaluate the error is to choose a certain tuple, consisting of a steering angle and an initial kink angle,

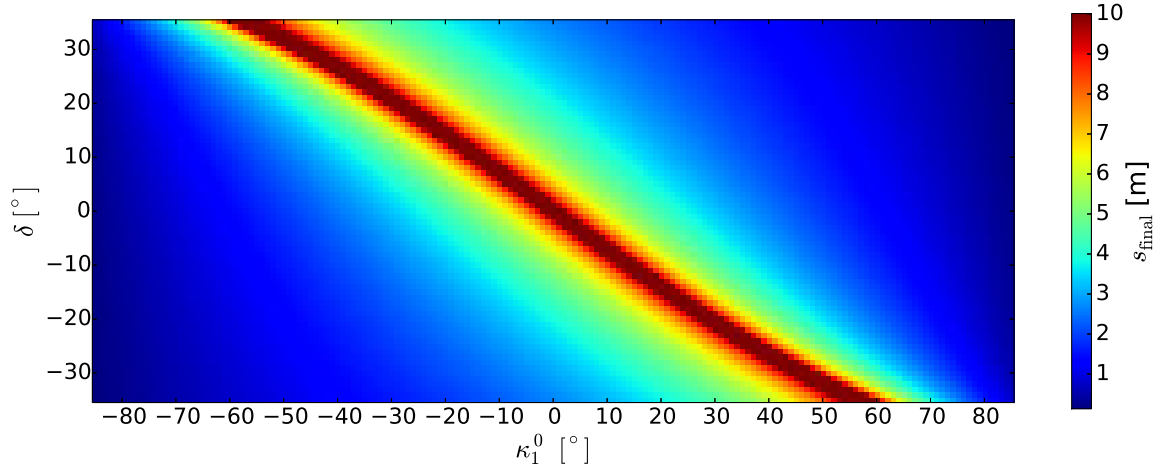


Figure 6.3: Maximum driven path s_{final} for various steering and initial kink angles

and compare the resulting distance to the distances of the neighbour tuples. Clearly, the error is depending on the system configuration, meaning that a constant error of the tuple would not lead to the same error, for different system configurations. The tuples of the lower left and upper right corner of Figure 6.3 nearly lead to the same travelled distances, resulting in a small error for uncertain tuples. However, there exist regions, where small uncertainties of the tuples lead to large errors in the resulting travelled distance. Especially the region, marked in red, is highly sensitive to slight changes of the initial tuple. The reason originates in the elaborated equation (6.3) for the vanishing kink angle rate. It is obvious, that a tuple, slightly differing from the configuration, which has a vanishing kink angle rate, results will reach a maximum kink angle, whereas the original configuration will not. That is why a large difference between the configuration arises. An uncertainty of 5° of the initial kink angle can result in a distance error of up to 3m, clearly an unsatisfying error. That is why it seems unclear, why an inaccuracy of 5° is tolerated in Ehlgens test [EPA08]. Another interesting thing to remark is, that equation (6.3) can be seen directly in Figure 6.3: the red marked region is reminiscent of an inverted sine function. Knowing that the arctan function is nearly linear in the range $[-1,1]$, the red area corresponds exactly to the mentioned equation.

Cutting it short, a slight change of the initial tuple can lead to large differences in the travelled distance and hence to a different trajectory. Especially configurations close to the vanishing kink angle rate suffer from this behaviour. On top of that it has to be noted, that in a manoeuvring situation, the system is aimed to be operated close to the vanishing kink angle configuration, since a fast bending of the trailer is undesirable.

7 Validation of the Model

Although the derivation of the model (4.9) was straight forward and logical, its reliability has to be proven, due to the strong simplifications, which have been assumed in advance. As a reminder, the strongest simplification was the negligence of the lateral slip on every axle

$$v_y = 0, \tag{7.1}$$

resulting in a pure kinematic model. Many investigations have used the bicycle model with together with this strong assumption (e.g. [EPA08], [MK15]). However, a test of the reliability of the model for a system with the size of a standard passenger car has not been found in the literature, except for the test of the kink angle development in [EPA08]. Even if some tests would exist, an inspection of the derived model from section 4 together with its implementation is still indispensable.

Basically, the model shall be proven in three steps, motivated by the available sensor data of the system. All three methods use data, gained by the same experiment. It was decided to start with a close to zero initial kink angle followed by a backward drive with a constant steering angle. Only in that way, the predicted and the actually driven driving path could be compared directly. Different scenarios were chosen, in order to test the system under nearly real conditions, namely, the steering wheel angle was set to

$$\varepsilon \in [-490^\circ, -180^\circ, -90^\circ, 0^\circ, 90^\circ, 180^\circ, 490^\circ].$$

This chapter describes the methods to prove as well as their results for different types of investigated trailers. Nevertheless, the constraints, which would define the validity of the model, had to be defined in advance.

7.1 Constraints Stating the Reliability of the Model

Before the validity of the model can be evaluated, the corresponding constraints have to be specified, which define, if the model delivers successful results. In nowadays camera-based parking assistance systems, the guidelines are presented wider, than the maximum width of the vehicle actually is. Several reasons enforce the introduction of this factor of safety. Beside the dynamic limit of the bicycle model, many optical influences may lead to errors in the projected guidelines. Theoretically, the guidelines are valid for a flat surface only, which is not guaranteed in several situations. According to some experience, it was decided to permit a maximum lateral deviation at the rear side of the trailer of 20 cm only. Nevertheless, the model should be aimed at to deliver a tolerance of 10 cm. The mentioned lateral deviation should be kept up to a predicted distance of at least 3 m in advance for the case, that the initial kink angle is close to zero. The greater the initial kink angle and the appropriate rate

of change in the increasing direction, the shorter the maximum driven distance. That is why the system might not even be capable of moving 3 m in some scenarios. Moreover, close to the maximum kink angle, dynamic effects are expected, so that the model might not deliver accurate results for these configurations. Therefore, the distance of 3 m in advance should be treated with caution.

7.2 Lateral Slip Analysis

The first step towards the validation of the model has been the analysis of the y-component of the towing vehicle's velocity at the rear axle, which should vanish, according to the main assumption of the model (7.1). In the derived model (4.9), the yaw-rate of the tractor vehicle can be predicted, but based on above's assumption. Beside the velocity of the rear axle and the steering angle, the yaw-rate is accessible through sensor measurements as well. The idea of the inspection is the verification the yaw-rate equation of the tractor vehicle of the model (4.9)

$$\dot{\kappa}_0 = \frac{v_R}{d_0} \tan \delta,$$

by a comparison of the the left and right side of the rearranged equation

$$\dot{\kappa}_0 \cdot d_0 = v_R \tan \delta. \quad (7.2)$$

The right side was evaluated with the help of the yaw-rate measurement whereas the left side was evaluated with the measurements of the rear speed and the steering angle. Finally, the difference of both sides of this equation forms the y-component of the velocity of the rear-axle, which should vanish, if the model is valid:

$$v_y = \dot{\kappa}_0 \cdot d_0 - v_R \tan \delta \stackrel{!}{=} 0. \quad (7.3)$$

7.2.1 Results

Both sides of equation (7.2) as well as their difference are presented in the upper plot in the analysis diagrams, placed in the appendix (figure 10.1 - 10.6 for the single-axle trailer and figure 10.7 - 10.12 for the two-axle trailer). Clearly, the lateral slip, if present, is very small, since the lateral velocity is almost zero for every time in every scenario. Only when the vehicle is starting or stopping, the lateral velocity is climbing above $5 \frac{\text{cm}}{\text{s}}$ in some cases (e.g. for the scenario $\varepsilon \approx \pm 490^\circ$, evaluated in figure 10.5 and 10.6 for the single-axle trailer and the scenario $\varepsilon \approx +490^\circ$ evaluated in figure 10.11 for the two-axle trailer), but even then, only for a short time. The reason for this short deviation could also originate in the dullness of the speed sensor, whereas the yaw-rate sensor is extremely sensitive, resulting in fuzzy data. The key result from the evaluation should be, that the lateral velocity at the rear axle of the towing vehicle is negligibly small for all scenarios, which gave rise for a further analysis of the model. An absolute comparison of the driven path with the predicted path is even necessary, since the lateral velocity at the axle can make no statement about the absolute deviation of the model's prediction from the reality. Theoretically, the lateral speed could be integrated, making an evaluation of the lateral deviation possible. However, due to the fuzzy data of the yaw-rate sensor, the integration would lead to worse results, the model is actually delivering. Moreover, statements about the trailer are necessary.

7.3 Kink Angle Behaviour

One step further is the analysis of the kink angle behaviour during the scenarios. The solution of the model (4.9) is a trajectory of states, depending on the driven path s of the towing vehicle's rear axle. Another sensor-algorithm combination of the system is able to deliver the increments in x - and y -direction, which can be used to process the driven path s . Furthermore, the kink angle κ_1 can be measured at any time. By synchronising the time, each kink angle κ_1 is related to a corresponding driven path s , so that a curve $\kappa_1(s)$ can be recorded. Clearly, this curve should be compared to the model's prediction.

7.3.1 Results: Single-Axle Trailer

For all investigated scenarios, the predicted and the measured curves are plotted in figure 7.1. The measured data points are displayed with crosses, whereas the predicted curve is repre-

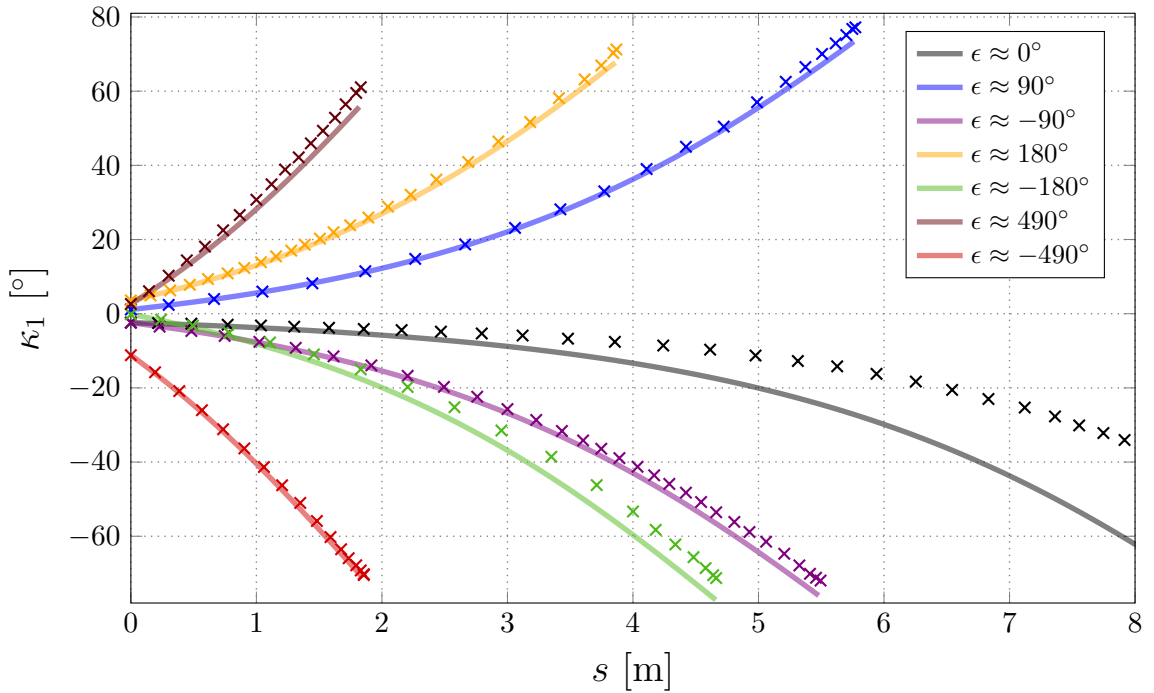


Figure 7.1: Kink angle development along driven distance for a single-axle trailer

sented by a solid line in a similar colour as its corresponding measurement points, so that their relation becomes obvious.

During the experiment, the kink angle could only be measured, after some distance was covered already. Hence, an initial condition for the kink angle was not available. According to the discussion in section 6.2, the curve of the kink angle development is only shifted for different initial conditions at a constant steering angle. That is why the prediction was started first, when the sensor delivered reliable data. The driven distance was set to zero and the prediction done from that point in time.

In order to be able to evaluate the absolute difference between predicted and measured kink angles, the differences along the driven distances are plotted in figure 7.1. The model was

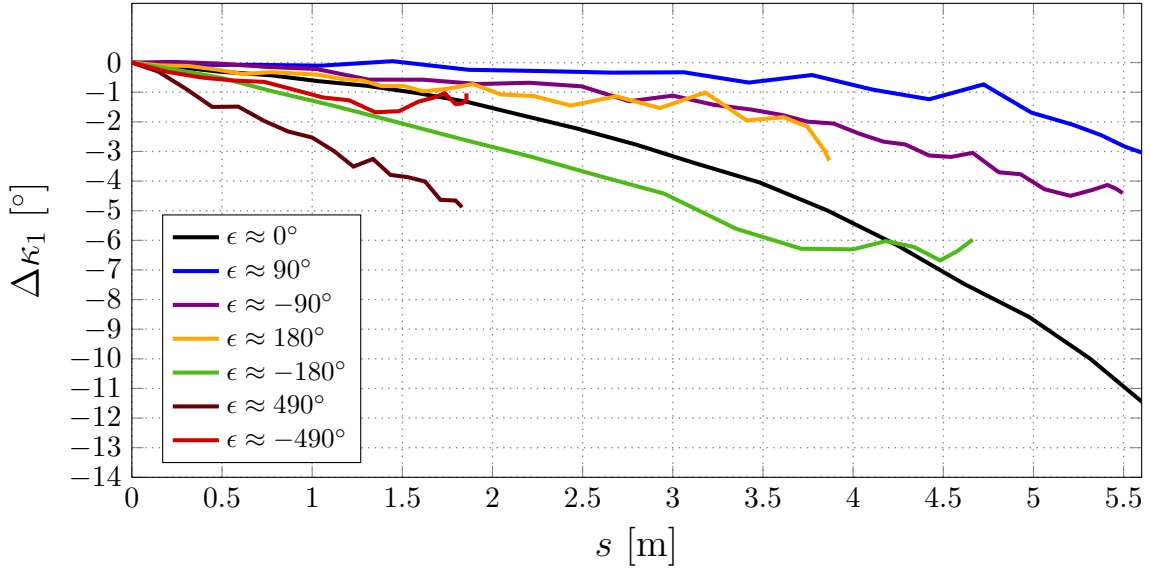


Figure 7.2: Kink angle deviation along driven distance for a single-axle trailer

aimed at to have maximum lateral deviations of 20 cm in each direction and should be valid for at least 3 m in advance. The maximum angular difference at 3 m is approximately 4.8° . With the distance from the junction to a corner of the trailer's rear side, the lateral distance Δ can be estimated from the given angular distance:

$$\Delta \approx d_1 \cdot \tan(\Delta\kappa_1)$$

Inserting the maximum angular difference results in a lateral deviation of $\Delta_{\max} \approx 31.6$ cm. This does not meet the defined constraints in section 7.1. However, only in two scenarios, the deviations are that large. The rest of the scenarios lead to a maximum deviation of 3° , equivalent to a lateral deviation of 19.7 cm. Clearly, the constraints are met for those scenarios. The scenarios, which do not meet the constraints are $\varepsilon \approx 490^\circ$ and $\varepsilon \approx -180^\circ$. Clearly, some scenarios are more accurate, than others. Probably this phenomenon arises due to uncertainties in the steering model (section 4.2). The disregard of the dynamic behaviour of the steering system may lead to a strong influence of the observed deviations.

Visually, the largest deviation seems to occur at the straight backward drive scenario. Nevertheless this may be an erroneous belief, because the prediction goes much further, than for scenarios with large steering angles. At a driven distance of 3 m, the scenario does not lead to the strongest deviation from its predictions. However, the deviation at a driven distance runs high until it reaches more than 10° . Clearly, this is caused by the instability of the system towards its initial conditions at roughly zero kink and steering angle (see section 6.6). Moreover, the quantization of the kink angle measurement is quite high. Together with the instability of this scenario, the strong deviation should have been expected. Another important observation to notice is the strength of the deviation of scenarios with large steering angles, compared to scenarios with a smaller steering angle. The greater the steering angle, the smaller the driven distance until the full bending of the system becomes. Apparently, the system suffers from dynamic effects at the state close to the maximum kink angle, since the kinematic model shows the largest deviation at large kink angles. This is not only the case for large steering angles, but for all scenario, as soon as the state gets close to the maximum

kink angle. Nevertheless, the deviations are only that strong, that the defined constraints are still kept.

A further reason for the deviations in all scenarios could be the unavailability of the kink angle at the beginning of the experiments. Although the applied method is motivated by the analysis in section 6.2, there may have occurred slight mistakes, leading to stronger effects in the analysis. Then, the resulting deviation would not have their reasons in the inaccuracy of the model, but rather in mistakes during the experiment.

Still, the analysis of the kink angle development showed, that the defined constraints were kept in most of the scenarios, so that the model has passed a further important test, at least for a single-axle trailer.

7.3.2 Results: Two-Axle Trailer

As discussed in section 3.2, a generalised axle has to be introduced, in order to be able to apply the model of a single-axle trailer to a trailer having multiple axles. However, the equation for the generalised axle (3.3) was originally derived for a truck, so that its validity for a trailer, is not guaranteed ad hoc. That is why the analysis for the kink angle development was done twice, first for the model of the generalised axle, based on equation (3.3) and secondly for the mean axle, based on equation (3.2). Only after the analysis, the better choice for the calculation of the generalised axle can be determined

Model of Generalised Axle According to the properties of the used trailer, the generalised axle, based on equation (3.3) was calculated and fed to the system's model. The rest of the procedure was equivalent to the analysis of the single-axle trailer. Finally, the development of the kink angle along the driven distance of the towing vehicle is shown in figure 7.3. It's corresponding deviation between the model and the actual kink angle development is presented in figure 7.4. The accuracy of the model is slightly better, compared to the experiment of the single-axle trailer, showing a maximum deviation at a predicted distance of 3 m of roughly 4.2° . However, this deviation corresponds to a lateral deviation of approximately 33.6 cm, due to different dimensions of the trailer. Obviously, this result is not meeting the set tolerance limit. Nevertheless, only two scenarios do not fulfil the constraints, namely $\varepsilon \approx -490^\circ$ and $\varepsilon \approx 180^\circ$. All remaining scenarios fulfil the requirements with a maximum deviation of 17.6 cm, what is clearly inside the defined tolerance limit. The resulting deviation gave rise to the investigation of the trailer, using the model of the mean axle 3.2. Maybe, the model 3.3 can not be used for trailers.

Model of Mean Axle Although the model of the generalised axle based on equation (3.3) delivered fairly well results, the investigation of the model, based on a mean axle was performed. The resulting kink angle development is shown in figure 7.5. The first contemplation gives rise to the assumption, that the model using the mean axle (3.2) leads to better results, than the model based on equation (3.3). The assumption is confirmed in the diagram, showing the absolute deviation between model and real data, depicted in Figure 7.6. Clearly, the maximum error at a predicted distance of 3 m is below 2.6° , being exactly at the limit of the set constraints. Again, only the scenario for $\varepsilon \approx -490^\circ$ lead to the large deviation. In the case of the mean axle, the maximum deviation still meets the constraints. Obviously, all other scenarios lead to deviations far below the limits. That is why the model of the mean axle should be preferred compared to the model of the generalised axle according to

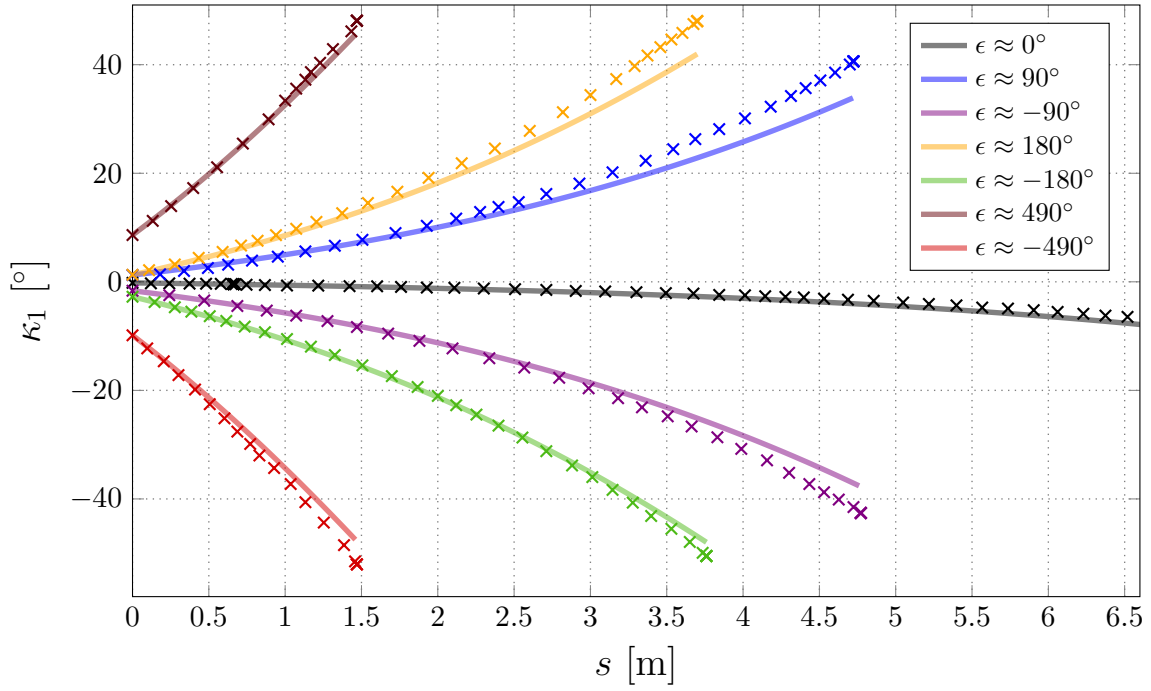


Figure 7.3: Kink angle development along driven distance for a two-axle trailer with used model (3.3)

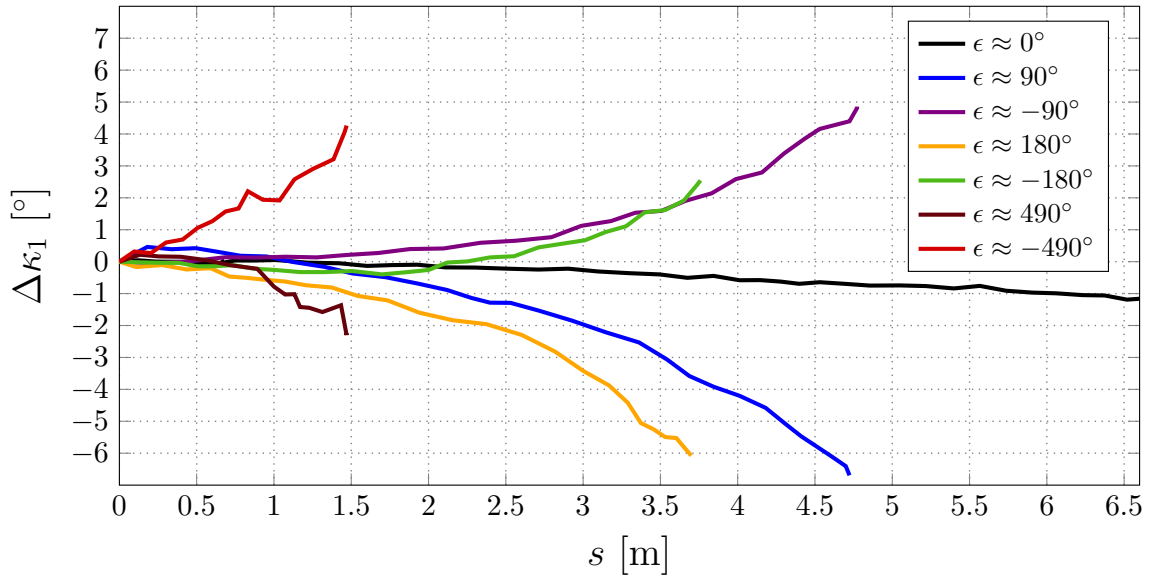


Figure 7.4: Kink angle deviation along driven distance for a two-axle trailer with used model (3.3)

equation (3.3). The results of the experiment of the two-axle trailer are even exceeding the success of the results of the experiment with the single-axle trailer.

However, the model based on equation (3.3) delivered fairly well results as well, so that it should not be discarded. One has to keep in mind, that the experiment was performed with an empty trailer. It may happen, that the quality of the results for the latter model improve, if mass load is added to the trailer, but distributed equally. The empty trailer was slightly

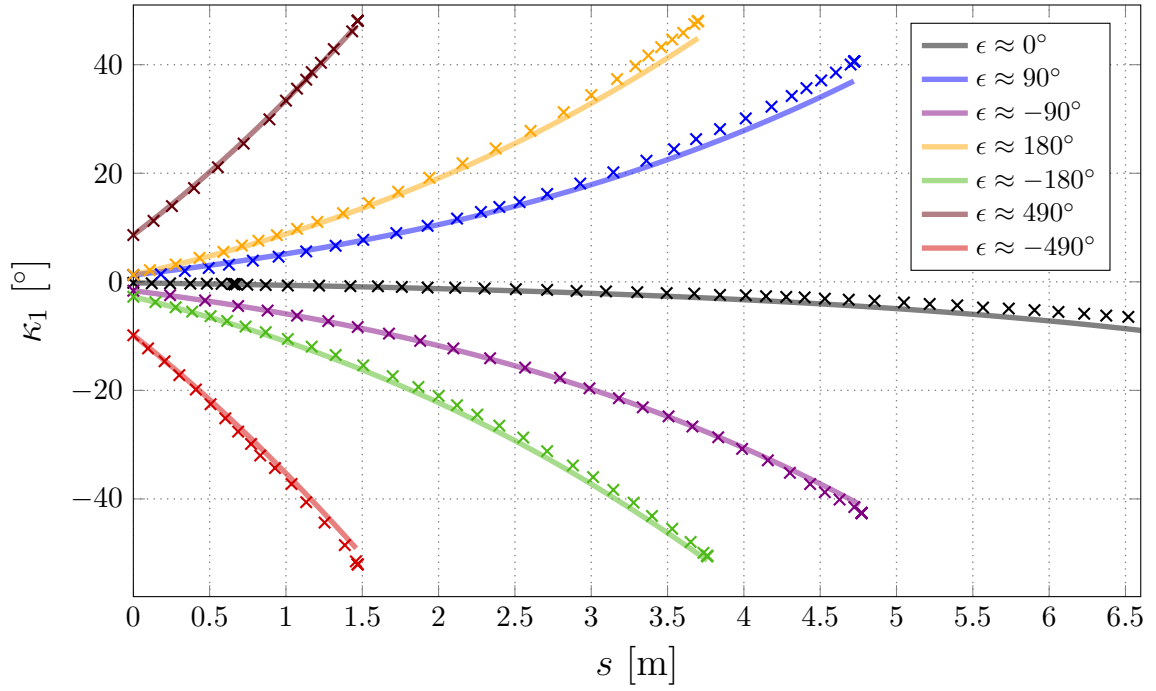


Figure 7.5: Kink angle development along driven distance for a two-axle trailer with used model (3.2)

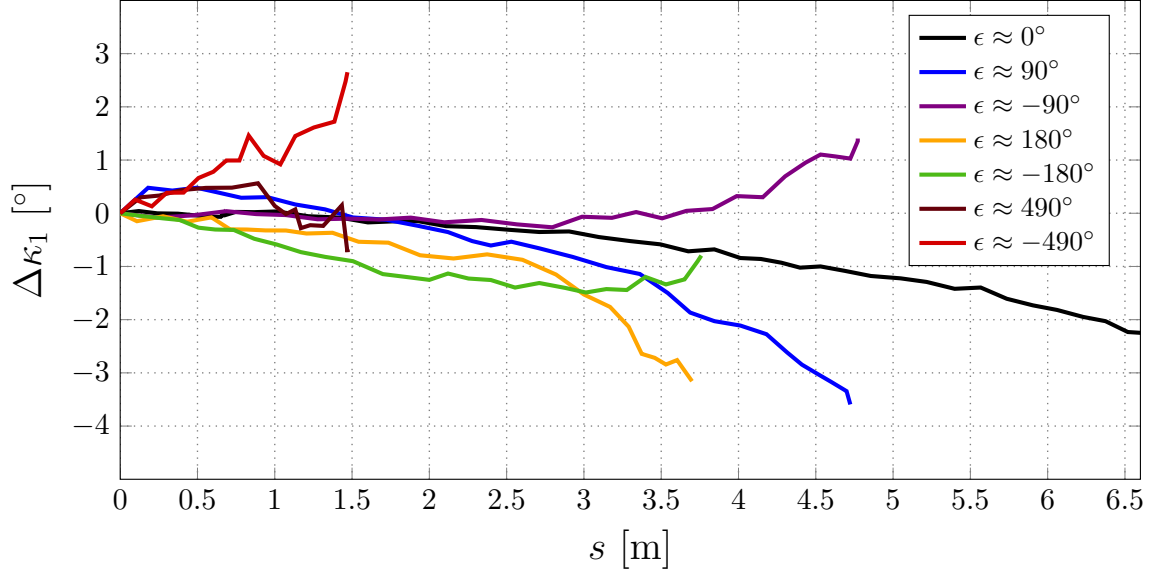


Figure 7.6: Kink angle deviation along driven distance for a two-axle trailer with used model (3.2)

inclined towards the front axle, due to the hitch position of the towing vehicle. That could have shifted the generalised turning axle towards the first axle. Still, the conclusion of this investigation is, that in general, the mean axle should be used for any attached trailer with multiple axles.

7.4 Absolute measurement

The previous tests of the model have only investigated the properties of the state vector of the system. What actually matters in the evaluation of the model is the lateral accuracy of the trailer's path, which has only been estimated so far. However, the path is not a property of the state directly, but has to be rather obtained from the trajectory of states (see section 5). A comparison can only be done, if the trailer's path can be measured absolutely. It was decided to record the system's action from above and further to process the resulting path from the video. In order to obtain a sufficient top-view video from the tractor-trailer system, a drone with a steerable camera was used. Compared to a static camera, placed at a large height above the ground, the drone can deliver a video view from directly above the tractor-trailer system, even though there are some difficulties, which arise by using a drone. Although nowadays position controllers of drones are quite accurate, an assumption of a static camera would not describe the reality accurately. Furthermore, present wind gusts can lead to abrupt changes of position and orientation of the camera. If every frame is taken from a different position and orientation, the camera calibration becomes necessary with every taken frame. Albeit this leads to higher computational effort, it should be noted, that the intrinsic calibration of the camera remains the same. In the end, an extrinsic calibration remains for every frame, before an accurate back projection of the image coordinates is possible. The computational effort is though not a problem, because the analysis of the video is done after the experiment.

The idea of the experiment is, to place targets on the ground, whose coordinates are known in advance. An algorithm can detect these targets and acquire the corresponding image coordinates. Knowing these mappings, the extrinsic calibration becomes quite easy with nowadays computing algorithms. Having the camera's pose together with its intrinsic parameters, everything is provided, to be able to calculate the image-to-world correspondences of the targets of interest, which are placed on the trailer. Finally the path, consisting of the retrieved points can be compared to the prediction according to the system's initial state.

The following section covers the whole methodology, which was required for the performance of the analysis. In the end, the results are presented and discussed.

7.4.1 Camera Calibration

An absolute measurement from a video sequence requires an ordinary calibrated camera. The calibration parameters split in extrinsic and intrinsic quantities. Whereas the extrinsic calibration has to be performed in every frame of the recorded video, the intrinsic calibration can be done only one-time before the experiment. Only extreme conditions of the environment may change these parameters, like temperature gradients. However, these changes are neglected.

Intrinsic Calibration The calibration procedure was performed according to the description by Zhang [Zha00]. Although there exist quite many methods to obtain the camera parameters, the method described by Zhang in [Zha00] is straight forward, uses only minimal and cheap equipment, does not require detailed knowledge of 3D geometry and computer vision and finally delivers good results. The algorithm behind the procedure requires at least two views from different orientations of a planar pattern with markers, whose coordinates are known. Using a maximum likelihood estimation, the resulting image-to-world correspondences

are the input parameters for the estimation of the camera's calibration parameters. However, during this step, the extrinsic parameters are not required, since the camera will have a different orientation during the experiment. Still, the algorithm delivers the extrinsic parameters for every view of the pattern, which can be used for a re-projection of the coordinates, evaluating the quality of the calibration.

A chessboard containing 14 rows and 19 columns was used as the calibration pattern (Figure 7.7). The lateral length of each panel was 2.05 cm. *OpenCV* provides an algorithm, which is able to detect the inner corners of a chessboard [Bra00]. As long as the recording conditions are well, the detection algorithm *findChessboardCorners* is very robust. An example of the detected inner corners can be seen in Figure 7.7. In each calibration frame, a coordinate sys-

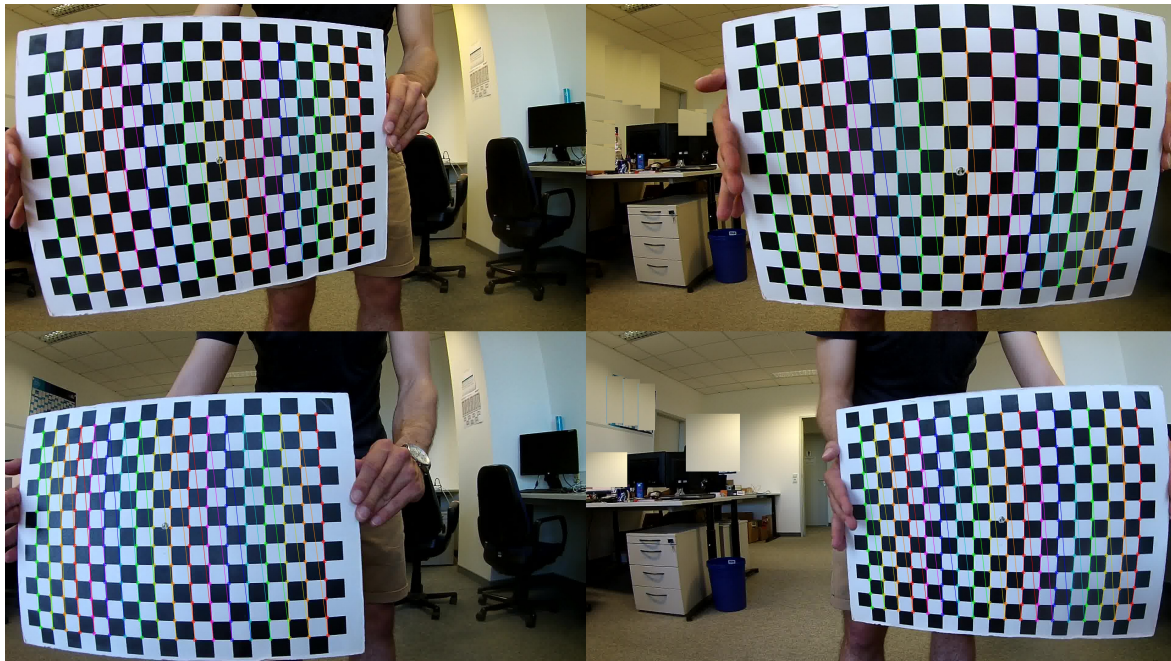


Figure 7.7: Calibration chessboard pattern at different views with detected inner corners

tem is defined, having the origin in the upper-right most inner corner and the x- and y-axis pointing along the rows and columns of the chessboard, respectively. With the properties of the chessboard, the world coordinates in the just introduced coordinate system of the detected points can be calculated. The *OpenCV* routine delivers the image coordinates of these points as well, so that the correspondences of image and world coordinates are known for each frame [Bra00]. Clearly, the more rows and columns the pattern has, the more accurate will be the mapping between image and world coordinates and the more accurate will be the intrinsic camera calibration.

According to Zhang [Zha00], the calibration can be improved with an increasing number of views of the pattern, even though two views are enough. However, the quality of the calibration has a limit, at which more views would not lead to any improvement. For the calibration of the camera of the drone, around 40 images with different orientations of the pattern have been used. Especially for a camera with fisheye effects, the pattern should cover as much as possible from the camera's field of view. Therefore, at least one frame in each corner of the camera image should be taken, as shown in Figure 7.7.

The *OpenCV* routine *fisher::calibrate* performs several steps of the described procedure by Zhang and its algorithm is moreover based on the stated equations [Zha00]. Beside the estimation of the intrinsic parameters, the radial distortion coefficients (refer to section 2.2.2) as

well as the extrinsic parameters are estimated [Bra00].

For the evaluation of the calibration, the intrinsic parameters and the radial distortion coefficients have been used to re-project the world points of the pattern in each frame. Of course, the extrinsic parameters of each frame has been used in this step. For every point, the quadratic norm to its actual detected point has been calculated. The mean error of every point in every frame was determined to be

$$\Delta p = 0.8 \text{ px},$$

what means, that a metric measurement of a world point in the image has a mean error less than a pixel. This is a very good result for a calibration of a camera, stating the strength of Zhang's method [Zha00].

Extrinsic Calibration The determination of the camera's pose, consisting of the orientation and translation of the camera's frame with respect to the world coordinate system, is called extrinsic calibration. It is usually expressed with Euler angles and a translation vector in Cartesian coordinates. Extrinsic calibration can be solved with the help of n world-to-image point-correspondences, known as the Perspective- n -Point problem (short: PnP) [V. 09]. Theoretically, three points would solve the problem, according to the six degrees of freedom of the problem, albeit most algorithms use more point-correspondences, in order to obtain higher accuracy. Moreover, an implementation already exists in *OpenCV's* Camera Calibration and 3D Reconstruction library: *solvePnp()* [Bra00]. *OpenCV's solvePnp()* function provides several implementations: An iterative method, based on the Levenberg-Marquadt Algorithm [Lev44] [Mar63], a solution for the P3P-problem, according to the paper [GHTC03], an efficient method for the PnP-problem, related to [V. 09] and a method, which even adapts the focal length of the camera [PSACMN13]. After some research about the accuracy and performance, it was decided to use the method based on direct least-squares (DLS) [HR11]. For the world-to-image point-correspondences, specific objects have to be used, which can be easily detected by an algorithm. Robert Giese presented a detection algorithm in his thesis [Gie15], for the specific target, shown in Figure 7.8. Due to its structure, a high accuracy of

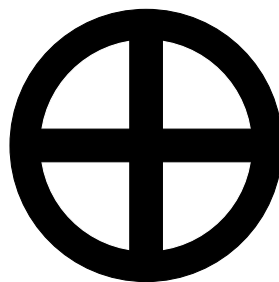


Figure 7.8: Used target structure for the extrinsic camera calibration

the centre of the target can be reached [Gie15]. The detection of the targets delivers the according image coordinates of the known world points. Together with the intrinsic parameters, the world-to-image point-correspondences are handled to *OpenCV's solvePnp()* method. Unfortunately, the function can not handle fisheye distorted images. That is why the frames are first undistorted with the *fisher::undistortImage()* function, before the detection algorithm is applied. Hence, the distortion vector, handled to the *solvePnp()* routine, is the zero-vector. Figure 7.9 shows beside the actual set-up of the absolute measurement, how recorded frames look like before and after the undistortion algorithm. With the help of the targets, placed on

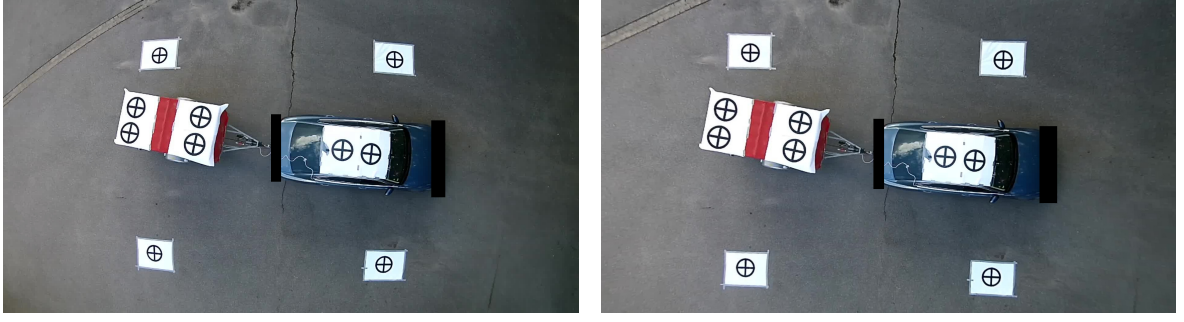


Figure 7.9: Recorded frame before (left) and after (right) undistortion

ground (Figure 7.9 - four targets which form the outer rectangle), the pose of the camera of the drone can be determined during the current frame.

Ground Pattern Coordinates Computation In order to obtain an accurate extrinsic calibration, the coordinates of the targets on ground have to be known with a high precision. It is, on the one hand, more accurate, to measure the absolute distances of the targets with respect to each other, instead of the absolute Cartesian coordinates in a pre-defined coordinate system. On the other hand, the coordinates of the targets have to be calculated out of their absolute distances to each other. Although the targets should be placed in a way, so that they form a rectangle, this could not be done with high precision in reality. The points would rather form a polygon, as demonstrated in Figure 7.10. However, the calculation of

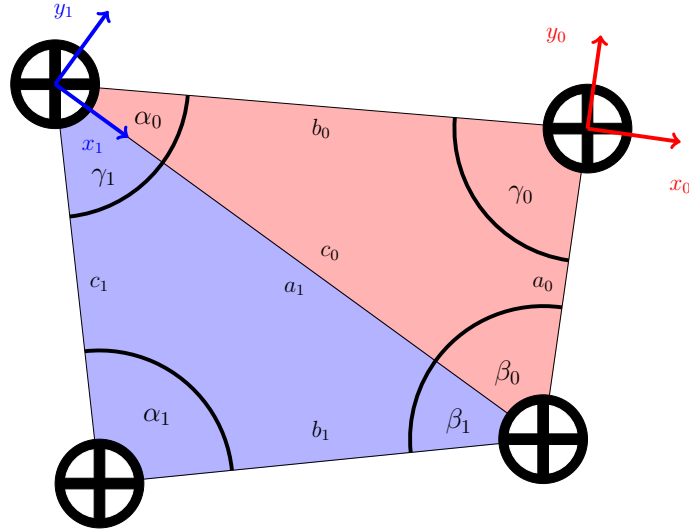


Figure 7.10: Calculation of world coordinates from absolute distances

the Cartesian coordinates has to be possible, according to the rule of congruence for triangles with three known side lengths. Therefore, an algorithm has been developed, which calculates the Cartesian coordinates out of the absolute distances of the points.

First of all, the targets should be placed roughly in a rectangular shape. From the resulting polygon, triangles have to be formed as shown in Figure 7.10. Starting with the most upper left target, all distances to the *next left*, *next lower* and *next right lower diagonal* targets have to be measured, for all targets. If there exists no target at any side, then the distance does not have to be evaluated. The origin of the world coordinate frame is formed by the

most upper right target. The z-axis is pointing out of the ground plane and the y-axis is parallel to the line, formed by the origin and the most right, second most upper target (red coordinate frame in Figure 7.10). Then, the coordinates of two points are known directly, namely the origin (0,0) and the target below the origin (0,- a_0). Knowing the side lengths and the coordinates of two points, the coordinates of the remaining point of the triangle can be calculated. However, the algorithm distinguishes between the calculation of an *upper* point (red triangle in Figure 7.10) and a *lower* point (blue triangle in Figure 7.10), with respect to the two known points of the triangle. The notation of the angles and side lengths should be done according to Figure 7.10. Then, depending on the type of the points, the following algorithm is performed:

Upper Case

$$\begin{aligned}\cos \gamma_i &= \frac{a^2 + c^2 - b^2}{2ac} & \sin \gamma_i &= \sqrt{1 - \cos^2 \gamma_i} \\ \cos \varphi_i &= \frac{P_{1,y} - P_{2,y}}{a} & \sin \varphi_i &= \frac{P_{1,x} - P_{2,x}}{a} \\ \tilde{P}_3 &= \begin{pmatrix} -c \sin \beta_i \\ c \cos \beta_i \end{pmatrix} \\ P_3 &= \begin{pmatrix} \cos \varphi_i & \sin \varphi_i \\ -\sin \varphi_i & \cos \varphi_i \end{pmatrix} \tilde{P}_3 + P_2\end{aligned}$$

Lower Case

$$\begin{aligned}\cos \beta_i &= \frac{a^2 + b^2 - c^2}{2ab} & \sin \beta_i &= \sqrt{1 - \cos^2 \beta_i} \\ \cos \varphi_i &= \frac{P_{1,y} - P_{2,y}}{a} & \sin \varphi_i &= \frac{P_{1,x} - P_{2,x}}{a} \\ \tilde{P}_3 &= \begin{pmatrix} b \sin \beta_i \\ b \cos \beta_i \end{pmatrix} \\ P_3 &= \begin{pmatrix} \cos \varphi_i & \sin \varphi_i \\ -\sin \varphi_i & \cos \varphi_i \end{pmatrix} \tilde{P}_3 + P_2\end{aligned}$$

The remaining point of the triangle is denominated with P_3 , whereas the both known coordinates are denoted with P_1 and P_2 . The coordinates of the points are labelled with an appropriated index.

Clearly, the algorithm is general, so that the coordinates of the targets forming any roughly rectangular pattern can be determined out of the determined distances to each other, even if the pattern contains more than four points. With the additional knowledge of the world coordinates of the calibration pattern, the world-to-image point-correspondences are complete, so that the extrinsic calibration can be performed afterwards.

7.4.2 Image-to-World Projection

Whereas the world-to-image projection is fully described by the camera model, the image-to-world projection requires the inverse mapping. However, the camera model is dropping

the information of one dimension. That is why the mapping is not bijective and the camera model can not simply be inverted. Nevertheless, rays in 3D space can be obtained from image coordinates [HZ04]. As soon as the plane, the point should lie on, is known, the 3D coordinates can be obtained by the intersection of the plane and the determined ray.

Before the image-to-world projection can be performed, the image should be undistorted, according to the distortion parameters k_i (section 2.2.2). A virtual pinhole camera, with the new intrinsic matrix $\tilde{\mathbf{K}}$, is created, which should be valid for all points in the image. The world-to-image projection can then be described with [HZ04]

$$\mathbf{x} = \tilde{\mathbf{K}}[\mathbf{R}_{\text{World}}^{\text{Cam}} | \mathbf{t}] \mathbf{X}$$

in this case. The corresponding ray \mathbf{d}^{Cam} , represented in the camera's frame, can be obtained by multiplication with the inverse of the camera matrix $\tilde{\mathbf{K}}$:

$$\underbrace{\tilde{\mathbf{K}}^{-1} \mathbf{x}}_{\mathbf{d}^{\text{Cam}}} = [\mathbf{R}_{\text{World}}^{\text{Cam}} | \mathbf{t}] \mathbf{X}$$

Furthermore, the ray should be normalized and represented in the world coordinate frame.

$$\begin{aligned} \mathbf{d}^{\text{Cam}'} &= \frac{\mathbf{d}^{\text{Cam}}}{\|\mathbf{d}^{\text{Cam}}\|} \\ \mathbf{d}^{\text{World}} &= \mathbf{R}_{\text{Cam}}^{\text{World}} \mathbf{d}^{\text{Cam}'} \end{aligned}$$

The resulting equation of a line in 3D space is only dependent on one parameter α

$$\Rightarrow \mathbf{x}(\alpha) = \mathbf{t}^{\text{World}} + \alpha \cdot \mathbf{d}^{\text{World}}$$

If the plane is known, which could be, without loss of generality, a plane parallel to the worlds $x - y$ -plane with known z -coordinate

$$Z = Z_0,$$

the independent parameter α can be calculated

$$\alpha = \frac{Z_0 - \mathbf{t}^{\text{World}}_z}{\mathbf{d}^{\text{World}}_z}$$

and finally the 3D point obtained by inserting the found parameter in the equation of the line:

$$\mathbf{x}^{\text{World}} = \mathbf{t}^{\text{World}} + \frac{Z_0 - \mathbf{t}^{\text{World}}_z}{\mathbf{d}^{\text{World}}_z} \cdot \mathbf{d}^{\text{World}} \quad (7.4)$$

7.4.3 Accuracy of Target Determination

Before a measurement can be performed, the accuracy of the operation has to be evaluated or estimated. The detection algorithm has a certain accuracy for the detection of the centre of the targets (Figure 7.8). Depending on the distance of the camera to the targets, this would lead to an error to greater or less extent, in terms of distance of the back projection. However, there are many other sources of error, like the possible inaccurate determination of the position of the targets on ground and the accuracy of the PnP algorithm, to mention only a few. An error

analysis would be a tricky task, in this case. Hence, the errors of the participating algorithms are not identified separately, but are not of interest neither. That is why it was decided, to make a test measurement, in which the targets positions are known, so that the results can be evaluated. The record of the video was done from a similar height, the drone was expected to have during the real experiment. In detail, the frames were taken from the third floor of a building, whereas the targets were placed on the ground floor, corresponding to a height difference of roughly 12.7 m. During the record, the camera was moved around in order to simulate conditions of the real experiment and to test their influences to the accuracy. The

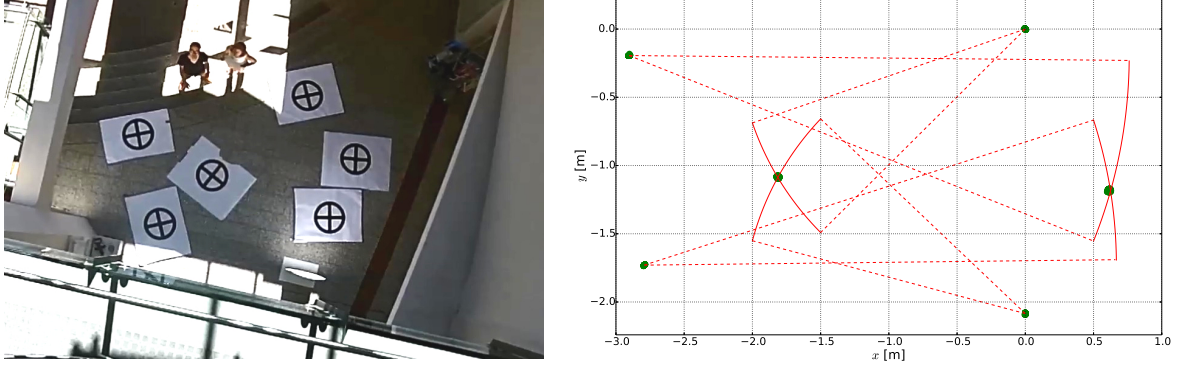


Figure 7.11: Detected points of accuracy measurement

left picture in Figure 7.11 shows a frame from the recorded video. Six targets were used, in which four are responsible for the extrinsic calibration and two should be determined by the algorithm. The right picture in Figure 7.11 shows all detected points for all frames, marked in green. The fact, that no target has a wide spread blob, can be treated as a confirmation of the reached accuracy.

The coordinates of both targets, which should be determined by the algorithm, were identified on ground, too, making a comparison of the detection algorithm to a reference possible. The following procedure was used: with the distance to two of the calibration targets, their position can be found via triangulation. The dashed red lines in Figure 7.11 show the radii of the points to the corresponding calibration target. The resulting arcs are presented with a red continuous line. Their intersection points mark the determined position of the targets. From a visual point of view, the detected targets match the intersections very well. Nevertheless, the centre the right-most target's blob has a slight deviation from its corresponding crossing. The effect arises certainly due to the location of the point with respect to the camera's centre. For both points, x-error, y-error and absolute error, with respect to the expected coordinate, are depicted in a histogram, with the use of the detected points from all frames of the record. The result for the point in the centre can be seen in Figure 7.12, the result for the right-most point in Figure 7.13. From left to right, the errors are shown in the same order, as mentioned above. For the binning of the green columns, the square-root of the number of points was used. The dashed line, marked in red, represents an idealized normal distribution with the mean error, marked in blue. Clearly, beside the standard deviation of the error, there exists an offset, represented by the mean value. This offset can be interpreted as a systematic error of the algorithm, whereas the standard deviation is a pure statistical error. The results for both points are presented in Table 7.1. The worst case would lead to a total error of approximately 16 mm. However, this is absolutely sufficient for the planned measurement.

Nevertheless, it should not be forgotten, that the targets, located at the top of the trailer will have a certain height above the ground. In order to be able to evaluate the deviations, resulting by the back projection of a certain height Z_0 , according to equation 7.4, a further

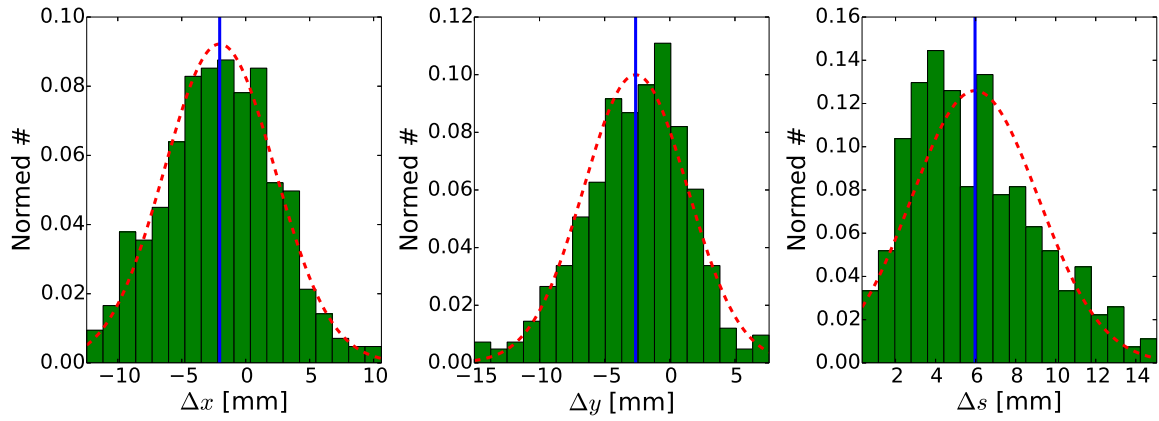


Figure 7.12: Mean error histogramm of the point in the centre

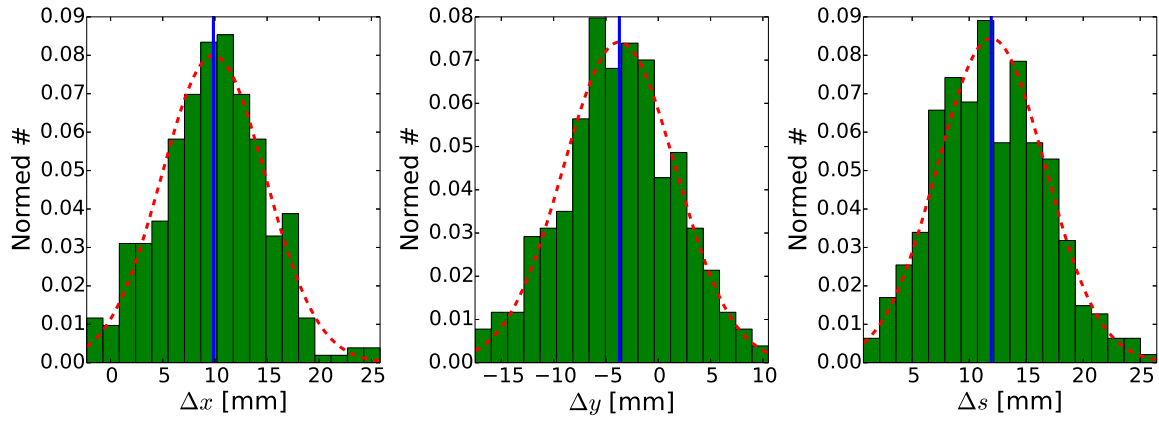


Figure 7.13: Mean error histogramm of the right-most point

test measurement was performed, but this time raising the right-most target to a height of 0.53 m above the ground. The corresponding histogram can be seen in Figure 7.14. The maximum deviation is slightly above the result for the case, when the targets were placed on ground. A maximum deviation of 27 cm, as depicted in Table 7.1 is still tolerable.

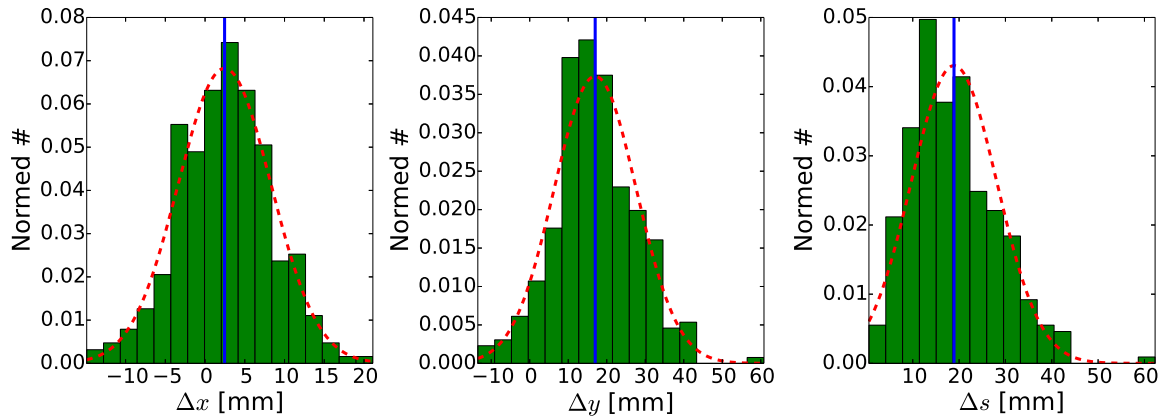


Figure 7.14: Mean error histogramm of the right-most point at a height of 0.53 m

Table 7.1: Accuracy results of both points on the floor and the right-most point at a height of 0.53 m

point	parameter	Δx	Δy	Δs
centre, ground	μ	-2.0 mm	-2.6 mm	6.0 mm
	σ	4.3 mm	4.0 mm	3.2 mm
right,ground	μ	9.9 mm	-3.7 mm	11.9 mm
	σ	5.0 mm	5.4 mm	4.7 mm
right, h=0.53 m	μ	2.5 mm	17.0 mm	18.9 mm
	σ	5.8 mm	10.7 mm	9.3 mm

7.4.4 Trajectory Comparison

After the image-to-world projection, a set of 3D-points is available, from which the x-y-plane coordinates are of interest only, due to the convention of the vehicle's moving plane. The set can be grouped according to the trajectories of the individual targets. Although the time information of the trajectories is not of interest, what would lead to the actual designation of *path*, the available sets of 2D-points will be called trajectories in this section, in the style of [RMJ07] [Rod09]. The subsets of measured points have to be compared to the predicted trajectories, also forming discrete 2D-point sets, due to the discrete implementation. However, it turns out, that the comparison of point sets is not as easy, as one might expect.

The first step towards the comparison is to bring the point sets to the same coordinate frame. While the predicted trajectories are described with respect to the centre point of the rear axle of the towing vehicle, the measured coordinates are related to the set origin, which is the upper right most target on the ground (see section 7.4.1 and Figure 7.10). Beside the targets on the trailer, two targets were attached to the car as well (see Figure 7.9), whose coordinates with respect to the tractor reference frame were determined in advance. With the help of the measurement of the drone video, these two points are known in the ground target reference frame as well. Having two point correspondences, the linear mapping, consisting of rotation and translation can be calculated and is further unique. With the obtained mapping, the points, gained by the video measurement of the drone were transformed to the tractor reference frame.

After the remapping the comparison is still a tricky process, for which no unique solution exists. Because of the lack of standard methods, trajectories are only compared qualitatively from their plots in most of the scientific literature [Rod09]. However, a qualitative check is not enough for the validation of the tractor-trailer system's model. Some investigations on trajectory comparison methods are though available in the literature, albeit not many. Roduit et al. have described some methods with the background of trajectories for mobile robots. The basis is formed by the description of a trajectory as a set of points, possibly extended by the related time [Rod09]. Since only the path of the tractor-trailer system is of interest, trajectories with time information will not be further investigated.

Even by having two sets of points, which should be compared, the question arises, what to compare and how. As an initial guess, the absolute distances of the points could be calculated. But due to the lack of the time information, it is no clear, which points of the two sets are causally related, so that their distance would have an actual meaning. The orthogonal distances could be evaluated, where orthogonal refers to only one of the two sets of points. The intersection of the resulting normal line with the remaining set of points forms the distance in that case. However, this scenario is quite tricky, since the normal line of a discrete point set is not easy to calculate.

In contrary, the methods proposed by Roduit et al. seem quite handy. For all methods, the keyword is sampling. In the first paper, a space-based sampling method along gates is described [RMJ07]. Gates are formed between boundary walls, in which the trajectory has to be situated. Necessarily, every trajectory crosses the vertical lines between the walls. At these points, the trajectories can be compared. In the case of the path of the tractor-trailer system, this method is not possible, since boundary walls were not present during the experiment. Further sampling methods are described in the resulting thesis of Roduit [Rod09]. Moreover, a method based on the area between two trajectories is described. Albeit this method seems quite reasonable for the researching problem, the total area only gives a scalar measure, which could be hardly evaluated in terms of goodness of the prediction.

In the end, a method in the style of the gate sampling [RMJ07] was developed. The absence of boundary walls was overcome by the fact, that each corner of the trailer was marked by a target. Hence, four trajectories for the trailer were available. Especially, the two rear corners were investigated. Their intersection line is orthogonal to the centre trajectory of the trailer. In the end, only the orthogonal deviation from the centre point is of interest, because the prediction should show for example, if a trailer fits into a parking spot or not. The main idea of the method is visualized in Figure 7.15. The blue markers depict the measured points of an example scenario of the rear left corner of the trailer whereas the violet markers represent the rear right corner respectively. The according predicted trajectories are drawn in orange with a continuous line. Each pair of left and right corner targets along the trajectories is connected and the resulting line extrapolated. If an intersection with the predicted trajectory occurs (green line in Figure 7.15), the absolute distance between the intersection point and the measured coordinate is calculated and treated as the difference of the trajectories at a given travelled distance. Clearly the distance is evaluated at every side of the trailer, labelled with Δ_l and Δ_r respectively. Nevertheless, it may occur, especially at the beginning and the end of the trajectories, that the extrapolated line will not cross the predicted trajectory (red line in Figure 7.15). In these cases, the deviation is simply not evaluated.

Beside the rear corners of the trailer, the front corners could have been investigated as well.

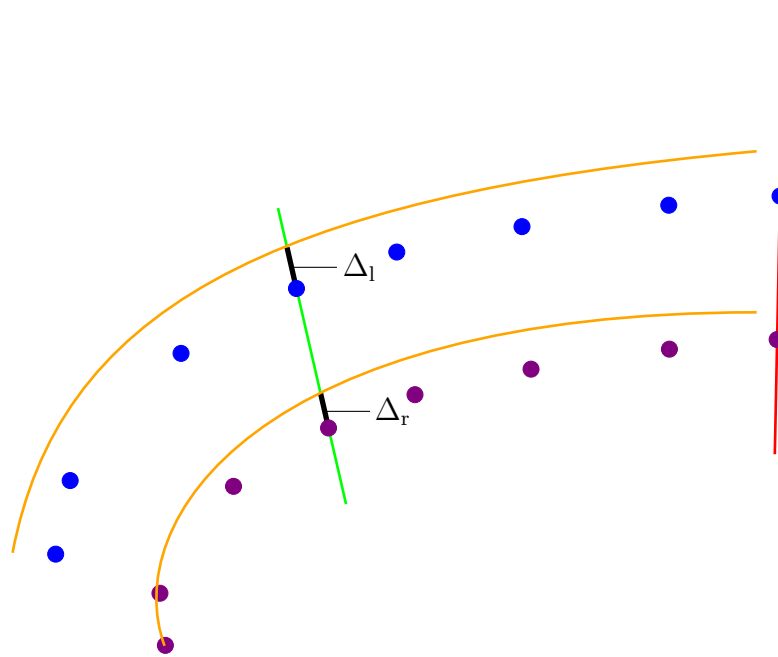


Figure 7.15: Method of trajectory comparison

However, the comparison of these trajectories were disregarded, since mainly the distance at the rear side is of interest in the actual application. The trajectories of the tractor have not been compared, too, because the targets were attached along the longitudinal axis of the car, so that the new method could not be applied. An additional method would have been necessary, whose development was regarded as an overkill for the actual problem.

7.4.5 Results: Single-Axle Trailer

For every scenario, two plots have been generated, showing the measured points versus the predicted path of the tractor-trailer system as well as the absolute difference of the trajectories, obtained by the algorithm described in section 7.4.4. Special attention is paid to the highlighting of the critical deviations, discussed in section 7.1. The yellow line indicates 10 cm deviation, whereas the red line signifies the critical deviation of 20 cm. Due to the huge space demand of the plots, they were placed in the appendix (Figure 10.1 - 10.6). Moreover, every figure is a bundle of one scenario, showing the lateral speed of the rear axle of the towing vehicle on top, followed by the just mentioned plots. In this section, only the two last plots of Figure 10.1 - 10.6 are of interest.

Again, the predicted paths are a result of an estimated initial kink angle. Due to the fact, that sensor data from the system as well as data from the drone record were used, two different time counting units were present. This makes the shift of the starting point of the prediction to the time, when the kink angle was delivered first, as it was done in the kink angle development analysis, quite impossible. The time synchronisation between two independent systems is a tricky and time consuming task. That is why it was decided to estimate the initial kink angle from the measured data points, which are obtained by the record of the drone: The angle between the line, formed by the two targets of the tractor, and the lines, formed by the connection of the rear targets and the front targets of the trailer were calculated. This led to two kink angles. The used kink angle was calculated by the mean of both. Clearly, this is only an estimation of the kink angle, since the method is very error sensitive. A slight inaccuracy of the targets' positions, would lead to a great error in the estimated kink angle. The usage of the mean of both determined kink angles was used for an error reduction. Still, prediction was done and the subsequent comparison to the data points performed. Clearly, this method can lead to a deviation of the trajectories, even, when the system has not started driving. Nevertheless, this represents the reality quite good, because it may occur, that the kink angle measurement is not precise, so that a trajectory prediction has to be done from an inaccurate measurement. In cases of large deviations even for the first detected points, the initial kink angle was adapted manually. Otherwise, the error of the kink angle estimation would have exceeded the actual inaccuracy of the model.

In contrast to the kink angle development analysis, a short note shall be done for every scenario. The summary with the most important information is, however, outlined in Table 7.2.

Scenario: $\varepsilon \approx 0^\circ$, $\kappa_1^0 \approx 0^\circ$ The qualitative analysis shows, that the prediction is only accurate for the first few metres. The further the system moves, the greater gets the deviation from the prediction. A large influence is clearly the inaccuracy of the steering model. If one has a look at the measured data points of the tractor and their prediction paths (Figure 10.1), one has to conclude, that even the model of the tractor has a certain deviation. A reason can be a inaccurate steering angle. Still, the defined requirements are kept: At a driven distance of 3 m, the deviation is only 4 cm for both sides, which is better than expected, based on the

results of the kink angle development in the previous section. For this scenario, the initial kink angle was adapted manually.

Scenario: $\varepsilon \approx 90^\circ$, $\kappa_1^0 \approx 0^\circ$ Both path sets, namely the one describing the tractor and the one describing the points of the tractor, are coinciding with the prediction very accurately. Over the total driven distance of 5 m, the lateral deviation is never exceeding 4 cm (Figure 10.2). The goodness of the steering model in this range lead to the good results of the whole tractor-trailer system in this scenario.

Scenario: $\varepsilon \approx -90^\circ$, $\kappa_1^0 \approx 0^\circ$ The corresponding scenario in the opposite direction shows nearly the same accuracy. Only when approaching large kink angles, the lateral deviation is increasing considerably. The steering model is quite accurate as well, as depicted in the plot in the centre of Figure 10.3. For this scenario, the manual adaptation of the initial kink angle was required. The result is, that the constraints are met with a large margin of safety.

Scenario: $\varepsilon \approx 180^\circ$, $\kappa_1^0 \approx 0^\circ$ Similarly to the results for a steering angle of 90° , this scenario shows very good results, too. Even after the prediction length of 3 m, the accuracy is far below 10 cm (Figure 10.4).

Scenario: $\varepsilon \approx -180^\circ$, $\kappa_1^0 \approx 0^\circ$ Unfortunately, the top-view record was not suitable for the developed algorithm, so that the analysis of this scenario could not be performed.

Scenario: $\varepsilon \approx 490^\circ$, $\kappa_1^0 \approx 0^\circ$ In section 7.3, it was found, that the steering model leads to the strongest deviations, for the maximum steering wheel angles, in both directions. The centre plot in Figure 10.5 confirms this fact again. Although the initial kink angle was adapted manually, the deviation grows enormously towards the maximum kink angle, so that the constraints are not kept any more. Clearly, the model of the tractor shows a stronger steering angle, resulting in a faster increasing kink angle. Maybe the constraints have to be loosened at very large kink angles. The model seems clearly not valid any more. Certainly, dynamic effects start to influence the system more than expected for these configurations. Still, until a certain limit of the kink angle, the prediction is tolerable. Moreover it has to be mentioned, that the used method for the comparison of trajectories is leading to strong deviations, if the trailer has a large kink angle. Its path is clearly forming a loop, so that the calculated distances to the model increase. That is why the deviations may be overrated for this scenario.

Scenario: $\varepsilon \approx -490^\circ$, $\kappa_1^0 \approx 0^\circ$ Obviously, the model lead to better results for this scenario than for the scenario in the opposite direction. Although the initial kink angle had to be adapted manually, the results are very accurate. Nevertheless, the steering angle is overestimated again (Figure 10.6), that is why the predicted rate of change of the kink angle is higher than in reality. It may be the case, that the axle angle of the towing vehicle is influenced by the attached trailer. Nevertheless, strong deviations only occur at high steering angles. Even for this scenario, the constraints are kept.

Table 7.2: Results of the absolute deviation for a single-axle trailer

Scenario	Maximum occurred deviation Δ at $s = 3$ m or maximum kink angle	Constraints met
$\varepsilon \approx 0^\circ, \kappa_1^0 \approx 0^\circ$	4 cm	✓
$\varepsilon \approx 90^\circ, \kappa_1^0 \approx 0^\circ$	2 cm	✓
$\varepsilon \approx -90^\circ, \kappa_1^0 \approx 0^\circ$	3 cm	✓
$\varepsilon \approx 180^\circ, \kappa_1^0 \approx 0^\circ$	4 cm	✓
$\varepsilon \approx 490^\circ, \kappa_1^0 \approx 0^\circ$	27 cm	✗
$\varepsilon \approx -490^\circ, \kappa_1^0 \approx 0^\circ$	15 cm	✓

7.4.6 Results: Two-Axle Trailer

The absolute analysis of the driven path for the two-axle trailer was executed for the model of the mean axle (3.2) only, due to its better results in the kink angle analysis. Again, a short comment is done for every scenario. The most important results are outlined in Table 7.3.

Scenario: $\varepsilon \approx 0^\circ, \kappa_1^0 \approx 0^\circ$ The algorithm was not able to analyse the data of this scenario. However, it is expected, that the results are slightly better than for the experiment with the single-axle trailer, due to the results of the kink angle analysis in section 7.3.

Scenario: $\varepsilon \approx 90^\circ, \kappa_1^0 \approx 0^\circ$ Although the initial deviation measures 3 cm already, the constraints were met during the whole test drive (Figure 10.7). Even the desired constraints of a maximum deviation of 10 cm was met. The tractor points were predicted precisely, too.

Scenario: $\varepsilon \approx -90^\circ, \kappa_1^0 \approx 0^\circ$ The equivalent scenario in the opposite direction shows the same results (Figure 10.8). Here, the desired deviations are kept, too.

Scenario: $\varepsilon \approx 180^\circ, \kappa_1^0 \approx 0^\circ$ With an increasing steering angle, the deviation of the model increases, as it occurred for the single-axle trailer already. However, the increase of the deviation does not begin before large kink angles are reached. The results indicate a phenomenon, which only occurs for a multi-axle trailers. Whereas the model of the single-axle trailer predicted a rate of the kink angle, which was too strong on average, the rate of change, predicted by the model, is too small in this case. Two reasons have been figured out, which could declare this phenomenon. First, an additional axle brings more stability to the system. That is why the kink angle rate could have been underestimated. Secondly, the trailer was slightly inclined during the experiment. A dislocation of the generalised axle towards the first axle, would lead to a behaviour, where the kink angle rate is higher. The smaller the distance from the junction to the (generalised) axle is, the larger is the rate of change of the kink angle. Nevertheless, all constraints were met for this scenario, as depicted in Figure 10.9.

Scenario: $\varepsilon \approx -180^\circ, \kappa_1^0 \approx 0^\circ$ Literally, the discussion of the previous discussed scenario could be copied for this scenario. Figure 10.10 shows the according results.

Table 7.3: Results of the absolute deviation for a two-axle trailer

Scenario	Maximum occurred deviation Δ at $s = 3$ m or maximum kink angle	Constraints met
$\varepsilon \approx 90^\circ, \kappa_1^0 \approx 0^\circ$	9 cm	✓
$\varepsilon \approx -90^\circ, \kappa_1^0 \approx 0^\circ$	3 cm	✓
$\varepsilon \approx 180^\circ, \kappa_1^0 \approx 0^\circ$	12 cm	✓
$\varepsilon \approx -180^\circ, \kappa_1^0 \approx 0^\circ$	13 cm	✓
$\varepsilon \approx 490^\circ, \kappa_1^0 \approx 0^\circ$	8 cm	✓
$\varepsilon \approx -490^\circ, \kappa_1^0 \approx 0^\circ$	15 cm	✓

Scenario: $\varepsilon \approx 490^\circ, \kappa_1^0 \approx 0^\circ$ The indication of the discussion of the previous experiments is confirmed in this scenario: the rate of the kink angle is slightly underestimated (Figure 10.11). Nevertheless, the constraints are met with a high precision.

Scenario: $\varepsilon \approx -490^\circ, \kappa_1^0 \approx 0^\circ$ The opposite scenario shows nearly the same behaviour, resulting in slightly greater deviations only (Figure 10.12). Still, all the requirements were met.

7.5 Conclusion

Several different methodologies have been performed, in order to investigate the derived model (4.9). Although the methods themselves did not necessarily lead to exactly equivalent results, the overall outcome showed, that the model delivers good results for not too large steering angles as well as until a certain threshold kink angle. Still, the range of validity is large, so that the model can be applied to the rear-view application system. For trailers with multiple-axes, the model showed fairly well results, too, even though the expected model for the generalised axle had to be adapted. The deviation at large kink angles could be overcome by enlarging the drawn guidelines on the one hand, or by an abortion of the model's integration at a smaller kink angle. For the determination of a quantitative value of the abortion kink angle, further test scenarios with different types of trailer are necessary.

8 The Overall System

The goal of the thesis was to implement the system in a prototypical manner. Especially importance was attached to the projection of the driving path into the camera image, beside the static distance markers. The mounting of the camera as well as the data transfer were less emphasized. Albeit the prototypical system is running well, many issues have to be clarified before the system is ready for a serial production. This section explains however, how the system was realised in terms of hardware and human-machine interface and further how it behaves under real test conditions.

8.1 Integration

Even if done in a prototypical manner, the camera had to be attached to the trailer's rear side. Since all of the test trailers were of box type and most other trailers have a similar shape as well, it was decided to construct an attachment, which can be hooked into the trailers rear barrier of the box. Figure 8.1 shows the mounting system of the camera. Two bars can be set tight with the help of locking screws, in order to guarantee a fixed pose of the camera with respect to the trailer. The camera itself is fixed at the front side of the mounting. With the help of a rotatable truss, the camera's inclination can be adapted. An angle of 45° with respect to the ground should be aimed at, in order to maximise the field of view of the ground. In Figure 8.9, the camera attachment is shown during a real experiment.

Another problem is the data transfer between the camera system at the rear side of the trailer and the communication unit inside the tractor. Beside the transfer of the camera image, the camera unit has to be powered with electricity as well. The electrical power supply is not tricky to implement, since the trailer is provided with electricity and signals via a standard socket. Theoretically, the power supply could be tapped from the trailers supply. However, in the prototypical implementation, engagements to the hardware of the trailer should be avoided, so that the camera unit was powered from the tractor unit via a long cable (see Figure 8.2). The transmission of the camera's image was done via Ethernet technology, according to its almost independence on transmission distance. Due to the lack of a digital communication port in the connection socket between trailer and tractor, a long cable was used as well, which is able to bridge the gap between trailer and towing vehicle (see Figure 8.2). However, the integration into the standard socket of the trailer is necessary for further applications and would therefore form an interesting topic to investigate. Yet, this issue is clearly beyond the scope of this thesis, so that it is not investigated further.

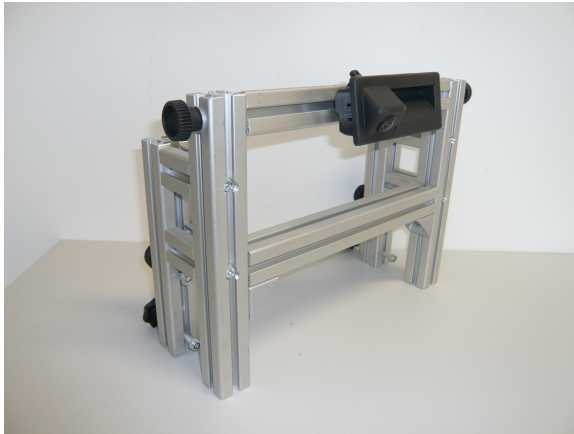


Figure 8.1: Mounting system of the rear view camera

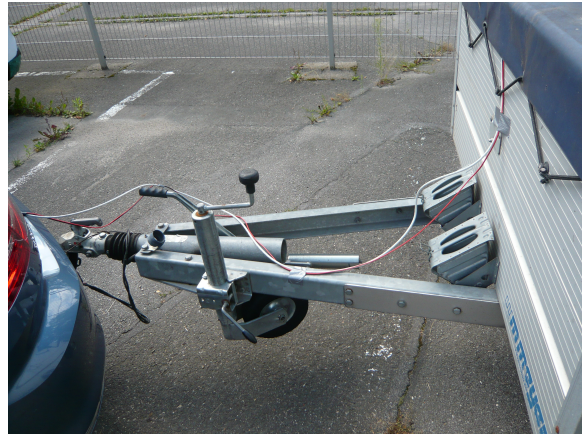


Figure 8.2: Wiring of the rear view camera

The most important section of the system is the human-machine interface (HMI), giving assistance to the driver. There should be no doubt, that the rear camera image including the overlays should be presented in any way. For a correct representation of the camera image and the superimposition of the guidelines, a calibration of the camera was necessary. The intrinsic parameters were determined using the method described in section 7.4.1. A correct projection of the guidelines was possible with the help of the formulas, derived in chapter 5. Attention should be paid to the overlays, namely the static distance markers and the driving path. As shown in Figure 8.3 and 8.4, the 1 m distance line is represented by a frame, coloured in green, whereas the 30 cm distance line is coloured in red, pointing out, that the system is close to a collision. In contrast, the driving corridor of the corresponding sub-vehicle, where the camera is mounted, is displayed in an orange colour, but only, if the rear gear is activated. Additional horizontal lines indicate, which points on the left and right guideline belong together. While this issue is clear for the driving path of an individual tractor, the trailer might turn in place, so that the associated points may not be figured out ad hoc. On top of that, the horizontal lines can form a great helping tool, if the trailer shall be placed parallel or perpendicular to a kerb stone edge or the marking of a parking spot. The distances between the horizontal lines represent equal driven sections of the towing vehicle.

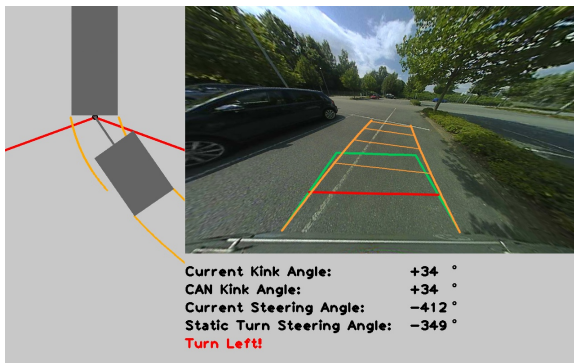


Figure 8.3: HMI - enabled Bird's Eye view and undistorted camera image

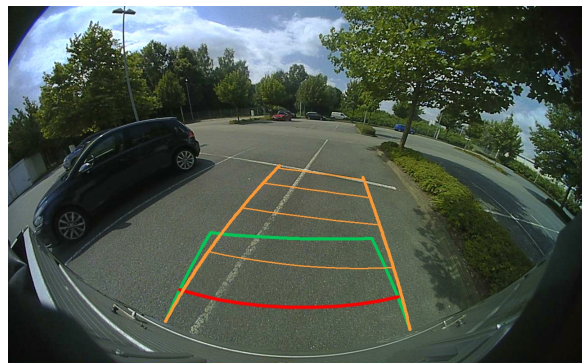


Figure 8.4: HMI - disabled Bird's Eye view with raw camera image only

However, it was decided to provide further support to the driver by an animation of a Bird's Eye view. Out of habit, the driver may concentrate on the camera image only, forgetting that the tractor can collide with the trailer's drawbar. With the help of the animation of the Bird's Eye view, the operator can control the kink angle while manoeuvring, so that the likelihood

of a collision can be reduced. Additionally, the Bird's Eye view shows the critical kink angle, discussed in section 6.5. The representation is done by two red lines, attached to the tractor's hitch, so that the angular difference to the trailer's drawbar can be assessed better.

Compared to the rear view image, the Bird's Eye view is showing the driving paths of every sub-vehicle. The required space for manoeuvring can be estimated better, if a top-view of the sub-vehicles paths is provided. Clearly, an image constructed from real camera images would be a better solution, as it is shown in Ehlgen's analysis [EPA08]. Although the Bird's Eye view is a helpful assistant, the driver has still the opportunity to disable the animation, in order to enlarge the camera's image inside the display. Another possibility is, to display the rear view image in a distorted or in an undistorted fashion. Figure 8.3 shows the undistorted rear view image together with the Bird's Eye view animation. With different settings, the scene illustrated in Figure 8.4 would appear to the driver, representing the raw rear view image only (distorted), but covering the maximum field of view (FOV), the camera is able to deliver.

If the Bird's Eye view animation is activated, the driver receives additional system information and manoeuvring hints, displayed below the rear view image (see Figure 8.3). The current kink angle and steering angle are retrieved from the CAN bus directly. If the quality of the kink angle raw value is below a certain threshold, the system predicts the kink angle based on the model (4.9) and the current system state. That is why the kink angle is displayed twice. Another displayed information is the *Static Turn Steering Angle*, which is calculated by the system according to equation (6.3). If the computed steering angle is applied, the kink angle between tractor and trailer would theoretically remain constant. However, a threshold of $\pm 10^\circ$ is added up to the computed steering wheel angle, in order to make the hint manageable to the driver. Nevertheless, the margin will result in inaccuracies, so that the constant kink angle is only guaranteed for a short distance. Still, an only slightly changing kink angle can be a helpful advice in manoeuvring an unstable system. According to the difference of the current steering angle and the computed steering angle, the hints *Turn Left!* or *Turn Right!* are displayed in red and *Keep Steering Angle!* are displayed in green respectively.

8.2 Performance

After the analysis of the driving path in section 7.4, the investigation of the accuracy of the projection of the guidelines to the camera image in section 5.4 and the integration of the rear view system to the trailer, a final performance test was done, in order to show the functionality of the subsystems together. As it was done in the validation of the model, the performance was proven for two different trailers, namely a single-axle trailer and a two-axle trailer. Nevertheless, the tests were performed differently.

8.2.1 Single-Axle Trailer

The performance test for the single-axle trailer was executed by marking the predicted driving path, displayed in the HMI, at the ground, and comparing it to the actual driven path. The idea is shown in Figure 8.5. Before the backward drive was started, yellow marks were attached to the ground. While the backward drive was performed, red marks were drawn related to the actual position of the trailer.



Figure 8.5: Used method of performance test for the single-axle trailer



Figure 8.6: Comparison of the driving path for two different steering angles for a single-axle trailer

The results for two different scenarios are shown in Figure 8.6, one using a large absolute steering angle and the other having a steering angle of approximately 160° . The test for the latter scenario showed very good results, so that the pre-marked corridor was coinciding with the actual driven path keenly (right path in Figure 8.6). However, the scenario with the large steering angle showed deviations to a greater extent (left path in Figure 8.6). Still, the deviation appeared, when the kink angle was close to its maximum only. When the kink angle was smaller, the paths showed a good agreement. This behaviour was determined in section 7.4.6 already: Figure 10.5 depicts, that the model reaches the maximum kink angle faster, than the system does in reality. In contrast, the model shows good results for steering angles around 180° (see Figure 10.4).

8.2.2 Two-Axle Trailer

The tests for the two-axle trailers have been performed differently. In detail, two methods have been applied. During the first one, which shall be called the *targeting test* from now on, the end of one side of the predicted driving path was placed at an outstanding object on the ground. Keeping the steering angle fixed, a backward drive was performed. After all, the final position of the trailer was compared with the prediction. Nearly the same was done in the second test, but referred to a parking spot. The goal was to fit the trailer in the desired parking spot with a fixed steering angle.

Targeting Test For the targeting test, a parking spot identification number was chosen to be the target (boxed in a reddish colour in Figure 8.7 and 8.9). Figure 8.7 shows the rear view image with the driving path overlay, during the experiment. From top to bottom, the scenes indicate increasing time. Clearly, the left guideline always hits the target, which is aimed at in the first frame already.

Figure 8.9 depicts, that the trailer really had reached the target at the end of the experiment, so that a wrong representation could be excluded. Furthermore, it should be noted, that the guidelines during the tests have represented the maximum width of the trailer, but transformed to the rear end, in case the maximum width appears somewhere in between. That is why a line parallel to the outer tires was drawn in Figure 8.9, in order to support the actual placement of the guideline points in the display. Clearly, the black line intersects the end of the trailer at the target, which is boxed in red.

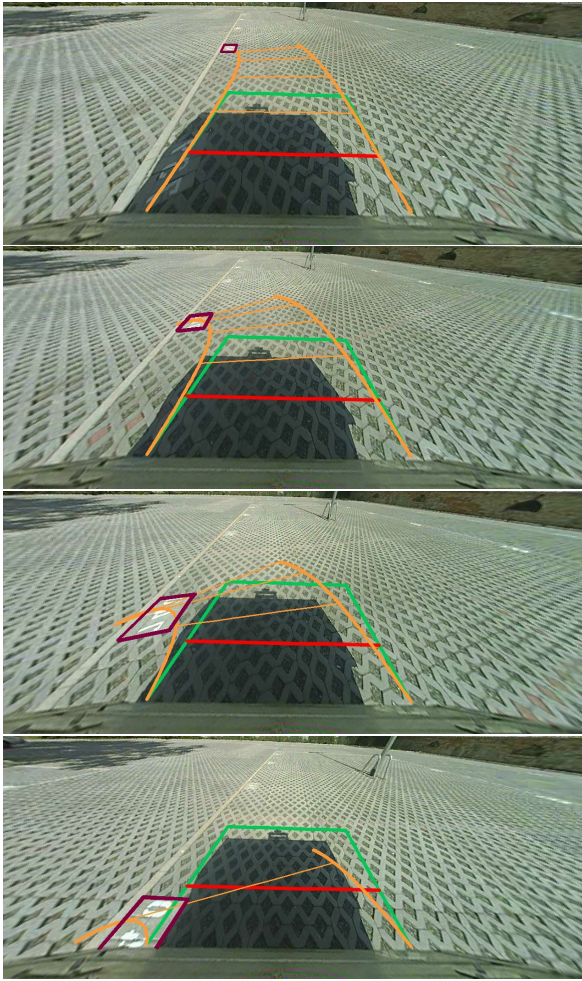


Figure 8.7: Rear view scenes during the target-
ing test: the trailer is approaching
the target (top to bottom)

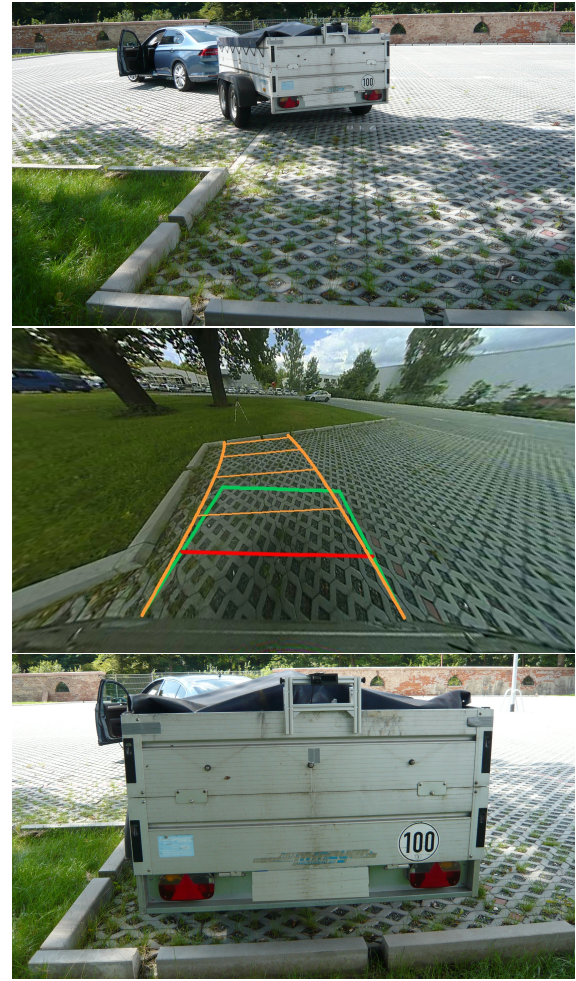


Figure 8.8: Initial position, prediction and fi-
nal position of the system during
the parking test

The second test was performed successfully as well. With a static steering angle, the trailer was manoeuvred from its initial condition (upper image in Figure 8.8) until it reached the parking spot, shown in the lower image in Figure 8.8. At its initial position, the rear view image with overlays looked like depicted in the image in the middle of Figure 8.8. It is obvious, that the prediction coincides with the final position of the trailer.

8.3 Conclusion

Several tests of the system have shown, that the rear view camera works well with respect to the set constraints. The prediction of the driving path as well as their mapping to the camera image represent the actual driving corridors, taking the defined error tolerances into account. However, a manoeuvring procedure in reality will not be based on fixed steering angles only, but rather on corrections during the driving process, during which the steering wheel has to be turned. Those scenarios are hard to test, but are, however, constructed by sequences with fixed steering angles. That is why the tests with fixed steering angles were indispensable. Several parking manoeuvres with corrections were performed as well, in which



Figure 8.9: Final position of the tractor-trailer system after the targeting test

the desired parking position was reached. Nevertheless, some additional error tolerances have to be accepted, since a changing steering angle while driving was not included in the model. Still, the system was tested successfully and has fulfilled the desired requirements.

9 Conclusion and Outlook

The thesis dealt with the prototypical implementation of a rear view camera system for a tractor-trailer combination. In order to obtain a reasonable visualisation, based on a rear-view camera image, several steps were necessary. Before the actual development had started, an extensive literature research was done, so that existing technologies in the close surroundings of the field of study could be evaluated and classified. The visualisation of the driving path, dependent on the current steering angle, requires an adequate mathematical model, which is able to predict the system's state along the driven path. The model for a system consisting of a towing vehicle including an arbitrary number n of attached trailers was derived based on the simple assumptions, that the lateral speed on every axle is vanishing (chapter 4.1). The derivation was strongly related to investigations in [Geo11], but extended to an arbitrary number of trailers. The result for an attached single-axle trailer is coinciding with stated equations in [Geo11] and moreover a generalisation for the model, mentioned in [Ada14]. A strict comparison was investigated in section 4.1.6. Since the actual influencing quantity of the kinematics of the system is the axle angle with respect to the body axle of the towing vehicle, but the steering wheel angle had been the only available data, a model for the steering system was introduced as well (section 4.2). With the help of the radii of driven circles of the tractor vehicle, the mapping between steering wheel angle and axle angle could be modelled. Before the model was derived, some simplifications of the model had to be made, which are described in chapter 3.

With the help of the derived model, a mathematical analysis of tractor-trailer combinations was possible. Especially the combination of a towing vehicle with an individual trailer was of interest and therefore investigated further. The systems reaction to several steering angles and initial conditions were studied and described in sections 6.1 and 6.2. In addition an error analysis was done for a certain system, which shows the sensitivity of the system with respect to uncertain properties (section 6.6). Beside the analysis, several interesting properties came out, which were later used for advising the operator of the tractor-trailer system.

A model of a physical system requires an investigation of its validity. Therefore, an extensive proof was performed, forming the main part of this thesis. Basically, the proof of the model was has been executed in three steps. The comparison of sensor data with the predictions of the model lead to the first confirmation, that the model seem to be valid for parking situations (section 7.2). The later comparison of the kink angle progress along the driven path with the prediction of the model lead to suitable results, too (section 7.3). In order to be able to make absolute statements about the validity of the model, a direct analysis of the resulting driving corridors has been performed (section 7.4). Before the driving path could be compared, the derivation of the equations for the calculation of the guidelines (section 5) was necessary. However, the absolute comparison had required plenty of preliminary work, before the actual analysis could be executed. In several test scenarios, the tractor-trailer system had been recorded by camera, mounted at a drone. Based on existing routines, an algorithm has been developed, which is able to extract the world coordinates of specific target

objects out of individual video frames of the recording (section 7.4.1 ff.). Its accuracy has been shown further in section 7.4.3. A technique for the comparison of trajectories, represented as point clouds suitable for the specific problem had been proposed and applied for the evaluation (section 7.4.4). Finally, the results have shown a strong validity of the model for parking situations. Two different types of trailers have been analysed, shown in section 7.4.6 and 7.4.6. Albeit equivalent models have been used widely in further investigations, a proof of its validity has not been found during the literature research. In the authors opinion, a validation had been an absolute necessity, but is still missing in the literature, except for the kink angle analysis in [EPA08].

The methods of the projection of the predicted guidelines was demonstrated and shown in section 5.3. The accompanied accuracy was analysed quantitatively in section 5.4.

A final test has shown the functionality of the overall system (chapter 8) during several parking scenarios. Especially the final test confirmed the achievement of the goals of this thesis.

9.1 Outlook

Clearly, the aim of this thesis has been fulfilled. Nevertheless, several steps are necessary, in order to make the system ready for a series production.

Although the model was tested for two different types of trailers, different test scenarios are necessary, in order to prove the overall validity for every type of trailer. The model is proposed for trains of trailers, so that a test for a tractor-trailer combination containing at least two trailers would be desirable. As a first step, a trailer with a movable axle should be investigated. Although the mean axle as an approximation for the generalised axle lead to the best results in the experiments, the situation may change according to the mass load. That is why a test with different mass loads should be conducted in the future, too. It may further confirm the single-track model together with the no-lateral-slip assumption or at least state its validity until a certain mass limit.

Still, for the executed experiments, the derived model delivered excellent results.

In addition to the validation of the model, the prototypical concept could be further integrated to the system of tractor and trailer directly. Possible extensions of the work of this thesis are clearly the integration of the data transfer and power supply to the standard sockets of trailers as well as the transfer of the developed visualisation to the standard HMI inside the tractor, to mention only a few.

Based on equation (6.3), steering hints are displayed as an additional support to the driver. The path planning methodology could be further implemented and integrated to the existing system, with the help of proposals like [MK15] and the mentioned functionality.

10 Appendix

10.1 Analysis of the Single-Axle Trailer

10.1.1 Scenario: $\varepsilon \approx 0^\circ$

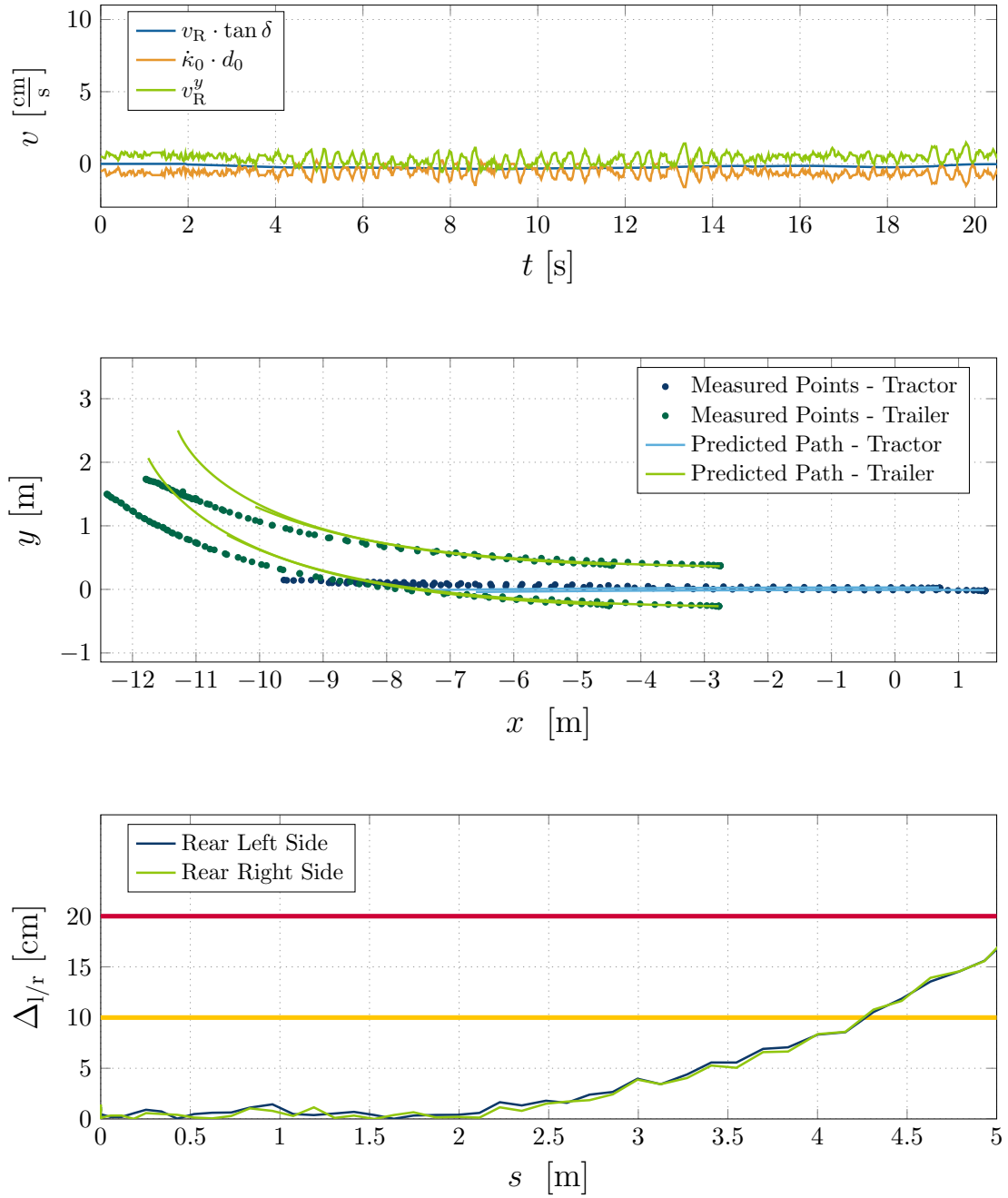
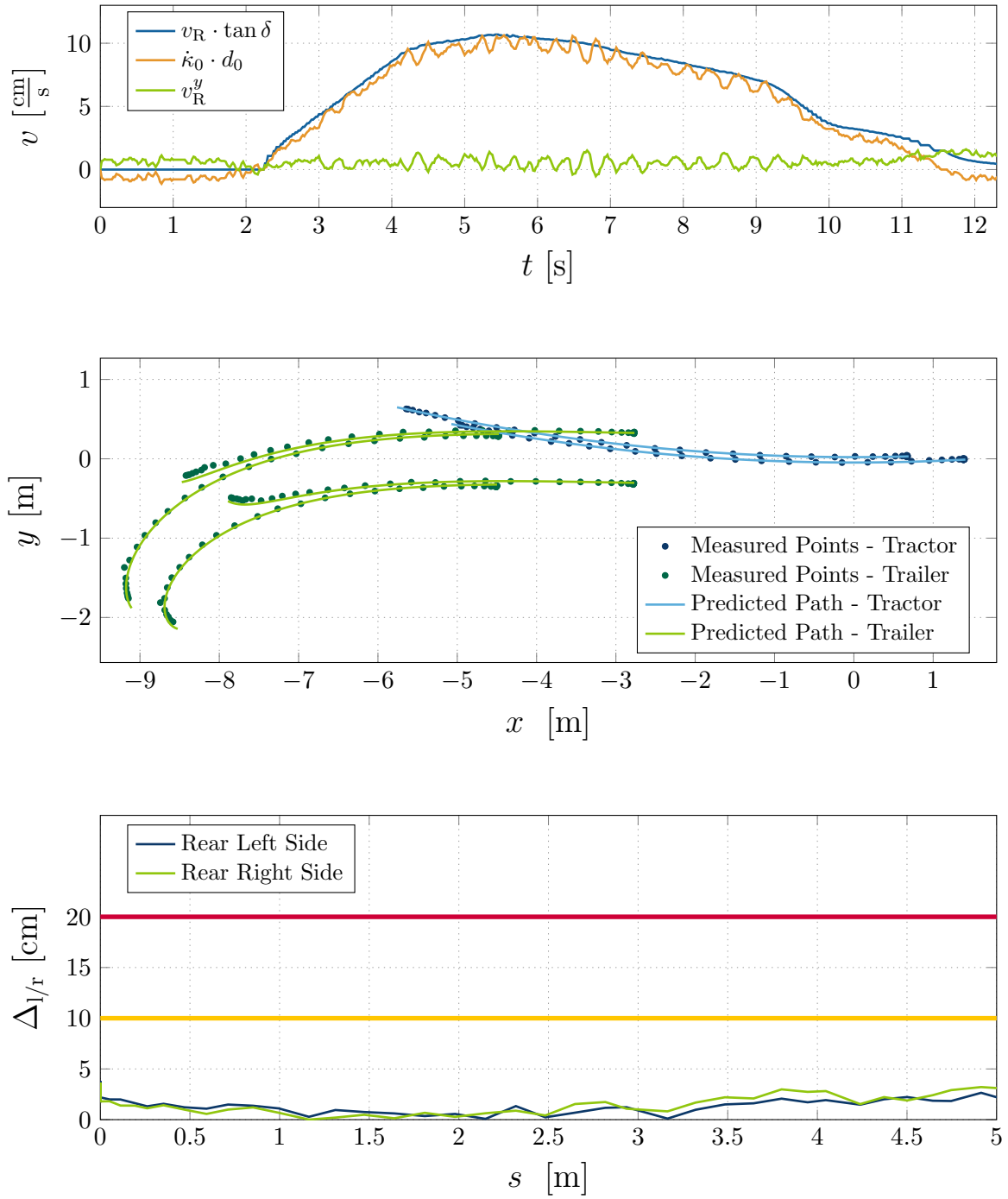


Figure 10.1: Analysis of single-axle trailer for 0° steering angle

10.1.2 Scenario: $\varepsilon \approx +90^\circ$ Figure 10.2: Analysis of single-axle trailer for $+90^\circ$ steering angle

10.1.3 Scenario: $\varepsilon \approx -90^\circ$

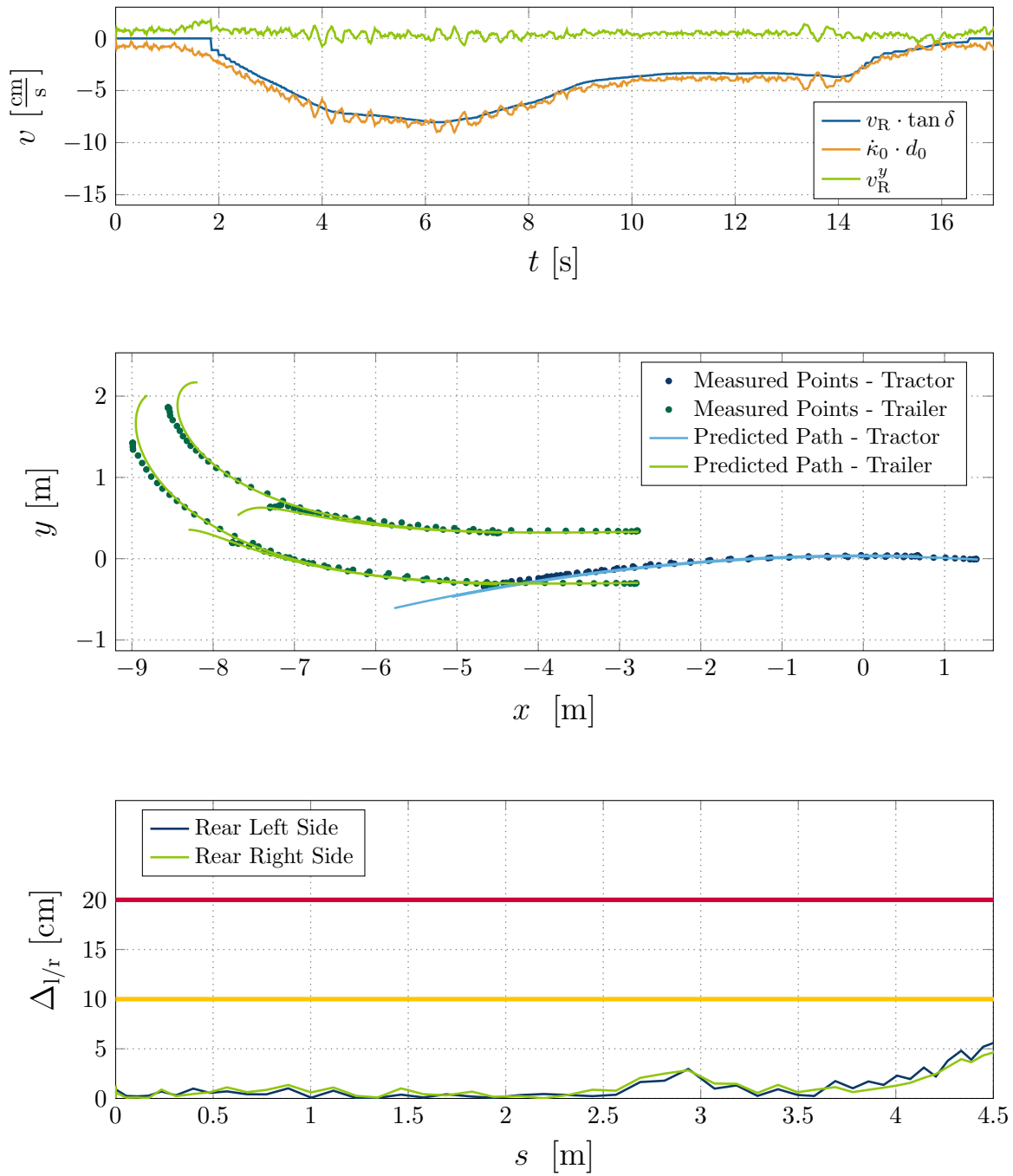
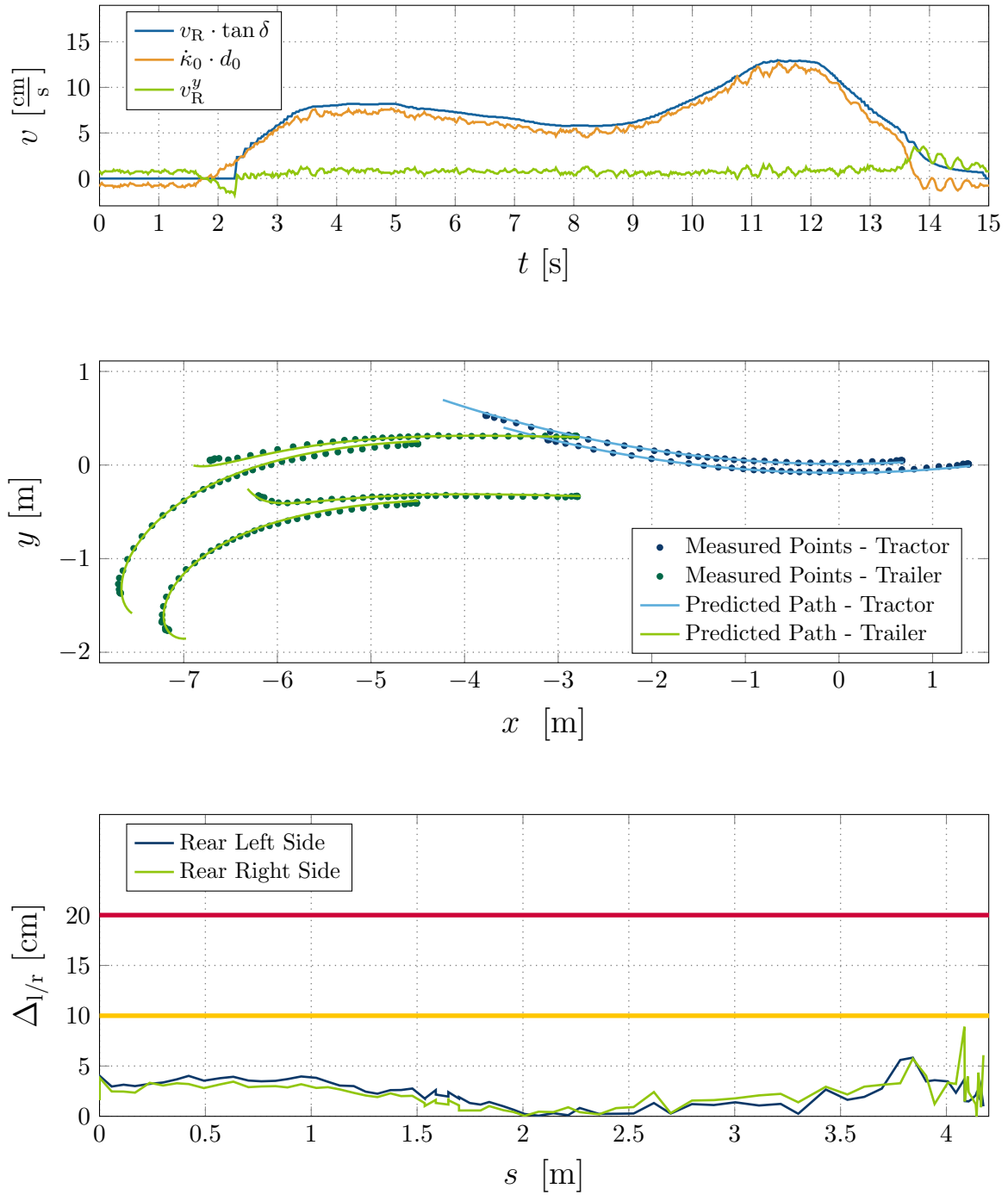


Figure 10.3: Analysis of single-axle trailer for -90° steering angle

10.1.4 Scenario: $\varepsilon \approx +180^\circ$ Figure 10.4: Analysis of single-axle trailer for $+180^\circ$ steering angle

10.1.5 Scenario: $\varepsilon \approx +490^\circ$

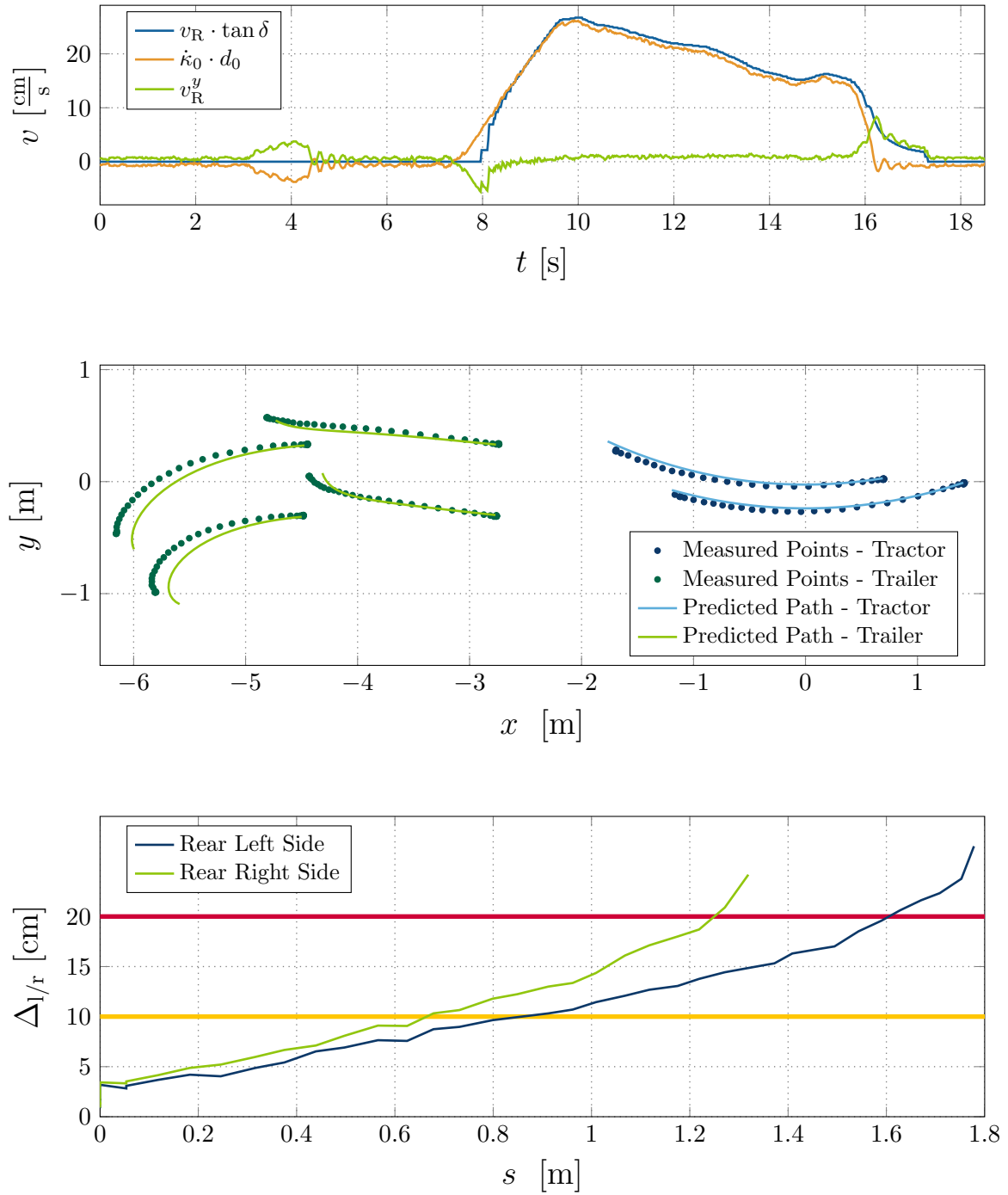


Figure 10.5: Analysis of single-axle trailer for maximum steering angle

10.1.6 Scenario: $\varepsilon \approx -490^\circ$

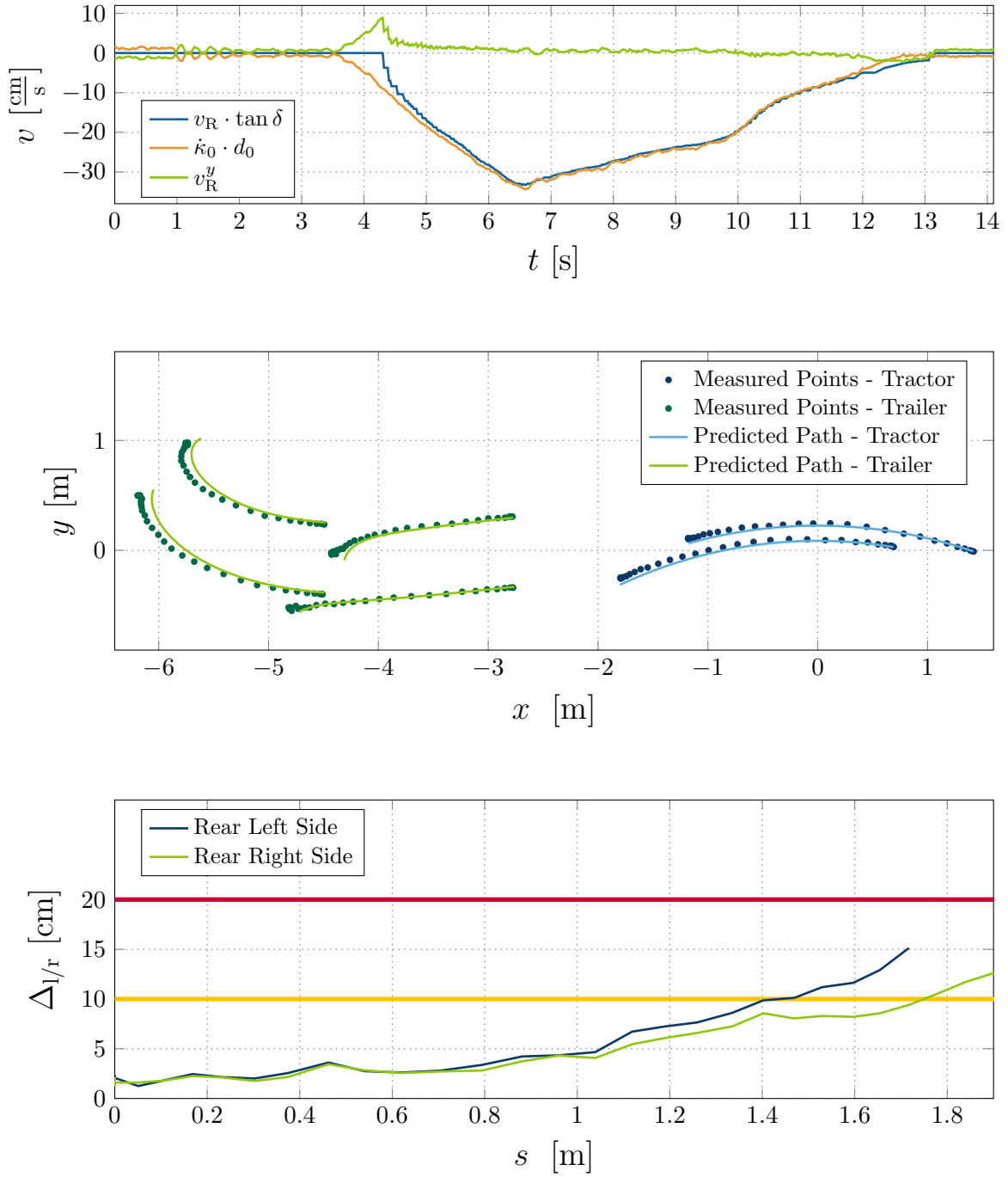


Figure 10.6: Analysis of single-axle trailer for minimum steering angle

10.2 Analysis of the Two-Axle Trailer

10.2.1 Scenario: $\varepsilon \approx +90^\circ$

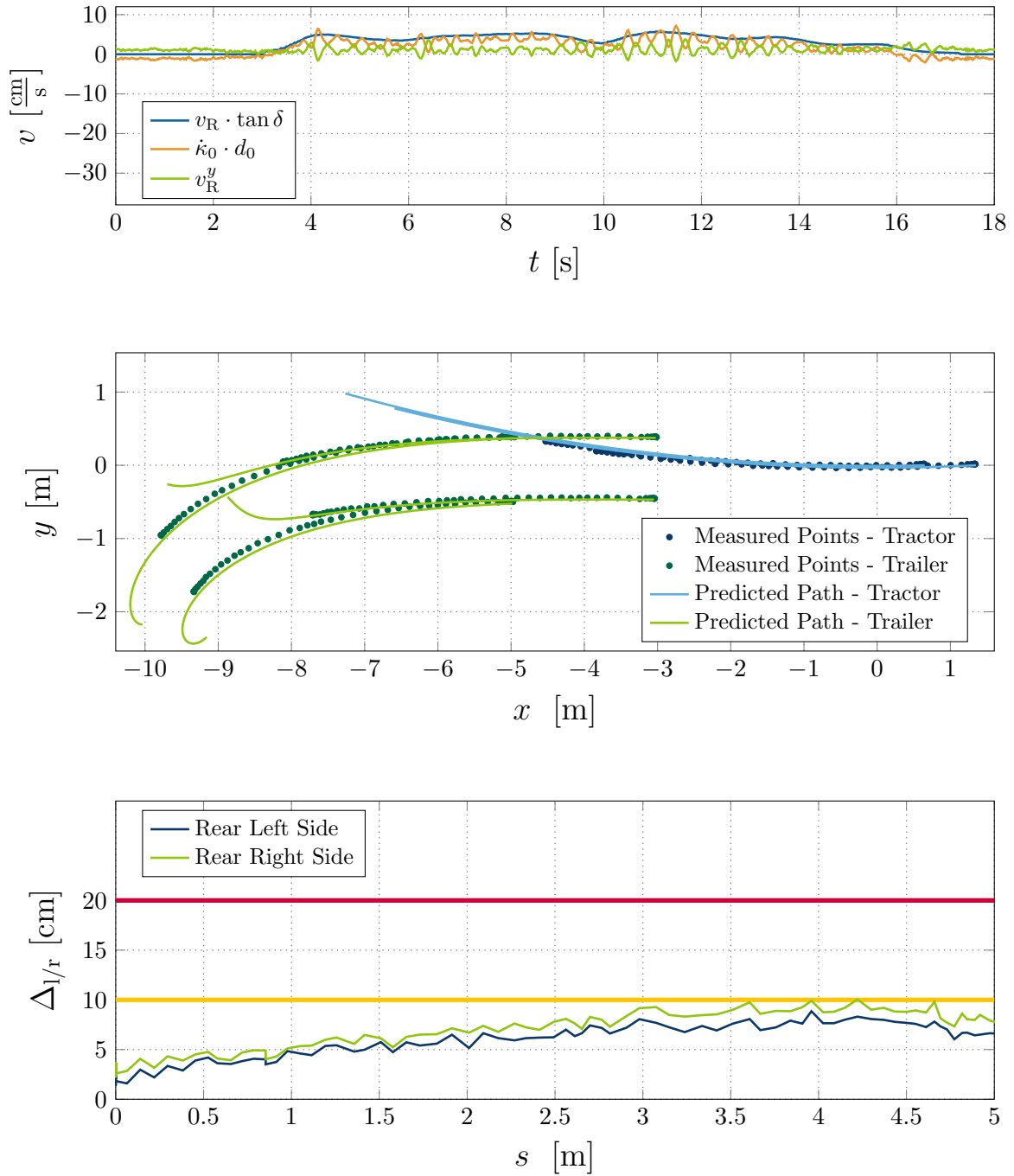
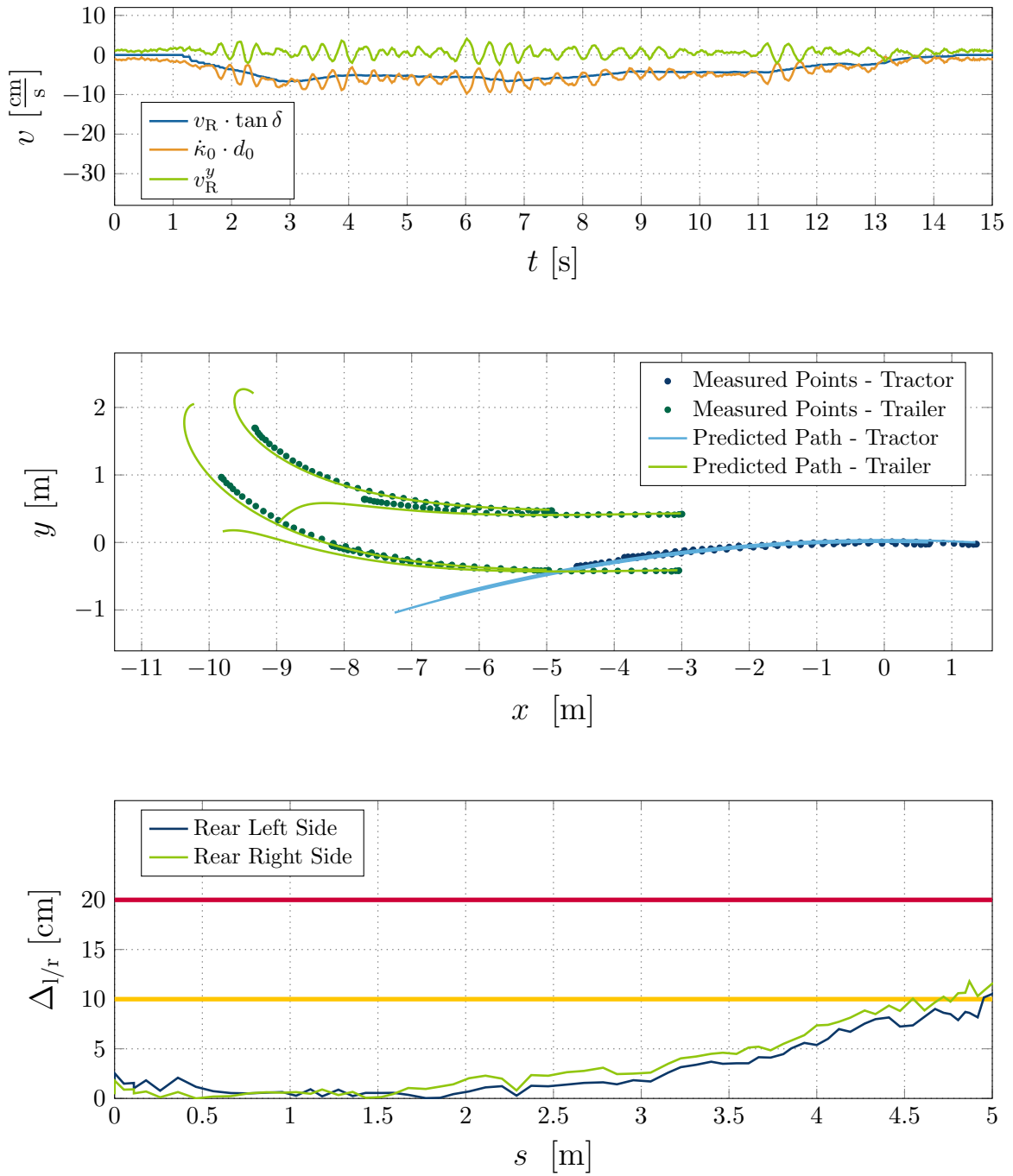


Figure 10.7: Analysis of two-axle trailer for $+90^\circ$ steering angle

10.2.2 Scenario: $\varepsilon \approx -90^\circ$ Figure 10.8: Analysis of two-axle trailer for -90° steering angle

10.2.3 Scenario: $\varepsilon \approx +180^\circ$

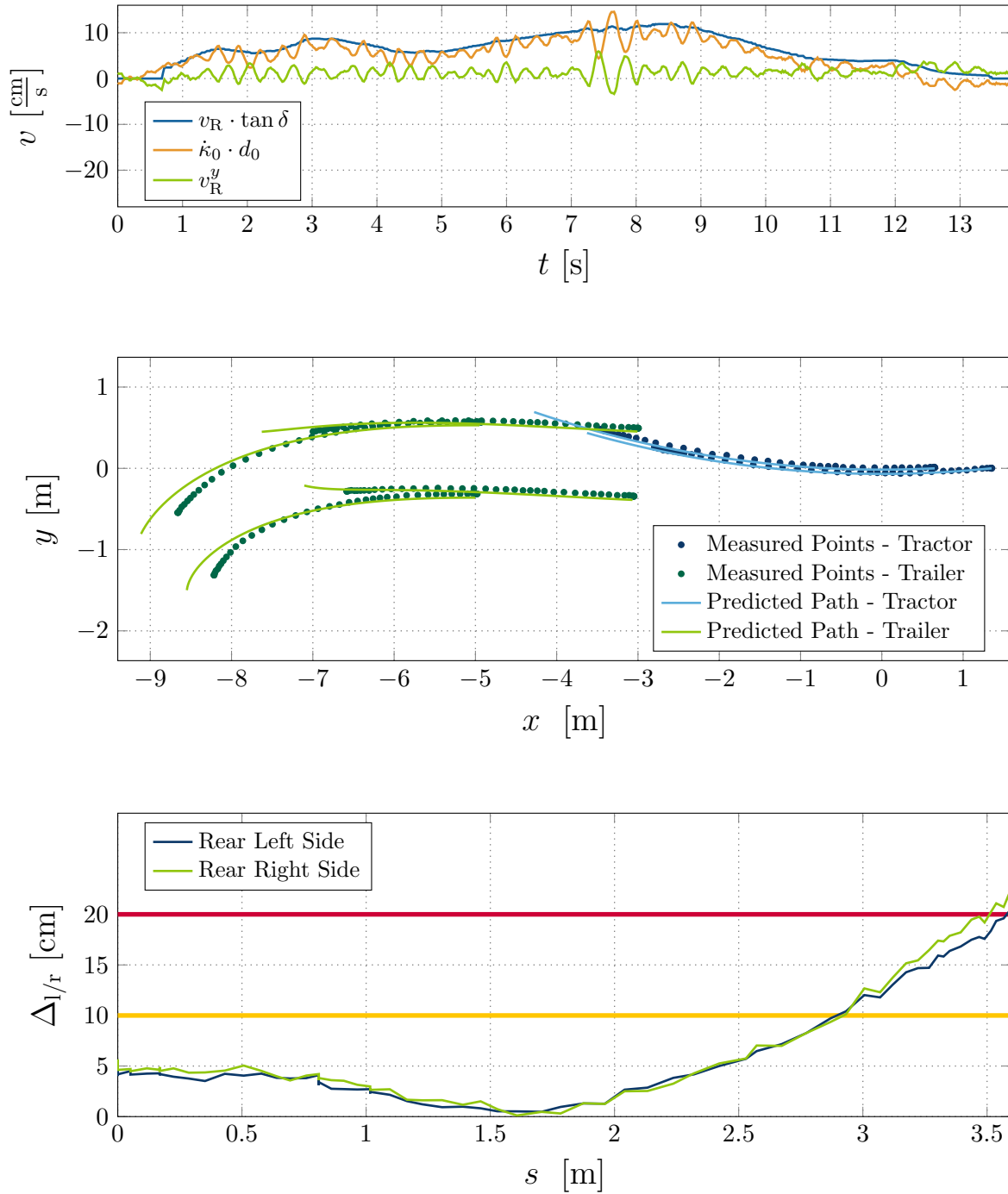
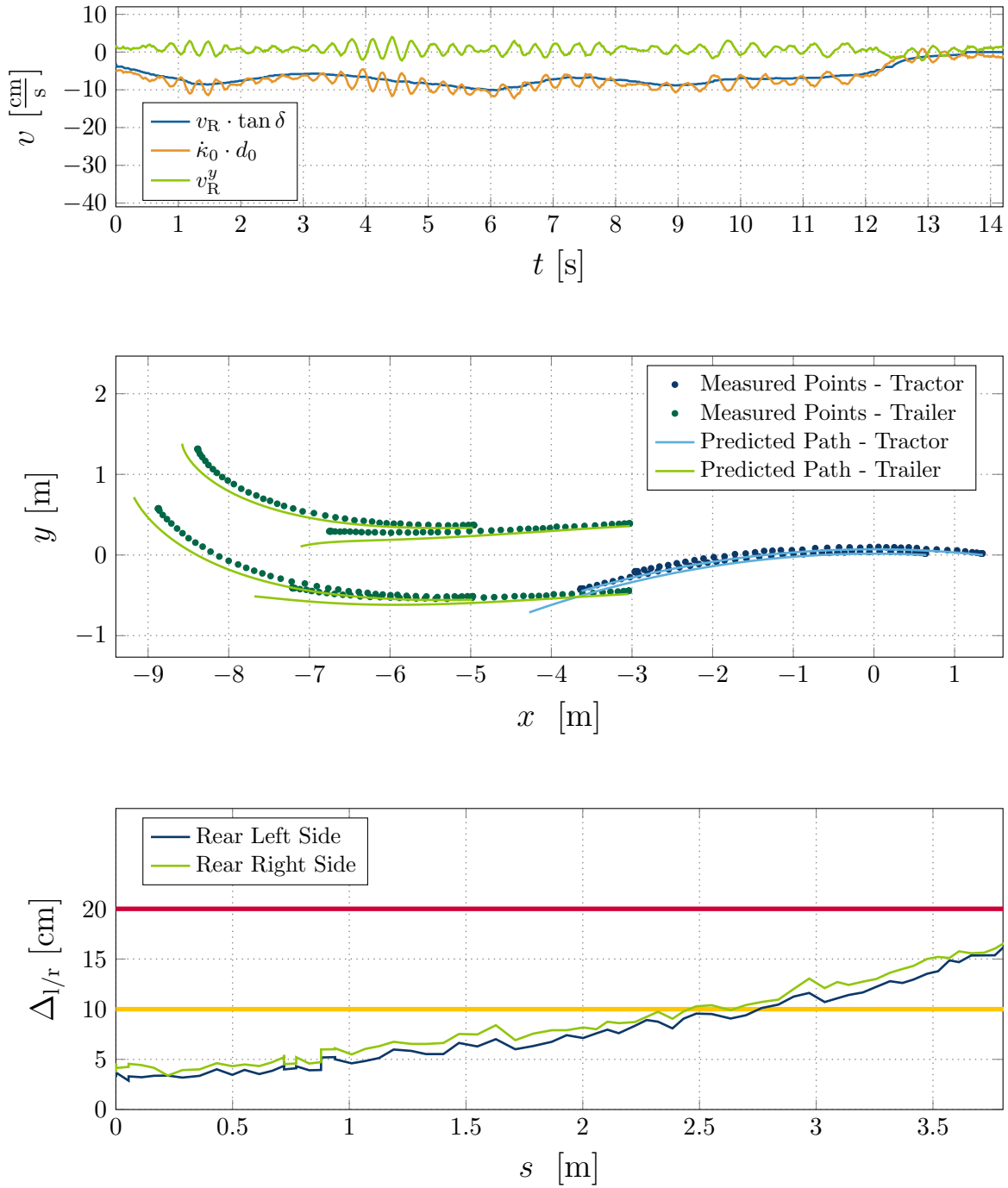


Figure 10.9: Analysis of two-axle trailer for $+180^\circ$ steering angle

10.2.4 Scenario: $\varepsilon \approx -180^\circ$ Figure 10.10: Analysis of two-axle trailer for -180° steering angle

10.2.5 Scenario: $\varepsilon \approx +490^\circ$

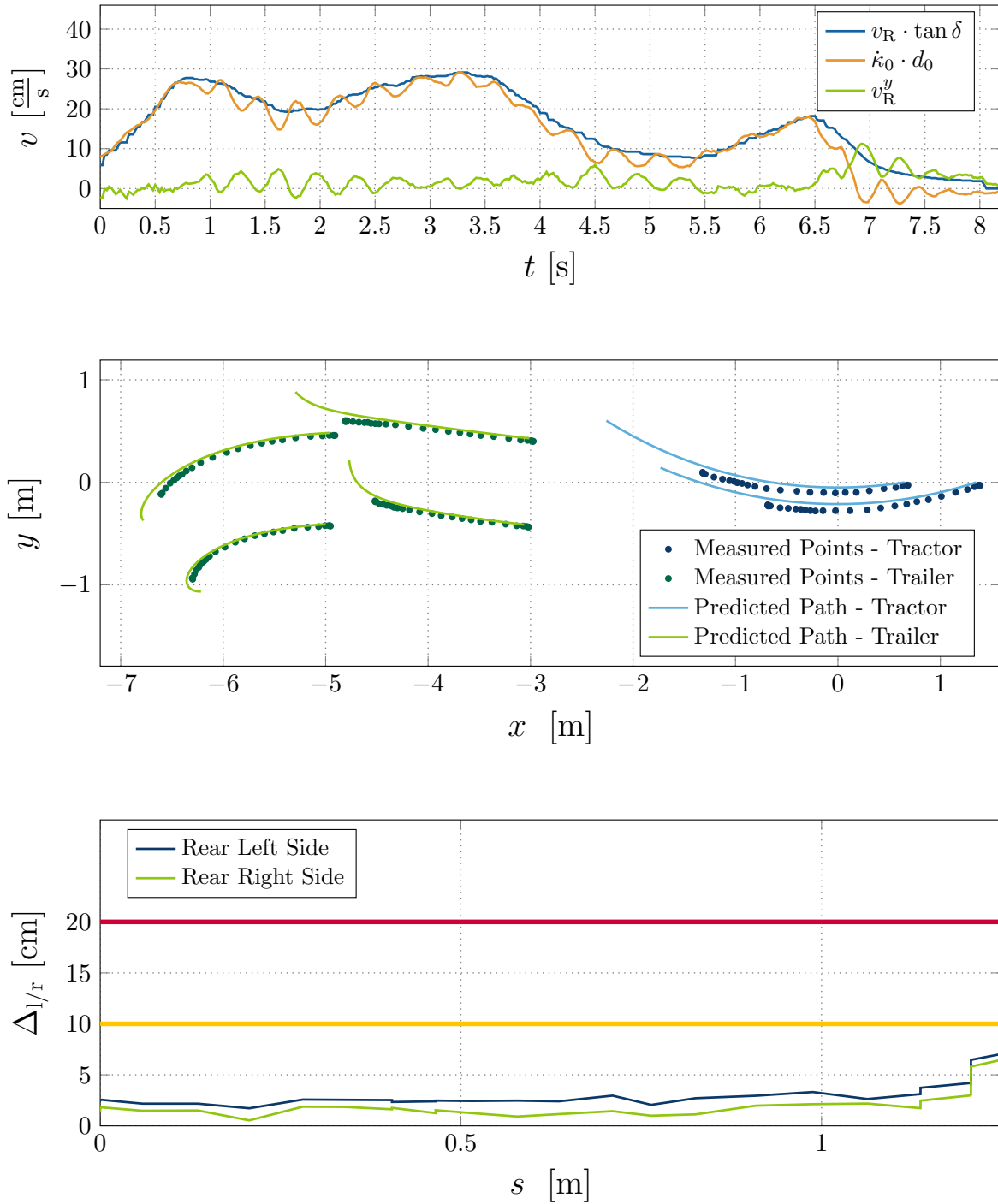


Figure 10.11: Analysis of two-axle trailer for maximum steering angle

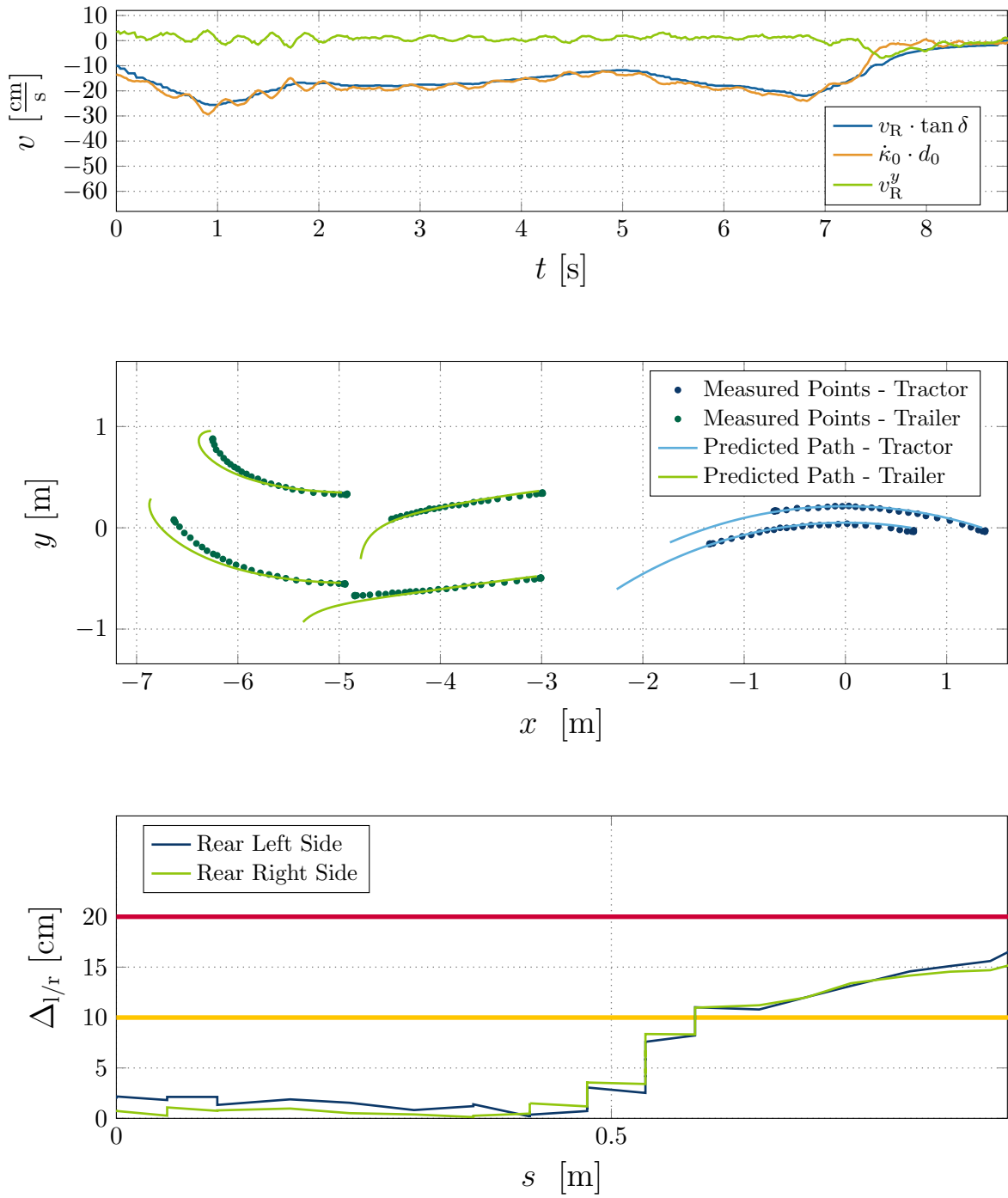
10.2.6 Scenario: $\varepsilon \approx -490^\circ$ 

Figure 10.12: Analysis of two-axle trailer for minimum steering angle

Bibliography

- [Ada14] Jürgen Adamy. *Nichtlineare Systeme und Regelungen*. Springer-Verlag, 2 edition, 2014.
- [Alt00] C. Altafini. Some Properties of the General n-Trailer. *International Journal of Control*, 2000.
- [Bra00] G. Bradski. OpenCV - Open Source Computer Vision Library. *Dr. Dobb's Journal of Software Tools*, 2000.
- [BTS95] L. G. Bushnell, D. M. Tilbury, and S. S. Sastry. Steering Three-Input Non-holonomic Systems: The Fire Truck Example. *The International Journal of Robotics Research*, 14:1428–1431, 1995.
- [Bul99] Vehicle Standards Bulletin. Building Small Trailers - Information for Manufacturers and Summarized Construction Requirements for Trailers less than 4.5 Tonnes Aggregate Trailer Mass, 1999.
- [CSMH13] L. Caup, J. Salmen, I. Muharemovic, and S. Houben. Video-based Trailer Detection and Articulation Estimation. In *Intelligent Vehicles Symposium (IV), 2013 IEEE*, pages 1179–1184, June 2013.
- [EPA08] T. Ehlgen, T. Pajdla, and D. Ammon. Eliminating Blind Spots for Assisted Driving. *IEEE Transactions on Intelligent Transportation Systems*, 9(4):657–665, Dec 2008.
- [FW07] P. Fancher and C. Winkler. Directional Performance Issues in Evaluation and Design of Articulated Heavy Vehicles. *Vehicle System Dynamics*, 45(7-8):607–647, 2007.
- [Geo11] Georg Rill. *Road Vehicle Dynamics - Fundamentals and Modeling*. CRC Press, 2011.
- [GHTC03] Xiao-Shan Gao, Xiao-Rong Hou, Jianliang Tang, and Hang-Fei Cheng. Complete Solution Classification for the Perspective-Three-Point Problem. *IEEE Trans. Pattern Anal. Mach. Intell.*, 25(8):930–943, 2003.
- [Gie15] Robert Giese. Entwicklung eines Verfahrens für die extrinsische Kalibrierung von im Fahrzeug verbauten Kameras, 2015.
- [Gil92] Thomas D. Gillespie. *Fundamentals of Vehicle Dynamics* -. Society of Automotive Engineers, Salzburg, 1992.

- [HR11] J. A. Hesch and S. I. Roumeliotis. A Direct Least-Squares (DLS) method for PnP. In *2011 International Conference on Computer Vision*, pages 383–390, 2011.
- [Hue14] Michael Huelsen. *Knowledge-Based Driver Assistance Systems - Traffic Situation Description and Situation Feature Relevance*. Springer, Berlin, Heidelberg, 2014.
- [HZ04] Richard Hartley and Andrew Zisserman. *Multiple View Geometry in Computer Vision* -. Cambridge University Press, Cambridge, 2004.
- [Jen15] Jens Stratmann. Wir leben in der Zukunft warum sehen wir nicht scharf? - Rückfahrkamera Vergleich: Welcher Hersteller verbaut die beste Kamera? <http://www.mobilegeeks.de/artikel/rueckfahrkamera-vergleich-welcher-hersteller-verbaut-die-beste-kamera/>, 2015. Accessed: 2016-07-02.
- [KB06] Juho Kannala and Sami S. Brandt. A Generic Camera Model and Calibration Method for Conventional, Wide-Angle, and Fish-Eye Lenses. *IEEE Trans. Pattern Analysis and Machine Intelligence*, 28:1335–1340, 2006.
- [Lev44] Kenneth Levenberg. A Method for the Solution of Certain Non-Linear Problems in Least Squares. *The Quarterly of Applied Mathematics*, (2):164–168, 1944.
- [Mar63] Donald W. Marquardt. An Algorithm for Least-Squares Estimation of Nonlinear Parameters. *SIAM Journal on Applied Mathematics*, 11(2):431–441, 1963.
- [MK15] M. M. Michałek and M. Kielczewski. The Concept of Passive Control Assistance for Docking Maneuvers With N-Trailer Vehicles. *IEEE/ASME Transactions on Mechatronics*, 20(5):2075–2084, Oct 2015.
- [MW14] Manfred Mitschke and Henning Wallentowitz. *Dynamik der Kraftfahrzeuge* -. Springer-Verlag, Berlin Heidelberg New York, 5 edition, 2014.
- [PSACMN13] A. Penate-Sanchez, J. Andrade-Cetto, and F. Moreno-Noguer. Exhaustive Linearization for Robust Camera Pose and Focal Length Estimation. *IEEE Transactions on Pattern Analysis and Machine Intelligence (PAMI)*, 35(10):2387–2400, 2013.
- [Raj11] Rajesh Rajamani. *Vehicle Dynamics and Control* -. Springer Science & Business Media, Berlin Heidelberg, 2. aufl. edition, 2011.
- [RDG10] Konrad Reif, Karl-Heinz Dietsche, and Robert Bosch GmbH. *Kraftfahrtechnisches Taschenbuch* -. Springer-Verlag, Berlin Heidelberg New York, 27 edition, 2010.
- [Rei14] Konrad Reif. *Brakes, Brake Control and Driver Assistance Systems - Function, Regulation and Components*. Springer, Berlin, Heidelberg, 2014.
- [RMJ07] P. Roduit, A. Martinoli, and J. Jacot. A Quantitative Method for Comparing Trajectories of Mobile Robots using Point Distribution Models. In *2007 IEEE/RSJ International Conference on Intelligent Robots and Systems*, pages 2441–2448, Oct 2007.

- [Rod09] *Trajectory Analysis using Point Distribution Models: Algorithms, Performance Evaluation, and Experimental Validation using Mobile Robots*. PhD thesis, École Polytechnique Fédérale de Lausanne, 2009.
- [Sch06] Martin Schönfeld. Implementierung einer Rückfahrkamera mit Einblendung von Trajektorien für das Rückwärtsfahren mit einachsigen Anhänger, 2006.
- [Sta11] Alexander Stanoyevitch. *Introduction to Numerical Ordinary and Partial Differential Equations Using MATLAB*. John Wiley & Sons, New York, 2011.
- [SV95] Petr Svestka and Jules Vleugels. Exact Motion Planning for Tractor-Trailer Robots. In *ICRA*, pages 2445–2450. IEEE Computer Society, 1995.
- [Tex15] Texas Instruments. *Advanced Driver Assistance (ADAS) Solutions Guide*, 2015. Accessed: 2016-07-02.
- [TMS93] D. Tilbury, R. M. Murray, and S. Sastry. Trajectory generation for the N-trailer problem using Goursat normal form. In *Decision and Control, 1993., Proceedings of the 32nd IEEE Conference on*, pages 971–977, Dec 1993.
- [TSBS95] Dawn Tilbury, Ole Jakob Sørдалen, Linda Bushnell, and S. Shankar Sastry. A Multisteering Trailer System: Conversion into Chained Form Using Dynamic Feedback. *IEEE Transactions on Robotics and Automation*, 11(6):807–818, 1995.
- [V. 09] V. Lepetit and F. Moreno-Noguer and P. Fua. EPnP: An Accurate $O(n)$ Solution to the PnP Problem. *International Journal Computer Vision*, 81(2), 2009.
- [Vol14] Volkswagen. VIAVISION: Volkswagen - Nachrichten aus der mobilen Zukunft. http://www.volkswagenag.com/content/vwcorp/info_center/de/publications/2014/01/VIAVISION.01.bin.html/binarystorageitem/file/ViaVision_D.pdf, 1 2014.
- [WA98] C. Winkler and J. Aurell. Analysis and Testing of the Steady-State Turning of Multi-axle Trucks. *International Symposium on Heavy Vehicle Weights and Dimensions*, 1998.
- [WHLS15] Hermann Winner, Stephan Hakuli, Felix Lotz, and Christina Singer. *Handbook of Driver Assistance Systems - Basic Information, Components and Systems for Active Safety and Comfort*. Springer International Publishing, Cham, Heidelberg, New York, Dordrecht, London, 1st ed. 2016 edition, 2015.
- [WHW⁺11] Hermann Winner, Stephan Hakuli, Gabriele (Eds.) Wolf, Hermann Winner, Stephan Hakuli, and Gabriele Wolf. *Handbuch Fahrerassistenzsysteme - Grundlagen, Komponenten und Systeme für aktive Sicherheit und Komfort*. Springer-Verlag, Berlin Heidelberg New York, 2 edition, 2011.
- [Zha00] Zhengyou Zhang. A Flexible New Technique for Camera Calibration. *IEEE Trans. Pattern Anal. Mach. Intell.*, 22(11):1330–1334, November 2000.
- [ZPW00] Dieter Zöbel, David Pollock, and Philipp Wojke. Steering Assistance for Backing up Articulated Vehicles. *Systemics, Cybernetics and Informatics*, 1(5), 2000.

CD Content

Table 10.1 summarises the content of the directories on the attached CD.

Table 10.1: CD Content

Directory	Subdirectory	Description
Thesis_PDF		Master's thesis in pdf format
Thesis_latex-figures		Appearing figures
	tikzpictures	Generated figures with TikZ
	fig	Used figures

